Deciphering the mechanism of the arrhythmogenic R735X nonsense PKP2 mutation

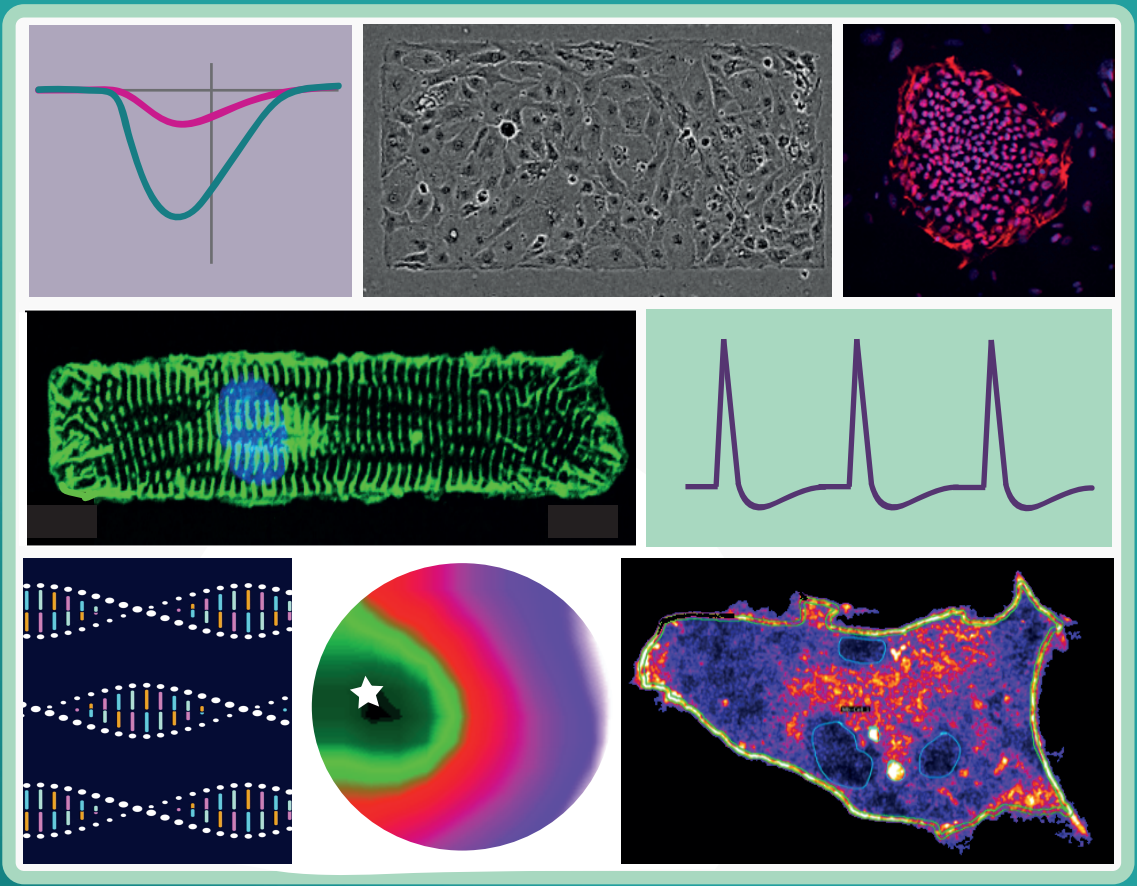

Cristina del Carmen Roselló
Doctoral thesis

Universidad Autónoma de Madrid
Programa de doctorado en Biociencias Moleculares
Madrid, 2019

Departamento de Bioquímica
Facultad de Medicina
Universidad Autónoma de Madrid

Deciphering the mechanism of the arrhythmogenic R735X nonsense PKP2 mutation

PhD candidate: Cristina del Carmen Roselló. Degree in Biotechnology.

Thesis director: Dr. Juan Antonio Bernal

Spanish National Center for Cardiovascular Research (CNIC), Madrid

AGRADECIMIENTOS

AGRADECIMIENTOS

Gracias a mi director de tesis, el Dr. Juan Antonio Bernal, por darme la oportunidad de trabajar en tu laboratorio. Por hacerme ver que estaba en el lugar adecuado. Por todo lo aprendido. Gracias por ayudarme a convertirme en una científica con criterio y en una mujer que puede con todo.

Gracias al Dr. José Jalife por compartir conmigo su gran sabiduría y experiencia. Por acogerme en tu laboratorio como a una más. Por ayudarme cuando ha sido necesario. Por tener siempre la puerta de tu despacho o la ventana de *Skype* abierta para mi. Ha sido una suerte y todo un honor.

A todos mis compañeros de laboratorio pasados y presentes, por vuestra inestimable ayuda. A Cristina, mi amiga y compañera, porque has estado, y estoy segura de que siempre estarás, en los peores agobios y en las mejores risas. Por compartir conmigo tu inteligencia, tu sensatez y tu prudencia. Por ser brillante y hacer brillar a los demás. A Silvia, la bondad personificada, gracias por tu inocencia y tus ganas de ayudar siempre. Por ver siempre el lado positivo de las cosas. Gracias a ambas por acompañarme a llegar hasta aquí. Sin vosotras, no habría sido capaz. Gracias a Ana, mi *cruso*, por tu buen humor, por tu cariño, por hacerme reír hasta el infinito. Gracias a Mariya, por tu desparpajo, por tu fidelidad, por cubrirme siempre.

A Briane, my partner of adventures, crepes, make-up, feminism… It has been amazing to meet you and grow up with you. A Ghislaine, merci pour ton grand sourire et ton courage, pour être un exemple pour toutes les autres. A Melisa, mi primera amiga en esto de la ciencia. Gracias por acogerme cuando llegué a CNIC, por tu empatía, tu salsa y tus patines. A Julio, Sergio y Jesús, por demostrar que una feria de abril en Madrid es posible. Por ser los mejores compañeros de ciencia y de fiesta.

A todos los "Mazanares", ejemplo de trabajo en grupo, gracias por transmitir esa energía y esas ganas por la investigación.

A todos los miembros del CNIC que a lo largo de estos años siempre han estado dispuestos a echar una mano, gracias.

To my Ann Arbor friends, thanks for turning those months in USA into one of the best experiences I will ever have in my life. Thanks to Eric, Erik, Roberto, Abuelito, Mary and my Juanes for taking me in your family and make me feel at home. For demonstrating that dancing does not understand about borders. To Ejona, mi amiga, for taking care of me like a sister, for being such a good friend.

A mi segunda familia, la familia que se elige. A ellas, espejo donde buscarme, mujeres todoterreno, ejemplos de valentía y fuerza. En especial a María, Mer y Ángela, mis psicólogas durante estos años. Gracias por caminar junto a mi cada día y alentarme a luchar. A ellos, por vuestra fraternidad y por recargarme siempre de energía positiva. A todos, por demostrar que la amistad no entiende de kilómetros y que hay cosas que son para siempre.

A todos mis tíos y primos. Por formar una familia tan maravillosa.

A todos mis abuelos , gracias por inculcarme tanto, por cuidarme siempre. A mi segunda madre, mi fan numero uno, gracias.

A mi hermano, mi persona favorita en este mundo. Gracias por aguantarme y sacarme una sonrisa siempre.

A mis padres, gracias por habérmelo dado TODO. Por haberme apoyado en mis decisiones por locas que os pudieran parecer. Por dejar que me equivoque y que acierte. Por haberme enseñado a ser responsable y persistente. Soy muy afortunada.

SUMMARY

SUMMARY

Ventricular arrhythmias (VA) appear during the concealed phase of arrhythmogenic right ventricular cardiomyopathy (AC). This VA can lead to sudden cardiac death, being in many cases, the first symptom of the disease. Mutations on the desmosomal gene *Plakophilin-2* (*PKP2)* have been described as the most prevalent genetic causes of AC. However, the molecular mechanism underlying these early electrical changes during AC development has not been elucidated. PKP2 integrates into the connexome protein network and may lead to changes in its components. In this thesis project we have demonstrated that R735X (a PKP2 truncation associated to AC phenotype) leads to a decrease of the voltage-gated sodium channel Nav1.5 at the plasma membrane of HEK293T and HL-1 cells. In order to study the effect of R735X on a human context, we have developed an AC model based on human induced pluripotent stem cell-derived cardiomyocytes (hiPSC-CM). We have study the role of R735X in hiPSC-CM electrophysiology by comparing electrical features of AC hiPSC-CMs (expressing R735X) with its hiPSC-CM isogenic control. Patch-clamp measurements indicate that R735X leads to a decrease in the fast depolarizing sodium current generated by Nav1.5 channel in hiPSC-CMs. Optical mapping showed an elongation of the action potential duration (APD) and slow down in the conduction velocity (CV) of the electrical impulse in mutant 2D hiPSC-CM monolayers, inducing arrhythmogenics events. These results highlight the arrhythmogenic character of R735X protein and could explain the electrical abnormalities reported in AC patients at early stages of the disease.

RESUMEN

RESUMEN

Pacientes con Cardiomiopatía Arritmogénica (siglas en inglés, AC) pueden sufrir arritmias ventriculares (AV) durante la fase subclínica de la enfermedad. Estas AV pueden provocar la muerte súbita del paciente, siendo en muchos casos, el primer síntoma de la enfermedad. Se ha descrito que la causa genética más prevalente de AC son mutaciones en el gen desmosomal *Placofilina-2* (siglas en inglés, *PKP2*). Sin embargo, el mecanismo molecular por el que se producen cambios eléctricos en el corazón en fases tempranas durante el desarrollo de AC no se conoce. PKP2 forma parte de la red proteica conocida como conexoma y puede provocar cambios en sus componentes. En esta tesis, hemos demostrado que R735X (una versión truncada de PKP2 relacionada con AC) hace que disminuya la cantidad de canal de sodio ($Na_V1.5$) en la membrana plasmática de células HEK293T y HL-1. Con el fin de estudiar el efecto de R735X en un contexto humano, hemos generado un modelo de AC basado en cardiomiocitos derivados de células madre pluripotentes inducidas (siglas en inglés, hiPSC-CMs). Hemos estudiado el papel de R735X en la electrofisiología de hiPSC-CMs las características eléctricas entre los hiPSC-CMs que expresan la mutación R735X y su control isogénico. Los experimentos de *patch-clamp* demostraron que R735X provoca la reducción en la corriente rápida que despolariza los cardiomiocitos. El mapeo óptico demostró que R735X provoca un alargamiento de la duración del potencial de acción y enlentece la velocidad de conducción del impulso eléctrico, provocando la aparición de arritmias. Estos resultados subrayan el carácter arritmogénico del mutante R735X y podría explicar las anormalidades eléctricas que se dan en pacientes con AC.

INDEX

ABBREVIATIONS

ABBREVIATIONS

AC	Arrhythmogenic cardiomyopathy
AP	Action potential
APD	Action potential duration
APD_{20}	Action potential duration at 20% of repolarization
APD_{80}	Action potential duration at 80% of repolarization
APD_{90}	Action potential duration at 90% of repolarization
ARVC	Arrhythmogenic right ventricular cardiomyopathy
BrS	Brugada syndrome
Ca_V	Voltage-gated calcium channel
CV	Conduction velocity
DSC2	Desmocolin-2
DSG2	Desmoglein-2
DSP	Desmoplakin
EGFP	Enhanced Green Fluorescent Protein
FRAP	Fluorescence recovery after photobleaching
HEK293T cells	Human embryonic kidney 293T cells
hiPSC-CMs	Human induced pluripotent stem cells-derived cardiomyocytes
hiPSCs	Human induced pluripotent stem cells
I_{Ca}	Calcium L-type current
IF	Intermediate filaments
I_{K1}	Inward rectifier current
I_{Na}	Sodium currents
K_v	Voltage-gated potasium channel
Na_V	Voltage-gated sodium channel
$Na_V1.5$	Voltage-gated sodium channel alpha subunit 5
PB	*Piggy*Bac
PDMS	Polydimethylsiloxane
PG	Plakoglobin
PKP2	Plakophillin-2
R735X	PKP2 truncated mutant
RPM	Resting membrane potential
s.d.	Standar deviation
s.e.m.	Standard error of the mean
SCD	Sudden cardiac death
$T_{1/2}$	Half-time of recovery
VA	Ventricular arrhythmias

INTRODUCTION

INTRODUCTION

1. Cardiac electrophysiology

The physiological mechanism whereby the heart pumps blood throughout the body via the circulatory system is a very complex and tightly regulated process. Electrical activity is initiated in the pacemaker cells in the sinoatrial (SA) node and propagated through the atria to the atrioventricular (AV) node. After a brief pause in the AV node, excitation spreads through the Purkinje fibers to the apex of the heart and into the ventricular myocardium (Figure 1). For the cardiomyocytes to contract, an electrical impulse generates an action potential (AP) associated to a contraction event. This event is followed by a relaxation and a refractory period until the next impulse is generated and propagated. An AP is a reversible change in the cell membrane potential that goes from the basal resting membrane potential (RMP, -85/95mV) to approximately +40/50 mV, and returns to the basal RMP. The cardiac AP is the result of the sequential activation and inactivation of ion channels that conduct depolarizing, inward (Na^+ and Ca^{2+}), and repolarizing, outward (K^+), currents. Action potential waveforms are different in each region of the heart, reflecting the heterogeneity of ion channel expression levels in each cell type (Nerbonne and Kass, 2005) (Figure 1).

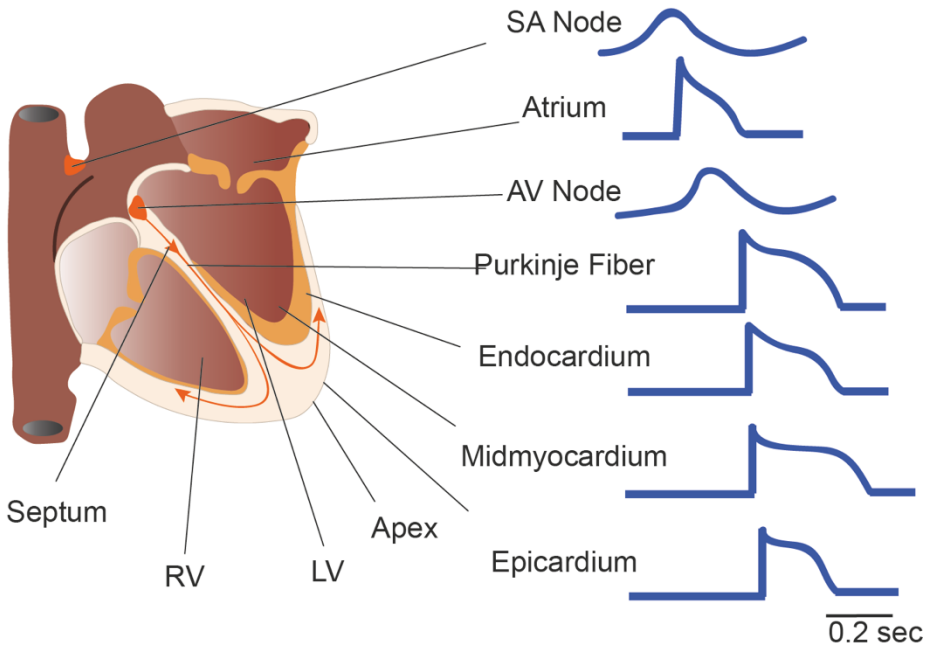

Figure 1. Electrical activity in the heart. Schematic of a human heart with detail of typical action potential waveforms recorded in different regions. Right ventricle (RV). Left ventricle (LV). Orange arrows represent direction of electrical impulse propagation. Solid red lines represent action potential wave forms. Adapted from Nerbonne & Kass, 2005

AP of ventricular cardiomyocytes have four phases (Figure 2) (Delpón, 2019) (Tamargo et al., 2004):

- Phase 0 or fast depolarization: is due to the rapid inward Na^+ current (I_{Na}) through the voltage-gated sodium channel (Na_V). These channels are rapidly opened and closed, becoming inactive.

- Phase 1 or initial rapid depolarization: is consequence of the rapid voltage-dependent inactivation of I_{Na} and the activation of the fast transient voltage-gated outward K^+ current (I_{to}).

- Phase 2 or plateau is the sum of:
    - inward depolarizing currents of Na^+ (late I_{Na} or I_{NaL}) through the fraction of channels that have not been inactivated completely and Ca^{2+} current (I_{CaL}) through the voltage-gated calcium (Ca_v) L-type channels. Ca^{2+} entry through L-type channels results in Ca^{2+} release from intracellular stores and is the main trigger for excitation-contraction coupling.

    - the different components of the delayed outward rectifier K^+ current through the voltage-gated K^+ channels (K_V) : rapid (I_{Kr}) and slow (I_{Ks}).

- Phase 3 of repolarization: Na_V and Ca_V channels are inactivated and the outward K^+ currents predominate, resulting in repolarization, bringing the membrane voltage back to the resting potential.

- Phase 4 or diastolic interval: at the end of phase 3 the inward-rectifier K^+ current is activated (I_{K1}). Kir channels conduct K^+ currents more in the inward direction than in the outward direction and play an important role in setting the RMP close to the equilibrium potential for K^+ (E_K, approximately - 90 mV) and in the repolarization of the AP.

Any factor altering this delicate process would change action potential waveforms, synchronization, and/or propagation, putting the heart at risk of potential life-threatening arrhythmias. Therefore, a thorough understanding of the cardiac electrophysiology and how it might be altered is essential to proper diagnosis and management of cardiac arrhythmias.

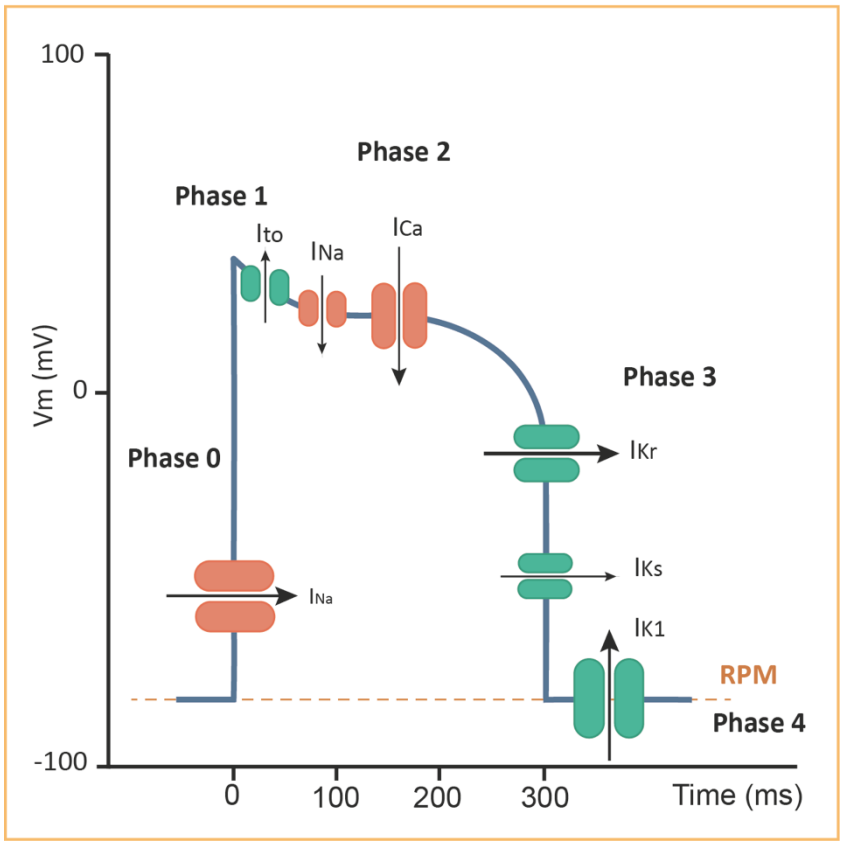

Figure 2. Action potential of a human ventricular cardiomyocyte. Membrane voltage (Vm) in millivolts (y-axis) is plotted against time in milliseconds (x-axis). Resting membrane potential (RMP) is represented at ~ -90mV. Black arrows represent inwards or outwards ion currents. Red and green ovals represent ion channels. Phase 0-4 of the action potential are indicated.

2. Inherited cardiac arrhythmias

Inherited cardiac arrhythmias have been classified in two different groups: hereditary arrhythmia syndromes and genetic arrhythmogenic structural heart disease (Beckmann et al., 2011). Hereditary arrhythmia syndromes or channelopathies include several different diseases, such as long QT syndrome (LQTS), Brugada syndrome (BrS), catecholaminergic polymorphic ventricular tachycardia (CPVT), short QT syndrome (SQTS), idiopathic ventricular fibrillation (IVF), and progressive cardiac conduction system disease (PCCD). Ventricular arrhythmias, typical of these syndromes, are caused by mutations of ion channels and their interacting proteins, mainly involving potassium, sodium, and calcium handling. However, in patients with this disease, the heart is typically structurally normal without showing macroscopic structural evidence of disease. In fact, many young people with these diseases suffer sudden cardiac death (SCD) and upon autopsy, they typically show no structural anomalies (Gray and Behr, 2016).

Among the most frequent genetic arrhythmogenic structural heart disease we can find Hypertrophic cardiomyopathy (HCM), Dilated cardiomyopathy (DCM) and Arrhythmogenic cardiomyopathy (AC). Mutations in different sarcomeric, cytoskeletal, desmosomal or nuclear envelope genes mediate structural changes in the cardiac tissue (hypertrophy, dilatation, fibrous infiltration, etc.) that have been related to arrhythmias and SCD (Nishimura Rick A. et al., 2017)(Reichart et al., 2019).

3. AC: a complex and challenging disease

Arrhythmogenic cardiomyopathy (AC), known for many years as arrhythmogenic right ventricular cardiomyopathy (ARVC) (Platonov et al., 2019) is a chronic, progressive and heritable cardiomyopathy. AC is one of the leading causes of **sudden unexpected cardiac death** in young and apparently healthy individuals. It has been classified as a rare cardiac pathology (ORPHA247) (Alcalde et al., 2014) and its estimated prevalence ranges from 1:1000 to 1:5000, sudden death being the first symptom of disease in many cases (Haugaa et al., 2016).

General AC disease progression has been divided into **three phases** (Haugaa et al., 2016):

1. Early 'concealed phase': in this phase individuals are often asymptomatic, but are at risk of ventricular arrhythmias and sudden cardiac death.
2. Overt 'electrical phase': individuals present with symptomatic arrhythmias. RV morphological abnormalities may still not be detectable by conventional imaging tools.
3. Diffuse, progressive disease resulting in right, left, or biventricular heart failure, often combined with ventricular arrhythmias.

However, it is important to note that 30% of patients with morphological criteria for AC have a so-called ECG-concealed form that does not fulfill the ECG diagnostic criteria.

Diagnosis of AC is one of the most challenging in the field of inherited cadiomyopathies due to two main reasons (Gandjbakhch et al., 2018):

- Its **variable expressivity** and **incomplete penetrance** in relatives.

AC clinical manifestations usually appear during adolescence, but can also manifest later on in adulthood. Disease progression is highly variable. For instance, life-threatening ventricular

arrhythmias may present as periodic bursts and “hot phases” instead of manifesting as a steady process. AC progression is strongly determined by environmental factors such as inflammatory processes and exercise. Clinical diagnosis of relatives is particularly difficult in AC because of the low penetrance of mutations. In fact, only one third of relatives fulfill definitive task force criteria diagnosis. Thus, clinical screening is usually not sufficiently accurate to predict their genetic status. Moreover, phenotype and penetrance in AC are age dependent, and phenotypically negative relatives may present with symptoms and cardiomyopathy years after initial screening (Gandjbakhch et al., 2018).

- Absence of specific unique diagnostic criteria.

In 2010, several **combined diagnostic criteria** (task force criteria, TFC) were reviewed and implemented, increasing diagnosis specificity (especially in family members and young athletes). However, AC 2010 TFC still lack sensitivity, in the early stages of the disease (Gandjbakhch et al., 2018). AC task force criteria include: global or regional dysfunction and structural alterations, tissue characterization of the ventricular wall, re- and depolarization or conduction abnormalities, arrhythmias, genetics and family history.

3.1. Anatomopathological features

AC main anatomopathological feature is the loss of myocytes and its replacement by fibrous or fibroadipose tissue in the RV free wall. LV pathological histology is frequently reported in autopsy cases or explanted hearts, even in the absence of macroscopic LV changes. It should be noted that fatty infiltration by itself is not required as a histological diagnostic criterion. In fact, a systematic study of myocardial biopsies showed the absence of specific RV fat infiltration in contrast to extensive fibrous tissue and myocyte loss (Gandjbakhch et al., 2018).

3.2. Electrocardiogram features

ECG-based TFC diagnostic criteria include: right precordial T-wave inversions, presence of epsilon waves, and increased duration of the terminal QRS. T-wave inversions in the right precordial leads are present in up to 87% of adult patients with AC and are directly related to RV dilatation, and may extend to the left precordium with time. Tanawuttiwat T. *et al*. performed a study where they showed the great variety of ECG presentations. It included 35 AC

patients with negative precordial T waves that were studied by epicardial and endocardial mapping, and MRI imaging. They showed the relationship between the QRS and disease localization and extent. For instance, when the QRS appeared normal, the extent of activation after the end of QRS was minimal and mostly subepicardial. On the other hand, the epsilon wave would correspond to epicardial perivalvular activation (Tanawuttiwat et al., 2016). This study reflects the heterogeneity found in electrocardiogram features among patients that is one of the reasons why AC diagnosis may be easily missed.

3.3. AC therapies

At present there is no effective treatment that can prevent the progression of AC. Therapies focus on symptoms treatment such as the prevention of lethal events. Implantable cardioverter defibrillator placement is the only therapy proven to improve mortality in AC patients. The rest of the treatments - medications (beta blockers and antiarrhythmics), radiofrequency ablation, surgery, cardiac transplantation, and lifestyle changes- help to treat symptoms but none of them have proved to decrease mortality (Idris et al., 2018)(Platonov et al., 2019)(Wang et al., 2019).

3.4. Genetics of AC

Molecular genetic reports have revealed AC to be mainly an autosomal dominant inherited disease (Haugaa et al., 2016). To date, up to 16 different genes have been associated with the AC phenotype. Nonetheless, the genetic cause of AC remains unknown for approximately 40% of patients. AC has been mainly associated with mutations in genes encoding the desmosomal proteins *plakophilin-2* (*PKP2*), *desmoglein-2* (*DSG2*), *desmoplakin* (*DSP*), and, more rarely, *desmocollin-2* (*DSC2*) and *plakoglobin* (*JUP*). In addition, non-desmosomal genes have also been identified as responsible for this pathology: *catenin-α-3* (*CTNNA3*), *cadherin-2* (*CDH2*), *transmembrane protein 43* (*TMEM43*), *lamin A/C* (*LMNA*), *desmin* (*DES*), *titin* (*TTN*), *phospholamban* (*PLN*), *ryanodine receptor type 2* (*RYR2*), *sodium voltage-gated channel α subunit 5* (*SCN5A*), *tumor protein P63* (*TP63*) and *transforming growth factor-β-3* (*TGFB3*) (Gandjbakhch et al., 2018). In table 1, all AC associated genes are enlisted together with their frequencies and other associated phenotypes.

Gene	Protein	Frequency in AC ‡	Structure	Phenotype AD
PKP2	Plakophilin-2	20%–45%	Desmosome	AC
DSG2	Desmoglein-2	4%–15%	Desmosome	AC, BiVCM
DSP	Desmoplakin	1%–13%	Desmosome	AC; ALVC, DCM, Cardio-cutaneous Sd, CCD†
DSC2	Desmocollin-2	1%–7%	Desmosome	AC, BiVCM cardiomyopathy
JUP	Plakoglobin	0%–1%	Desmosome	AC
CTNNA3	α-T-catenin	<1%	Intercalated disc	AC
CDH2	N-Cadherin	2%* of patients with negative genetic screening (missense)	Intercalated disc	AC
TMEM43	LUMA	<1%	Nuclear envelop, Intercalated disc, sarcolemma	AC EDMD
LMNA	Lamin A/C	3%–4%	Nuclear envelop	DCM/BiVCM/AC with CCD, AF, VAs _ muscular dystrophy
DES	Desmin	<1%	Intermediate filament	DCM/BiVCM/AC with CDD, AF, VAs _ muscular dystrophy
TTN	Titin	18%* of AC patients with negative genetic screening (missense)	Sarcomere	AC/BiVCM
PLN	Phospholamban	0%–12% (Netherlands)	Calcium regulatory protein	DCM, BiVCM, AC, HCM
RYR2	Ryanodine receptor type 2	9%* of AC patients with negative genetic screening (missense)	Calcium regulatory protein	CPVT _ right ventricular involvement AC
SNC5A	$Na_V1.5$	0%–2%*	Cardiac sodium channel	Brugada Sd, Long QT Sd, AF, CDD, DCM, AC, MEPPC
TP63	P63	1 case report	Transcription factor	Ectodermic dysplasia. AC†, ADULT Sd
TGFB3	TGF-beta 3	2 families	Transforming growth factor	AC

***Frequency of rare missense variants. †Unique observation in the literature. ‡Patients with AC/D phenotype fulfilling task force criteria. AD: autosomal dominant; AF: atrial fibrillation; ALVC: arrhythmogenic left ventricular cardiomyopathy; BiVCM: biventricular cardiomyopathy; CCD: cardiac conduction disease; CPVT: catecholaminergic polymorphic ventricular tachycardia; DCM: dilated cardiomyopathy; del: deletion; EDMD: Emery-Dreifuss muscular dystrophy; HCM: hypertrophic cardiomyopathy; H: heart failure; ins: insertion; MEPPC: Multifocal ectopic Purkinje-related premature contractions; SCD: sudden cardiac death; Sd: syndrome.**

Table 1. List of genes associated with AC. Adapted from Gandjbakhch *et al*. 2018.

4. AC and the desmosome

Desmosomes are membrane protein complexes that play an important role in intercellular adhesion and maintenance of the structural integrity of tissues subjected to mechanical stress, such as the heart and skin. Hemidesmosomes integrate transmembrane proteins: Desmocolin-2 (DSC2) and Desmoglein-2 (DSC2), that attach to their neighbor hemidesmosome transmembrane proteins; and inner face proteins: Plakophilin-2 (PKP2), Plakoglobin (PG), Desmoplakin (DSP), that associated with transmembrane proteins and intermediate filaments (IF) (Figure 3). DSP (member of the plakin family of cytolinkers) serves as a core constituent of the dense plaque. DSP anchors IF to the plasma membrane by its C-terminus and is tethered

indirectly to DSC2 and DSG2 (plasma membrane cadherins) by its N-terminus. N-terminal tethering of DSP is facilitated by PG and PKP2 (armadillo family) [13] .

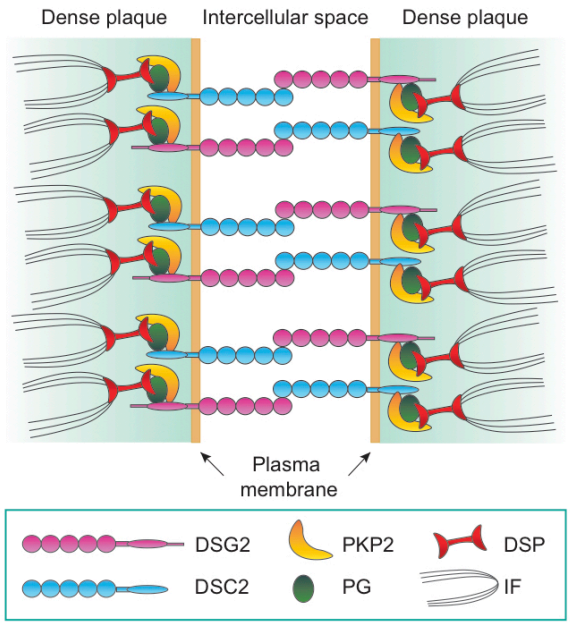

Figure 3. Cardiac desmosome. Organized desmosomal proteins and intermediate filaments (IF) are represented. DSC2: Desmocolin-2, DSG2: Desmoglein-2, PKP2: Plakophilin-2, PG: Plakoglobin, DSP: Desmoplakin.

Mutations in desmosomal genes have been identified in 33% to 63% of AC probands in different patients cohorts. These mutations usually have an autosomal dominant mode of inheritance with incomplete penetrance, leading to an isolated cardiac phenotype. Various types of mutations -missense, stop-gain, splice-site, frameshift, and large deletions- have been reported. PKP2 is the major AC disease-causing gene, accounting for 36% to 92% of mutations identified in desmosomal genes (Cox et al., 2011)(Bao Jingru et al., 2013)(Groeneweg Judith A. et al., 2015)(Fressart et al., 2010). PKP2 mutations are mostly autosomal dominant and are more likely to lead to isolated RV involvement and a conventional phenotype than other desmosomal mutations(te Riele et al., 2013).

5. PKP2 and the arrhythmogenic phenotype

AC patients present an arrhythmogenic phenotype that may exist even from the subclinical or concealed phase of the disease, without being paired with dysfunction and structural alterations. The mechanisms responsible for life-threatening arrhythmias in the concealed

phase of AC still remain unclear. There are studies suggesting that, even though most of the AC associated mutated genes do not codify for channel proteins, their proteins would associate with molecules that are crucial for the heart electrical performance. Historically, it has been described that cardiac cells are in direct contact at the site of end-end cell apposition through the intercalated discs (ID). Different separated molecular complexes were defined at the ID: gap junctions, desmosomes, adherens junctions and the voltage-gated sodium channel (Na_V) complex. However, the current experimental data support that instead of being independent, these molecular complexes form a common protein interacting network at the ID, the so-called "connexome". This protein network will have the role of controlling excitability, electrical coupling and intercellular adhesion. Thus, alterations in one the components of the connexome, could have an effect on the other components (Agullo-Pascual et al., 2014). For instance, an immunohistochemical study (Noorman et al., 2013) performed on human AC patient biopsies (61% of them had PKP2 mutations) revealed that immunoreactive signal of $Na_V1.5$ (the pore forming α-subunit of Na_V complex) at the intercalated disc was decreased in 65% of AC patients; although immunoreactive signals of the mechanical components appeared generally unaffected. Hence, they propose the decrease of $Na_V1.5$ at the ID as a possible component of the electrophysiological substrate present in AC patients.

Whole-cell patch-clamp experiments performed on isolated cardiomyocytes from heterozygous null PKP2 mice (PKP2-Hz) revealed that average peak I_{Na} density in PKP2-Hz cardiomyocytes was significantly reduced when compared with control cells. Same experiment performed on flecainide-treated isolated cardiomyocytes showed a more acute and faster block in PKP2-Hz cells. Electrical epicardial activation mapping of Langendorff-perfused whole heart preparations showed that flecainide caused a most pronounced decrease in longitudinal propagation velocity in PKP2-Hz hearts. Moreover, 50% of PKP2-Hz animals showed flecainide- induced ventricular arrhythmias, while none was observed in any of the WT mice tested (Cerrone et al., 2012). Thus, electrophysiological characterization of the PKP2 haploinsufficient mouse indicate that a decrease in normal levels of PKP2 associates with sodium channel dysfunction and increase of susceptibility to ventricular arrhythmias. Moreover, it has been shown that a reduction of PKP2 levels in HL-1 cell (PKP2-KD HL-1 cells) correlates with a reduction in sodium current density and a decrease of co-localization between $Na_V1.5$ and N-cadherin at site of cell contact. They also showed how transient transfections of *PKP2* in PKP2-KD HL-1 cells was able to restore normal levels of I_{Na} and normal co-localization levels between $Na_V1.5$ and N-cadherin, while overexpression of different *PKP2* missense mutants were not (Cerrone et al., 2014).

6. PKP2 stop-gain mutations: R735X

In 2014, Alcalde et al. performed genotype-phenotype correlations of a small AC Spanish cohort (30 patients) to establish the diagnostic value of genetics and to assess the role of mutation types in age-related penetrance in AC. After screening the desmosome genes, they found that stop-gain PKP2 mutations were the most prevalent desmosome-related gene mutation in AC Spanish patients (Figure 4) (Alcalde et al., 2014).

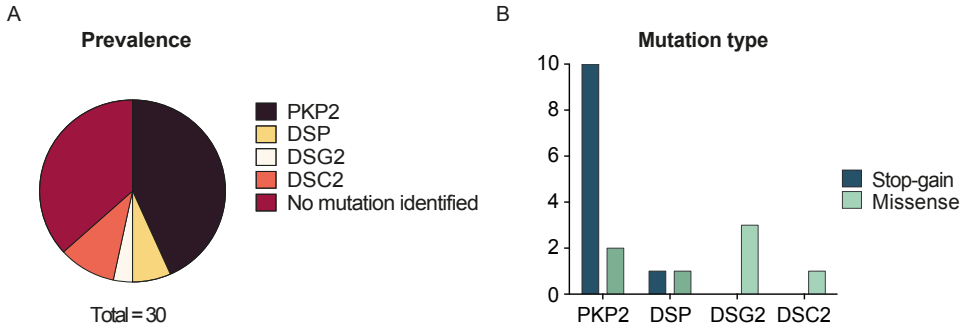

Figure 4. Representation of genetic screening in AC Spanish cohort (30 patients). A. Prevalence of desmosomal gene mutations. B. Prevalence of stop-gain and missense mutations. Adapted from Alcalde et al.2014

A stop-gain mutation may lead to an haploinsuffiency related phenotype, if the resultant peptide is degraded. However, stop-gain mutations may lead to an actual, "new" protein whose role is to be determined. Thus, we focused on one of the reported PKP2 truncating mutations to further investigate its molecular mechanism in AC development. Specifically, we chose the mutation c.2203C>T which codifies for an early stop codon in exon 11 (R735X) since this exon is a hot spot of recombination that give raise to several PKP2 truncations reported in AC patients (Syrris Petros et al., 2006)(Gerull et al., 2004)(Tan et al., 2010). The wild-type sequence of PKP2 has an HR2 domain at its N-terminus and 8 armadillo repeats domains (ARM) and R735X causes the lost of partially ARM6 to C-terminus (Figure 5).

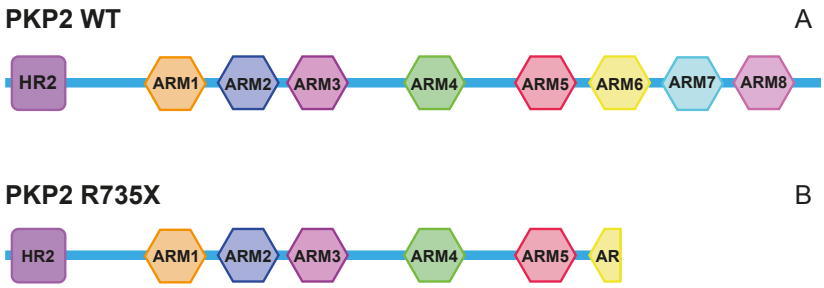

Figure 5. Diagram of PKP2 sequence. A. Representation of PKP2 wild-type sequence: HR2 domain (square) and 8 armadillo (ARM) repeats (hexagons). B. Representation of truncated PKP2. R735X early stop codon mutation causes the loss of partially ARM6 to C-terminus. Adapted from Alcalde et al. 2014.

The AC patient carrying the mutation R735X described by Alcalde et al. (2014) is a 52 years old female that suffered syncope and presents RV dysfunction and structural alterations, repolarization abnormalities, ventricular arrhythmias and family history of SCD. An example of her EGC can be found in figure 6. R735X mutation has also been found in other patient cohorts that presented with syncope, ventricular tachycardia, right ventricular and in some cases left ventricular involvement and family history (Gerull et al., 2004). Moreover, the characterization of the wild-type mice injected with adeno-asociated virus (AAV) encoding for R735X demonstrated that the truncated PKP2 functions as a dominant-negative protein. R735X mice showed a reduction in right ventricular ejection fraction and poor contractility when subjected to endurance training (Cruz et al., 2015).

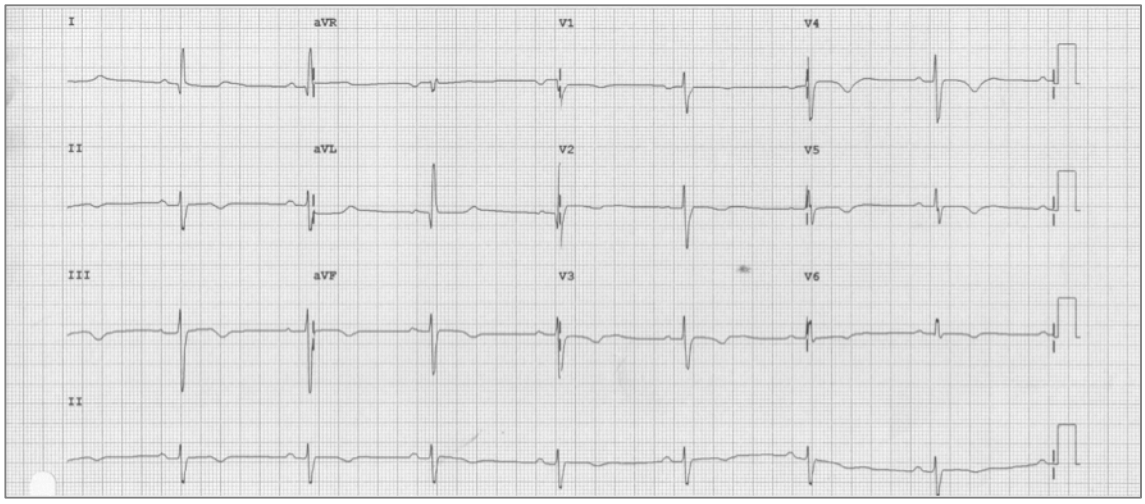

Figure 6. Electrocardiogram of a patient carrying c.2203C>G p.R735X mutation in *PKP2* gene. Patient was diagnosed with mayor repolarization abnormalities according to the TFC of the European Society of Cardiology/International Society and Federation of Cardiology criteria for ARVC(Alcalde et al., 2014).

7. hiPSC-CM as a model of AC

Animal models or cell-derived animal models have helped to enlight the pathogenesis of AC. Indeed, during this thesis project, different cell models (such as HEK293T and HL-1 cells) have been used to characterize the molecular biology of R735X. However, regarding electrophysiological studies, the significant differences between these models and the human electrical features may interpose limits on the interpretation and application of the obtained data. However, the study of AC electrical mechanisms in human cardiomyocytes is extremely limited because obtaining cardiac samples from early stages of human AC hearts is not always possible since AC is commonly diagnosed at later stages or post-mortem, and biopsies may result in cardiac perforation. At this point, development of human induced pluripotent stem cell-derived cardiomyocytes (hiPSC-CMs) technology appears as an alternative platform to study the effect of AC-related mutations in the human electrophysiology.

7.1. Generation of PKP2 hiPS cell lines

Since hiPSCs generation technology and optimization of differentiation protocols became popular, many studies have been done comparing hiPS cells derived from patients and hiPSCs from healthy donors. This system is interesting because these hiPSC lines carry the genetic identity of each patient including disease-causing mutations and its genetic context. However, interpretation of its endpoints can be challenging due to differences in their genetic background. On the other hand, using genome-editing technologies, such as CRISPR/Cas9 system, to introduce or correct specific mutations in hiPSCs has become an alternative to overcome this problem (Paul J Tesar, 2018).

Instead, we decided to create a platform that allow us to generate hiPS cell lines that overexpress specific disease-related transgenes over a common, irrespective of patient's genetic background using the *piggy*Bac (PB) technology. PB technology allows for the efficient and rapid integration of a DNA sequence of interest into a host genome. The PB system used in this project was composed by two different elements: the PB transposon and the PB transposase. The PB transposon is a mobile genetic element consisting of any sequence that is flanked by a specific inverted terminal repeats (5'-TRs and 3'TRs). The transposase is an enzyme that recognize the TRs placed on both ends of the transposon sequence and insert the transposon into TTAA genome sites through a "cut-and-paste" mechanism in a very efficiently way (Allan Bradley, 2007). This approach has been proved to be a simple and versatile way to

stably integrate and express transgenes in hiPSCs. It is a robust and straightforward method to gene delivery into hiPSCs compared with classical delivery viral or BAC vectors. The cargo capacity of PB is massive compared to virus and does not have the risk of resection or fragmentation seen with random BAC integration (Kim et al., 2016). This method is less time consuming and more efficient that CRISPR/Cas9 system. Moreover, it allows to perform comparative studies between different transgenic lines with isogenic background. As a proof of concept of this approach, we have developed an AC model based on hiPSC-CMs consisting on (Figure 7):

- A non-modified hiPS cell line generated from reprogramed somatic cells of a healthy donor (control line).
- A R735X hiPS cell line generated by integrating the mutant transgene (R735X) into the control line.
- A PKP2 hiPS cell line generated by integrating the wild-type version of the transgene (PKP2) into the control line.

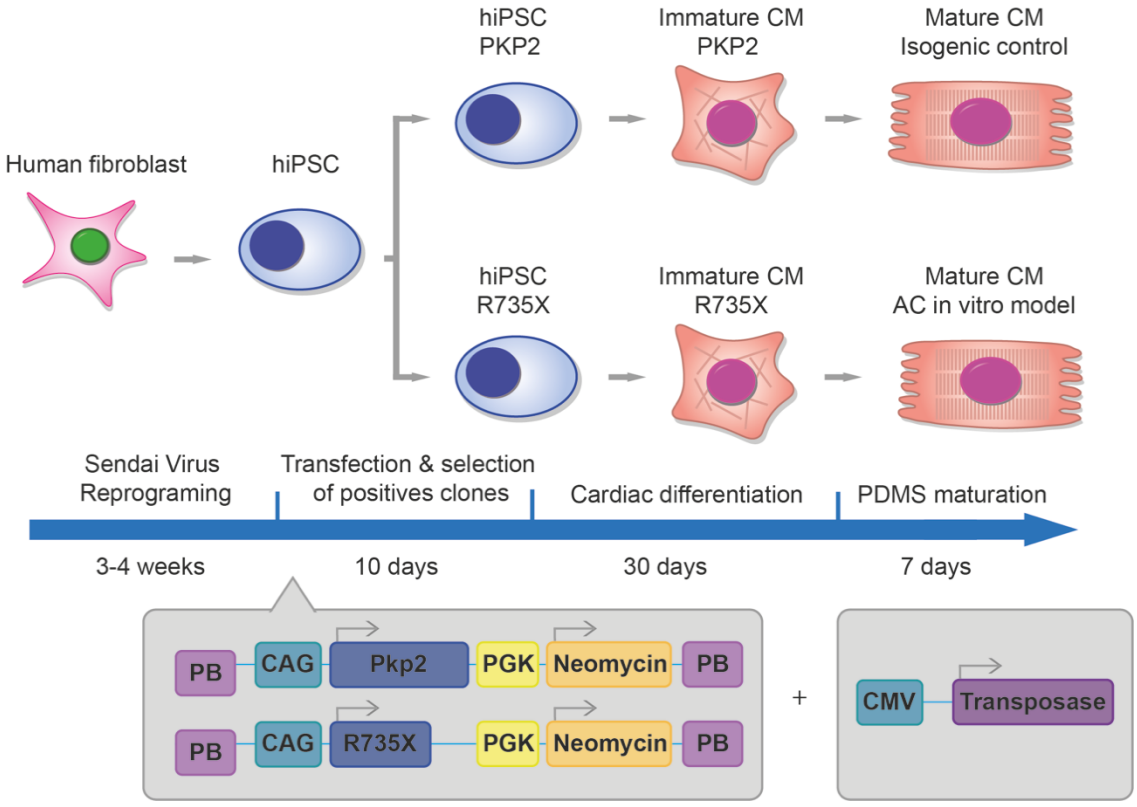

Figure 7. Generation of the AC model based on hiPSC-CM. Human dermal fibroblast were reprogramed into hiPS cells. hiPSCs were co-transfected with the constructs *pPB-CAG-PKP2-PGK-Neomycin-PB* or *pPB-CAG-R735X-PGK-Neomycin-PB*, and *pCMV-Transposase*. CMV, human cytomegalovirus promoter. CAG, CMV enhancer fused to the chicken beta-actin promoter. Neomycin, Neomycin resistance gene. Transposase, Transposase gene. Positives clones were selected with Neomycin treatment. hiPSC were differentiated into cardiomyocytes using a small molecule based protocol (see Materials and Methods). Resultant hiPSC-CM were maturated for 7 days on PDMS. R735X hiPSC-CM and its isogenic control (PKP2 hiPSC-CM) were characterized.

OBJECTIVES

OBJECTIVES

1. To study the impact of the mutation R735X in the localization and mobility of the PKP2 protein.

2. To study the effect of R735X on the voltage-gated sodium channel $Na_V1.5$.

3. To generate an AC model based on hiPSC-CM as a proof of concept of a potential platform to study the role of dominant negative mutations over the same genetic background.

4. To characterize the effect of R735X on single hiPSC-CM electrophysiology.

5. To evaluate the potential arrhythmogenic effect of R735X in hiPSC-CM monolayers.

MATERIALS AND METHODS

MATERIALS AND METHODS

1. DNA constructs

Fluorescent-tagged proteins

The wild-type sequence of *plakophillin-2* (*PKP2*) gene was purchased from Gene Cube. The stop codon in the amino acid 735 was introduced in the wild-type sequence of *PKP2* gene by PCR to generate the truncation R735X in *PKP2*. The sequence of the *SCN5A* gene (hH1a isoform) codifying for the sodium voltage-gated channel alpha subunit 5 ($Na_V1.5$) was kindly provided by Dr. Eva DelPón, Autonomous University of Madrid.

SCN5A was cloned into the plasmid *pEGFP-C1* (Clontech) to generate the plasmid codifying for the fusion protein EGFP-$Na_V1.5$ (N-terminal EGFP). The same strategy was followed to generate the plasmids codifying for both EGFP-PKP2 and EGFP-R735X proteins (N-terminal EGFP). Plasmids codifying for tdTomato-PKP2 and tdTomato-R735X proteins (N-terminal tdTomato) were generated by substitution of the *EGFP* sequence for the *tdTomato* sequence, kindly provided for Dr. Joan Insern (CNIC).

*Piggy*Bac constructs

To generate stable cell lines, both *PKP2* and *R735X* genes were cloned into a *piggy*Bac (PB) vector. Both PB vector and PB transposase vector were kindly provided by Dr. Allan Bradley (Sanger Institute).

All the plasmids were cloned and propagated in the Stbl3 E. coli strain (Invitrogen, C737303).

2. Molecular biology

Western Blot

25 µg of proteins were mix with loading buffer (60 mM Tris-Cl pH 6.8, 2% SDS, 10% glycerol, 5% β-mercaptoethanol, 0.01% bromophenol blue) and boiled at 95ºC during 10 min. Boiled proteins were loaded in home-made 6% acrylamide mini (8.6 x 6.7 cm) SDS-PAGE gel, together with molecular weight markers. Gels were run at 30mA in running buffer (25mM Tris, 190mM

Glycine, 0.1%SDS). When resolving smaller proteins was needed, Novex™ NuPAGE™ 4-12% Bis-Tris Protein Gels (Invitrogen, 10472322) were used. These gels were run on ice at 80V. Proteins were transferred from the gel to a PVDF membrane (Membrana Immobilon-P, 0,45 µm, Merck, IPVH00010) in a transfer tank filled with transfer buffer (50mM Tris, 380mM Glycine, 10% methanol) at 30V during 16h at 4ºC.

Nonspecific binding sites were blocked with 5% BSA-TBST buffer during 1 hour at room temperature in agitation and subsequently, incubated overnight with primary antibodies (Table 2) diluted in 1% BSA-TBST buffer in agitation at 4ºC. Membranes were washed with TBST buffer and incubated for 1 hour with secondary antibodies (Table 2) diluted in 1% BSA-TBST buffer in agitation at room temperature. Membranes were washed again and we proceeded to analyze them either using the Odyssey imaging system (Li-Cor) for secondary antibodies conjugated to a fluorophore or using Amersham ECL Western Blotting Detection Reagent (GE Healthcare, RPN2209) for secondary antibodies conjugated to a HRP (horseradish peroxidase). Densities of proteins were measured using Image J software.

Antibody	Reference	Source	Dilution
$Na_V1.5$	Alomone, ASC-005	Rabbit	1:1000
PKP2	Everest Biotech, EB10841	Goat	1:1000
GAPDH	Santa Cruz Biotechnology, sc-32233	Mouse	1:1000
N-Cadherin	Santa Cruz Biotechnology,	Mouse	1:1000
Na^+/K^+ ATPase	Abcam, ab7671	Mouse	1:1000
Anti-Mouse Immunoglobulins/HRP	Dako, P0447	Goat	1:5000
Anti-Rabbit Immunoglobulins/HRP	Dako, P0448	Goat	1:5000
Anti-Goat Immunoglobulins/HRP	Dako, P0449	Rabbit	1:5000
Alexa Fluor 680 Anti-Mouse IgG (H+L)	Invitrogen, A-21158	Goat	1:5000
Alexa Fluor 680 Anti-Rabbit IgG (H+L)	Invitrogen, A-21109	Goat	1:5000

Table 2. Primary and secondary antibodies used for Western Blot.

Total protein extraction

Cells were washed twice with PBS and resuspended in total protein extraction buffer (10% SDS, 0,2M Tris pH6,8) supplemented with Protease Inhibitor Cocktail (Merck, 535140). Total protein was extracted by constant agitation at 4ºC during 30 minutes. To remove cell debris, samples were centrifuged at 16000xg during 15 minutes and the pellet was discarded. Proteins were quantified using the colorimetric assay DC Protein Assay (Biorad, 5000111).

Total membrane protein extraction

To purify integral membrane proteins and membrane-associated proteins, we used the kit Mem-PERTM Plus Kit (Thermo Scientific, 89842Y). One p100 plate of HEK293T cells at 70% of confluence was co-transfected with *pEGFP-$Na_V1.5$*, and *pEGFP-PKP2* or *pEGFP-R735X*. After 48 hours of transfection, cells were collected with a scraper and washed with 3mL of Cell Wash Solution buffer. Cells were resuspended in 0.75mL of Permeabilization buffer and incubated 10 minutes at 4°C with constant mixing. Permeabilized cells were centrifuged for 15 minutes at 16,000×g. Pellet was resuspended in 0.5mL of Solubilization Buffer and incubated at 4°C for 30 minutes with constant mixing. Samples were centrifuged at 16,000×g for 15 minutes. Supernatant containing solubilized membrane and membrane-associated proteins was saved for later analysis by Western Blot.

Plasma membrane protein extraction

To separate plasma membrane proteins from the rest of cell proteins, we used the kit Plasma Membrane Protein Extraction Kit (abcam, ab65400). Six p150 plates of HEK293T cells at 70% of confluence were co-transfected with *pEGFP-$Na_V1.5$*, and *pEGFP-PKP2* or *pEGFP-R735X*. After 48 hours of transfection, cells were washed with ice-cold PBS, collected with a scraper and washed again with ice-cold PBS. Cells were resuspended in 2ml of Homogenize Buffer supplemented with Protease Inhibitor Cocktail and homogenized using a Dounce homogenizer 50 times on ice. Cytosolic and plasma membrane proteins were obtained from different density gradient centrifugations. Cell protein fractions (cytosolic and plasma membrane proteins) were analyzed by Western Blot.

Cell surface biotinylation assay

To isolate plasma membrane proteins, HL-1 cells were labeled with EZ-Link™ Sulfo-NHS-SS-Biotin (Thermo Scientific, 21331). This is a biotinylation reagent that reacts with primary amines ($-NH_2$) of the proteins present in the cell surface, since it is a reagent negatively charged and is not able to penetrate the plasma membrane. Cells were plated at 80% of confluence in supplemented Claycomb medium. Cells were washed twice with ice-cold PBS pH8.0 and incubated with diluted EZ-Link™ Sulfo-NHS-SS-Biotin (0,5mg/ml) in ice-cold PBS pH8.0 during 1 hour at 4ºC in agitation. Cells were washed twice with PBS pH8.0. To quench the rest of reactive

biotin, cells were incubated with Glycine 100mM (nzytech, MB01401) during 10 minutes at 4ºC in agitation. Cells were washed twice with PBS pH8.0 and lysated using a protein extraction buffer (25mM Tris HCl pH7.5, 150mM NaCl, 1mM EDTA, 1% Triton X-100).

Proteins were quantified, and 300ug of protein were incubated with 180µl of Pierce™ Streptavidin Magnetic Beads (Thermo Scientific, 88816) overnight at 4ºC in agitation. Before the incubation, magnetic beads were washed 3 times with protein extraction buffer. After overnight incubation, magnetics beads were pulled down with a DynaMag™-2 Magnet (Invitrogen, 12321D), supernatant was collected and saved for analysis, and beads were washed 3 times with protein extraction buffer. Proteins labeled with EZ-Link™ Sulfo-NHS-SS-Biotin were separated from the Streptavidin Magnetic Beads by incubating the complex with a 10% SDS buffer (10% SDS, 0,2M Tris pH6,8) at 60ºC during 1 hour in agitation. Precipitated proteins were analysed by Western Blot. In this case, proteins were mix with a loading buffer that do not contain β-mercaptoethanol and they were not boiled before loading the proteins in the acrylamide gel to avoid cleavage of the link between proteins and biotin.

Genomic DNA extraction, RNA extraction and PCR

Genomic DNA extraction: cells were lysate with 400µl of buffer lysis (0.1 M TrisHCl pH8.5, 5m EDTA, 0.2%SDS, 200mM NaCl) supplemented with proteinase K (100µg/ml) and incubated overnight at 37ºC. DNA was precipitated with 2-propanol/sodium acetate and etanol 70%.

RNA extraction and cDNA synthesis: RNA was extracted with the kit Direct-zol™RNAMiniPrep kit (Zymo, R2051) and reverse transcription was performed with the kit High-Capacity cDNA Reverse Transcription (ThermoFisher, 4368814).

PCR was performed by following the protocol of AccuPrime™ Pfx DNA Polymerase (ThermoFisher, 12344024). Primers are enlisted in table 3.

Primers	Sequence	Length
PKP2-F	AACCTCACGGCCGGAAGTGGACCAATGCCGACATC	PKP2-652pb
PKP2-R	GGTTGTGCCGCCTTTGCAGGTGTATCTTATACACG	R735X-209pb
Neo-F	AGGATCTCCTGTCATCTCACCTTGCTCGTG	485 bp
Neo-R	AAGAACTCGTCAAGAAGGCGATAGAAGGCG	
hc-Myc-F	CGCCCAGCGAGGATATCTGGAAG	224 bp
hc-Myc-R	CCGGGTCGCAGATGAAACTCTGG	
hKlf4-F	AGATCGTTGAACTCCTCGGTCTC	251 bp
hKlf4-R	ATCTTTCTCCACGTTCGCGTCTG	
h0ct4- F	CGGGACACCTGGCTTCGGATTTC	284 bp
h0ct4-R	CCTCAGGCTGAGAGGTCTCCAAG	
hSox2-F	AGATGCAGCCCATGCACCGCTAC	207 bp
hSox2-R	CTGGAGTGGGAGGAAGAGGTAAC	
SV-F	GGATCACTAGGTGATATCGAGC	181pb
SV-R	ACCAGACAAGAGTTTAAGAGATATGTATC	

Table 3. List of primers used to study the expression of pluripotency markers to genotype hiPSCs.

3. Cell culture

HEK293T cell line culture and transfection

HEK293T cell line is a cell line derived from human embryonic kidney cells. HEK293T cells were maintained in DMEM medium supplemented with 10% fetal bovine serum (FBS), 4mM L-glutamine and 1% penicillin-streptomycin. Cells were maintained as a monolayer and passaged twice a week when reached 90-100% of confluence. Plates were kept in an incubator at 37ºC, 5% CO_2.

HEK293T cells were transitory transfected with PEI 25K (Polyethylenimine, Linear, MW 25000, Transfection Grade, Polysciences, 23966-1). Cells were plated at 70% of confluence in supplemented DMEM medium, and they were incubated overnight with a mix of DNA and PEI in a ratio 1:3 (w/v).

HL-1 cell line culture and transfection

HL-1 cell line is a cardiac muscle cell line, derived from the AT-1 mouse atrial cardiomyocyte tumor lineage. These cells maintain the ability to contract and retain differentiated cardiac morphological, biochemical, and electrophysiological properties. HL-1 cells were cultured in Claycomb medium supplemented with 100µM norepinephrine, 10% FBS, 4mM L-glutamine and

1% penicillin-streptomycin and plated in 0.02% gelatin/fibronectin (Sigma Aldrich)-coated plates. HL-1 cells were maintained as a monolayer and passaged every other day when reached the 90-100% of confluence. Plates were kept in an incubator at 37ºC, 5% CO_2.

To achieve a 30-40% of HL-1 cells transfected, we optimized the protocol for the transfection reagent jetPRIME® (Polyplus transfection, 114-07). Cells were plated at 70% of confluence in supplemented Claycomb medium, and they were incubated overnight with a mix of DNA, JetPRIME® and jetPRIME® buffer. The optimized ratio DNA-jetPRIME® was 1:3 (w/v).

HL-1 stable cell lines

To generate HL-1 cell lines stables for the expression a gene of interest, we used the *piggy*Bac (PB) transposon system. This technology allows the efficient insertion of a DNA sequence into a host genome in a one-step transfection. Cells were transfected with JetPRIME® and a mix of DNA containing the constructs *pPB-CAG-PKP2-PGK-Neomycin-PB* or *pPB-CAG-PKP2-PGK-Neomycin-PB*, and *pCMV-Transposase* in a ratio of 1:5 (w/w). PB transposase will mediate the integration of the PB cassette into the genome. Forty-eight hours after transfection, we started the selection of the stably transfected cells by adding 300ng/µl G418 (Neomycin, Merck, G8168) to the culture media. Cells were treated with G418 during at least 10 days (Figure 8).

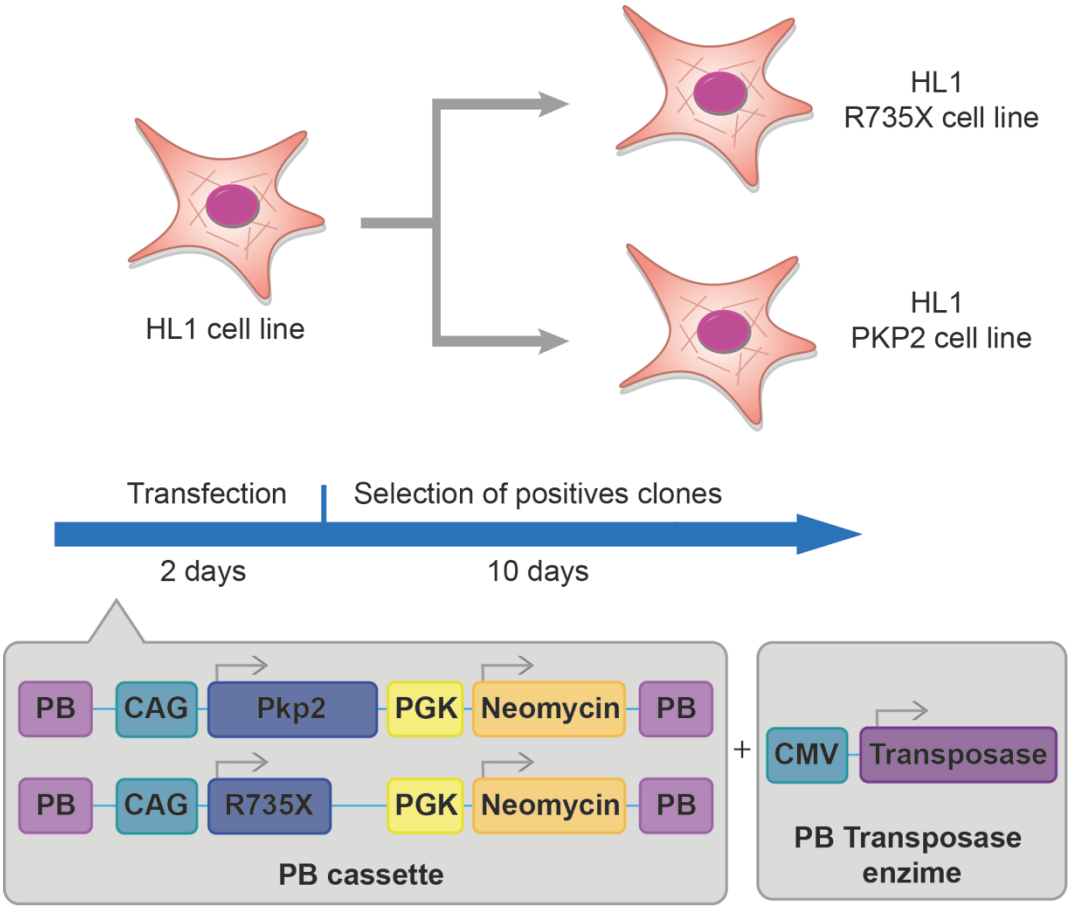

Figure 8. Generation of HL-1 stable cell line. HL-1 cells were co-transfected with the constructs *pPB-CAG-PKP2-PGK-Neomycin-PB* or *pPB-CAG-PKP2-PGK-Neomycin-PB*, and *pCMV-Transposase*. *CMV* (human cytomegalovirus promoter). *CAG* (CMV enhancer fused to the chicken beta-actin promoter). *Neomycin* (Neomycin resistance gene). *Transposase* (Transposase gene). Positives cells were selected with Neomycin treatment during 10 days. R735X HL-1 and its isogenic control (PKP2 HL-1) were characterized.

4. hiPSCs and hiPSC-CM culture

Human dermal fibroblast reprogramming

hiPSCs were generated from human dermal fibroblasts (HDFa, ScienCell Research Laboratory cat # 2320 , before #2310). HDFa were reprogrammed using the non integrative method CytoTune iPS 2.0 Sendai Reprogramming Kit (Invitrogen, A16517). HDF were trasduced with CytoTune™ 2.0 Sendai reprogramming vectors codifying for the reprogramin factors: hOct3/4, hSox2, hKlf4 and hc-Myc.

Twenty-four hours after transduction, fibroblast medium was refreshed. Cells were cultured during 6 days with media changes every other day. Seven days after transduction, fibroblast cells

were transferred to MEF coated culture dishes. Twenty-four hours later, fibroblast media was change to iPSC medium. During the next days, cells were monitored under a microscope for the emergence of cell clumps indicative of reprogrammed cells. 3-4 weeks after transfection, colonies were manually picked and transfered onto MEF plates. hiPS clones were expanded and tested for pluripotency and stemness.

hiPSCs culture

Human induced pluripotent stem cells (hiPSCs) were cultured using the commercial culture media StemMACS iPS-Brew XF (Miltenyi Biotec). hiPSCs were maintained as colonies and passaged every 7 days on plastic plates coated with matrigel (500 µg/mL; BD Biosciences). Every day, the cells that differentiate spontaneously were marked and removed manually before the media change. Plates were kept in an incubator at 37ºC, 5% CO_2.

hiPSCs stably transfected cell lines

hiPSCs were cultured in StemMACS iPS-Brew XF supplemented with 10 µM Rock Inhibitor for 24 hours. Cells were washed with HBSS (Hank's Balanced Salt Solution, Gibco, 14025092) and treated with Acutase for 5 minutes at 37ºC. Single cells were transferred to a 15ml conical tube and centrifuged at 1000rpm during 5 minutes. Approximately 10^6 cells were resuspended in the transfection mix (82µl of P3, 18µl of supplement, 1µg of PB cassette vector and 250µg of PB transposase plasmid) and transferred to a cubete. Cells were electroporated with 4D-Nucleofector System (Lonza) using the program H9. Cells were re-plated in a p100 with StemMACS iPS-Brew XF supplemented with 10 µM Rock Inhibitor. Forty-eight hours after transfection, we started the selection of the stably transfected cells by adding 50µg/ml G418 (Neomycin, Merck, G8168) to the culture media. Cells were treated with G418 during at least 10 days. After that, independent colonies were picked and transferred to separate wells to establish different clonal cell lines.

Cardiac differentiation protocol

Cardiac differentiation was achieved using a protocol based in small molecules, commonly known as the GiWi protocol (Lian et al., 2012)(Lian et al., 2013). hiPSCs were separated with Versene Solution (EDTA 48 mM in PBS, Gibco, LS15040066), plated in monolayers in 6 well plates (1×10^6 hiPSCs/ well aprox.) and maintained in StemMACS iPS-Brew XF (Miltenyi Biotech, 130-

104-368) culture media during 1 or 2 days until the cells cover completely the well surface (90-100% of confluence). On day 0 of the protocol, hiPSCs monolayers were washed with HBSS (Hank's Balanced Salt Solution, Gibco) and cultured in RPMI media supplemented with B27 without insulin (RPMI/B27-insulin, Life Technologies, A1895601) and the glycogen synthase kinase-3 inhibitor, CHIR99021 (12 µM, Miltenyi Biotec, 130-103-926). After 24 hours, CHIR99021 was removed and fresh RPMI/B27-insulin was added. On day 3, we added a mix composed of half of the volume of used media and half of fresh media (RPMI/B27-insulin) and the inhibitor of Wnt production-4, IWP4 (5 µM, Stemgent, 686772-17-8). On day 5, IWP4 was removed and fresh RPMI/B27-insulin was added. On day 7, cells were cultured in RPMI/B27+insulin (Life Technologies, A3582801). On day 8, we could start seeing some cells beating as a signal of success in the cardiac differentiation process. Human induced pluripotent stem cells derived cardiomyocytes (hiPSC-CMs) were cultured in RPMI/B27+insulin during 30 days with media changes every two days.

Purification of hiPSC-CM

The cardiac differentiation protocol is not 100% efficient and not all the cells differentiate into cardiomyocytes, obtaining mixed cultures. At day 30 of differentiation, cells were trypsinized and incubated with a cocktail of antibodies that recognize epitopes of non-cardiomyocytes cells (Miltenyi Biotec, PSC-derived cardiomyocyte isolation kit-human, 130-110-188). Then, these cells were incubated with a secondary antibody conjugated with magnetic beads. Magnetically labeled cells were retained in LS columns (Miltenyi Biotec, 130-042-401) inserted into a magnetic field. LS columns matrix is composed by ferromagnetic spheres, which amplifies the magnetic field. This magnetic-activated cell sorting targets and depletes non-cardiomyocytes from the whole cell population, enriching the sample in cardiomyocytes up to 98%.

Maturation of hiPSC-CM

Purified hiPSC-CMs were plated in wells covered with PDMS (transparent sheets of vulcanized silicon of polydimethylsiloxane) that improves the maturation of these cells. PDMS sheets were 40D, (D, Durometer o ≈1000 kPa) and obtained from Specialty Manufacturing, Inc. 15 mm diameter PDMS coverslips were cut manually and placed in 24 well plates. Each plate was sterilized using ethylene oxide. To promote cell adhesion, PDMS coverslips were coated with matrigel 1hour prior to plate cells. hiPSC-CM were maintained in culture on matrigel-PDMS coated plates during 7 days, with RPMI/B27 + insulin before any experiment.

PDMS micropatterns

PDMS stamps are printed with a micropattern composed by lines of a single cell size and squares where small monolayers (around 100 cells) can be seeded. These small monolayers will be around the single cells and will support their survival. PDMS stamps were cleaned with scotch tape followed by sonication in 70% ethanol for 20 minutes. In the hood, they were air dried and incubated with 250µl matrigel diluted in water (100 µg/mL) at room temperature for 1hour. After that, the matrigel solution from the PDMS stamps was aspirated.

In parallel, 18 mm PDMS circles were sonicated in 70% ethanol for 20 minutes and transferred, under the hood, to a 6-well plate where ethanol was air dried. The culture dish was UVO treated for 10 minutes. Before the re-plating of the cells, plates were cleaned with Penicilin-Streptomicin antibiotic for 1 hour and exposed to UV light during 15 minutes. Once PDMS stamp and PDMS circles were ready, dried stamps were inverted onto each PDMS circle and removed one by one after ~2 minutes. The micropatterned PDMS plates were incubated with pluronic-F27 overnight at room temperature.

Single cell re-plating

hiPSC-CMs monolayers that have been plated 7 days on PDMS were dissociated by using trypsin 0,025% with EDTA for 8-10 minutes. Dissociation was stopped by adding RPMI/B27+insulin supplemented with 10% FBS. Cells were filtered using a 70µm filter to removed non-dissociated cells and were centrifuged at 700 RPM for 3 min. Then, cells were resuspended in warm re-plating media (RPMI/B27+insulin with 2% FBS and 5µM of rock inhibitor). Approximately, 60K cells resuspended in 350µL of media were placed in the center of the micropatterned area. After 5 hours, 2ml of re-plating media was added very gently. Media change was performed at day 1 and 3 after re-plating the cells. Cells must be on micropatterns (Figure 9) at least 4 days before patch-clamping experiments.

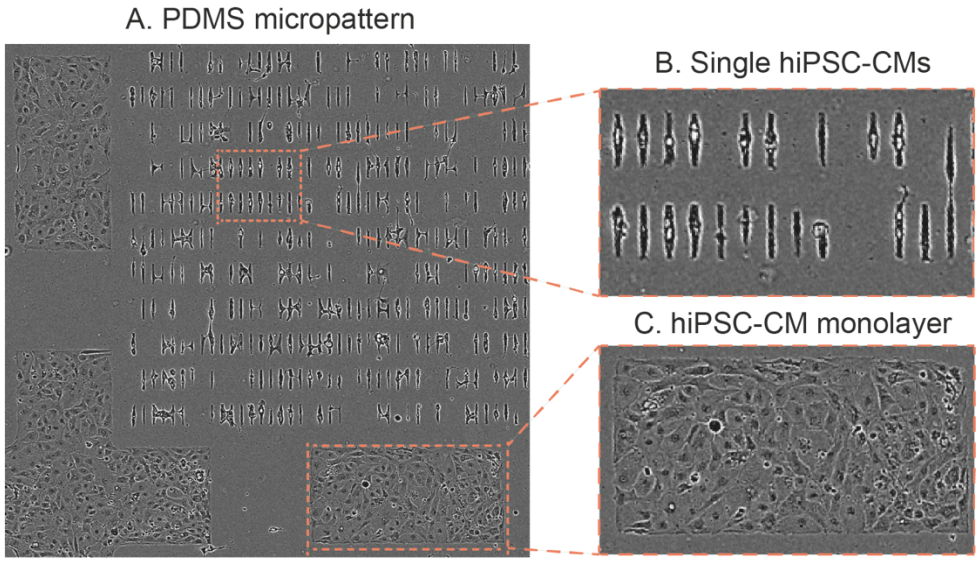

Figure 9. hiPSC-CMs plated on a PDMS micropattern. A. hiPSC-CMs are plated in PDMS microppatterns as single cells. Small monolayers of hiPSC-CM are plated surrounding single hiPSC-CMs to improve single cell survival. Image obtained under bright field microscope, objective 40x. B. Digital magnification of single hiPSC-CMs. C. Digital magnification of small hiPSC-CM monolayers.

5. Electrophysiology

Patch-clamp recordings in hiPSC-CM

Standard patch-clamp recording techniques were used to measure I_{Na}, I_{Ca}, and I_{K1}. All the experiments were performed at room temperature (22°C–25°C).

Voltage clamp experiments were controlled and analyzed with an Multiclamp 700B amplifier and pClamp 10.2/Digidata 1440A acquisition system (Molecular Devices, Sunnyvale, CA, USA) and OriginPro9 software (OriginLab Corporation, Northampton, MA, USA). Data were filtered at 5 kHz and sampled at 5–20 kHz. Activation curve data were fitted to a Boltzmann equation, of the form g = gmax / (1 + exp(V1/2 − Vm)/k), where g is the conductance, gmax the maximum conductance, Vm is the membrane potential, V1/2 is the voltage at which half of the channels are activated and k is the slope factor.

Pipettes were formed from aluminosilicate glass (AF150-100-10; Science Products, Hofheim, Germany) with a P-97 horizontal puller (Sutter Instruments, Novato, CA), and had resistances between 2 and 3 MΩ for patch-clamp experiments when filled with the respective pipette solutions (see below).

For I_{Na}, a pulse protocol from -80 mV to +55 mV with a holding potential of -160 mV was used. Recordings were made in a bath solution that consisted of 10 mM NaCl, 1 mM $MgCl_2$, 0.1 mM $CdCl_2$, 20mM HEPES, 11 mM Glucose, 60 mM CsCl, and 72.5 mM Choline chloride, pH = 7.35 adjusted with CsOH. The pipette solution contained 60 mM CsF, 5 mM NaCl, 10 mM EGTA, 5 mM HEPES, 5 mM MgATP, and 75 mM Choline chloride, pH = 7.2 adjusted with CsOH. Chemicals were purchased from Sigma.

I_{K1} was elicited from a holding potential of -50 mV by 500-ms steps from -120 to +40 mV. The external recording solution contained 148 mM NaCl, 0.4 NaH_2PO4, 1 mM $MgCL_2$, 5.5 mM Glucose, 1.8 mM $CaCl_2$, 5.4 mM KCl, 15 mM Hepes, and 5 µM Nifedipine pH = 7.4 adjusted with NaOH. 1 mM BaCl2 was used to isolate IK1 from other background currents (subtract solution). The internal solution contained 1 mM $MgCL_2$, 5 mM EGTA, 140 mM KCl, 5 mM HEPES, 5 mM Phosphocreatine, 4.4 mM K_2ATP, and 2 mM -Hydroxybutyric acid, pH = 7.2 adjusted with KOH.

I_{Ca} was evoked applying a voltage-step protocol from -40 mV to +80 mV with a holding potential of -50 mV. The cells were bathed in 137 mM TEA-Cl, 5.4 mM CsCl, 1 mM $MgCl_2$, 1.8 mM $CaCl_2$, 4 mM Aminipyridine, 10 mM HEPES, 30 M TTX, and 11 mM Glucose, pH=7.4 adjusted with CsOH. The pipette solution contained 20 mM TEA-Cl, 120 mM CsCl, 1 mM $MgCl_2 \cdot 6H_2O$, 5.2 mM Mg-ATP, 10 mM HEPES, 10 mM EGTA, pH=7.2 adjusted with CsOH.

Data analysis was performed using Clampfit 10.2 (Axon Instruments), a custom-made software (for AP), OriginPro 9, and GraphPad Prism 7.01 (San Diego, USA) software.

Optical mapping of hiPSC-CM monolayers

hiPSC-CM were plated on PDMS-matrigel coated wells in 2D monolayers during 1 week ($2*10^5$ cells / p24 well). hiPSC-CM monolayers were loaded with FluoVolt (F10488, Life Technologies), a voltage sensitive fluorescent probe that responds to changes in membrane potential. After 30 minutes of incubation, cells were washed with HBSS. Cells were positioned on a heating block to keep them at physiological temperature (37 °C) and below a high speed CCD camera (200 fps, 80 × 80 pixels). Blue LED illumination with the CCD camera via appropriate emission filter (515 nm, green light, Chroma) was used to record spontaneous or electrically paced action potentials. Electrical pacing was done using a custom made frame of point stimulation electrodes to enable electrical pacing of 6 x 6 array of wells. Recorded data was analyzed using Scroll, custom software developed by Dr Jalife's laboratory, University of Michigan, Ann Arbor

(USA). Scroll allowed us to calculate action potential duration at different percentage of repolarization and conduction velocity of the electrical impulse.

6. Immunofluorescence

hiPSC-CMs were washed with PBS and then fixed with 3% paraformaldehyde for 10 minutes and rinsed twice before adding blocking-permeabilization solution (10% normal donkey serum, 0.1% Triton X-100 in PBS) for 40 minutes at room temperature. Primary antibodies (Table 4) were diluted in 5% normal donkey and 0.05% Triton X-100 in PBS and incubated overnight at 4ºC. Subsequently, cells were washed three times with 10% normal donkey and 0.1% Triton X-100 in PBS. The secondary antibodies (Table 4), diluted in the same solution as the primary antibodies, were applied to cells and incubated at room temperature in the dark for 2 hours. After incubation, cells were washed three times with 10% normal donkey and 0.1% Triton X-100 in PBS and once with PBS only. Then, the nuclei were stained with DAPI (1:1000, Invitrogen) for 10 minutes in the dark at room temperature. Coverslips were mounted on slides for confocal imaging. Slides were analyzed under a Confocal System Nikon A1R coupled to an Eclipse Ti microscope (Nikon Corp., Japan) using a Plan Apo VC 60x/1,4 Oil objective, with the command of NIS Elements AR 4.30.02. Build 1053 LO software.

Antibody	Reference	Source	Dilution
α-actinin	Sigma, A7732	Mouse	1:400
SMA-Cy3	Sigma, C6198	Mouse	1:400
AFP	Dako, GA500	Rabbit	1:400
Tuj1	Covance	Mouse	1:100
GFAP	Dako, GA524	Rabbit	1:400
Alexa Fluor 488 Anti-Mouse IgG (H+L)	Invitrogen, A-11001	Goat	1:400
Alexa Fluor 488 Anti-Rabbit IgG (H+L)	Invitrogen, A-21109	Goat	1:400
Alexa Fluor 562 Anti-Rabbit IgG (H+L)	Invitrogen, A-21109	Goat	1:400

Table 4. Primary and secondary antibodies used for Immunofluorescence.

7. Confocal live imaging

For all the experiments involving confocal live imaging, HL-1 cells were plated in p35 glass-bottomed plates (MatTek, P35G-1.5-14-C). Before imaging, growth media was replaced with phenol-red free medium (Leibovitz's L-15 Medium, no phenol red, 21083027).

For EGFP-PKP2 and tdTomato-PKP2 imaging, HL-1 were transfected 24h before the experiment. Confocal live imaging was performed using a Confocal System Nikon A1R coupled to an Eclipse Ti microscope (Nikon Corp., Japan) using a Plan Apo VC 60x/1,4 Oil objective. Microscope was equipped with an incubator chamber to provide controlled temperature (37°C) and humidity, all under the command of NIS Elements AR 4.30.02. Build 1053 LO software. Images were acquired as a z-stack with step size of 0.2 µm to give a total of 75 slices. Images were saved as ND2 files and maximum intensity projection images were obtained from the z-stacks. Image processing was performed using Image J software.

For EGFP-$Na_V1.5$ imaging, HL-1 were transfected 48h before the experiment. Confocal live imaging was performed using a Confocal TCS Leica SP8 coupled to a DMi8 microscope (Leica Microsystems GmbH, Germany) using a HC PL Apo CS2 63x/1.4 OIL objective. Microscope was equipped with an incubator chamber to provide controlled temperature (37°C) and humidity, all under the command of LAS X 3.1.1. 15751 software. Images were acquired as a z-stack with step size of 0.17 µm to give a total of 8 slices. Pixel size was set following Nyquist sampling theorem to apply deconvolution on the acquired images later on.

Deconvolution

Deconvolution process is a combination of optical and computational techniques aimed to increase resolution, gain a better contrast and improved signal-to-noise ratio when imaging a biological specimen. Optical microscopes have inherent limitations that cause out-of-focus light, forming images that are not a true representation of the biological specimen. Deconvolution uses mathematical models to predict the distribution of this out-of-focus light and apply computer algorithms to compensate it (Biggs, 2010).

The quality of EGFP-$Na_V1.5$ images was low and deconvolution process was needed to improve the resolution and the signal-to-noise ratio. Images were deconvolved with Huygens Software (Scientific Volume Imaging B.V., The Netherlands), using the GMLE algorithm, with SNR:5 and 10 iterations. After deconvolution, images were analyzed by measuring the intensity of the plasma membrane and the cytoplasm. To do so, we drew regions of interest (ROIs) defining the plasma membrane and the cytoplasm, and excluding the nucleus and big vacuoles on each cell. Then, we calculated the ratio plasma membrane/cytoplasm intensity as a way to normalize the intensity of the plasma membrane with the level of transfection on each cell.

To study the co-localization of EGFP-$Na_V1.5$ and tdTomato-PKP2 we performed the same decolvolution process described above. Using the Huygens Software, we drew a 3 µm lines on the plasma membrane area and analyzed profiles of intensity on both EGFP and tdTomato signal. We identified peaks matching with the plasma membrane and we measured the distance between EGFP and tdTomato peaks as an indirect way to study the co-localization of $Na_V1.5$ and PKP2 proteins in HL-1 cells.

Fluoresce recovery after photobleaching (FRAP)

FRAP experiment was performed on a Confocal System Nikon A1R coupled to an Eclipse Ti microscope (Nikon Corp., Japan) using a Plan Apo VC 60x/1,4 Oil objective. Microscope was equipped with an incubator chamber to provide controlled temperature (37°C) and humidity, all under the command of NIS Elements AR 4.30.02. Build 1053 LO software.

In cells transfected with EGFP-Nav1.5, EGFP was bleached by radiating a circular region of interest (ROI) of 1,5 µm of diameter, using 488mn laser at 100% of power during 4 s (one lighting iteration). Pinhole was set to 35µm. In cells transfected with EGFP-PKP2/R735X, EGFP was bleached by radiating a circular regions of interest (ROIs) of 1,5 µm of diameter, using 488mn laser at 100% of power during 7,77 s (four lighting iterations). For prebleach and postbleach periods, images were captured every 2 s and laser power was kept to 15%.

In both cases, postbleaching captures continued for 120 seconds. Data were normalized to the initial fluorescence intensity (value=1) and to after bleaching intesity (value=0), after background subtraction. Half-time of recovery ($T_{1/2}$) and mobile fraction (MF) were calculated with nonlinear regression software, GraphPad, using the one-phase association equation.

8. Statistics

Statistical analyses were performed with GraphPad Prism 7. Data are presented as means ± s.e.m (standar error of the mean) or means ± s.d (standar deviation) as indicated. Differences were considered statistically significant at p-value < 0.05. In each figure p-value is represented as follows: *p<0.05, **p<0.01, ***p<0.001, ****p<0.0001 y ns p>0.05. Test used to calculate p-value are detailed in figure legends. Student's t-test was used to compare two groups. One-way o two-way ANOVA with Tukey's or Sidak's multiple comparison post-test was used to compare several groups.

RESULTS

RESULTS

1. R735X characterization

1.1. Subcellular distribution of R735X

It has been previously shown that some PKP2 mutants fail to localize at the plasma membrane and are found in the intracellular space(Joshi-Mukherjee et al., 2008a). These results led us to question whether our truncated PKP2 protein R735X would be mislocalized. The study of the subcellular distribution of PKP2 by immunofluorescence was limited since endogenous PKP2, and both exogenous PKP2 and R735X proteins are recognized by the same antibody. Therefore, we tagged PKP2 proteins with EGFP to be able to track them by confocal microscopy. The tag was placed at the N-terminal of PKP2 proteins since it has been described that N-terminal EGFP tag does not alter PKP2 localization (Godsel et al., 2010). We transiently transfected *pEGFP-PKP2* and *pEGFP-R735X* constructs in HL-1 cells to study the subcellular distribution of PKP2 and R735X proteins in a cardiac cell context. HL-1 is a mouse cardiac muscle derived cell line that has differentiated cardiac features (morphological, biochemical, and electrophysiological) and maintains the ability to contract (Claycomb et al., 1998). We observed that EGFP-PKP2 localized mainly at the border of the cells, following a continuous linear pattern surrounding the cytoplasm and in a patchy pattern in areas where the cell was in contact with the plate. In contrast, most of the EGFP-R735X signal was found in the cytoplasm and not at cell borders (Figure 10). This would indicate that R735X is mislocalized from the inner face of the plasma membrane to the intracellular space, away from junctional complexes.

To test whether R735X might alter the localization of PKP2 protein and *vice versa*, we performed co-transfections of PKP2 and R735X in HL-1 cells. We also tagged both PKP2 and mutant R735X proteins with the fluorescent protein tdTomato and co-transfected with PKP2 or mutant counterpart tagged with the EGFP to track both proteins in the same cell by confocal microscopy. We observed that cells expressing EGFP-PKP2 and tdTomato-R735X presented a green signal at the cell membrane and a red cytoplasm. On the other hand, cells expressing tdTomato-PKP2 and EGFP-R735X showed a cell membrane stained in red and a green cytoplasm (Figure 11). Thus, data showed in figure 10 and 11 indicate that R735X fails to localize at the inner face of the plasma membrane and is mainly found at the cytoplasm, independently of the tag. It also shows that R735X does not disrupt the proper localization of PKP2.

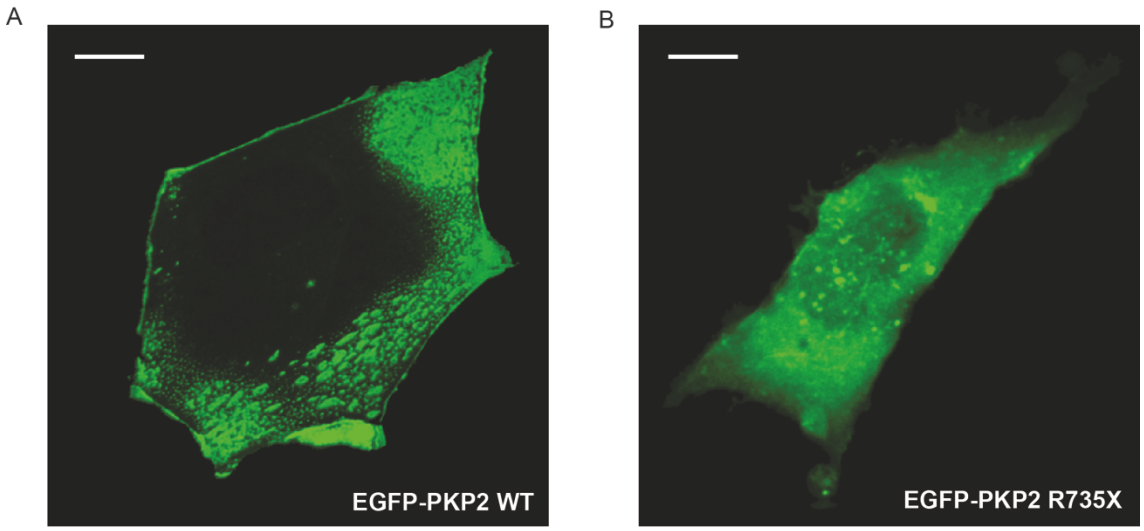

Figure 10. PKP2 C-terminal deletion alters subcellular localization. Subcellular distribution of PKP2 (*pEGFP-PKP2*) and R735X (*pEGFP-R735X*) in HL-1 cells. A. Z-stack projection of a HL-1 cell transiently expressing EGFP-PKP2. B. Z-stack projection of a HL-1 cell transiently expressing EGFP-R735X. Scale bar =10 µm.

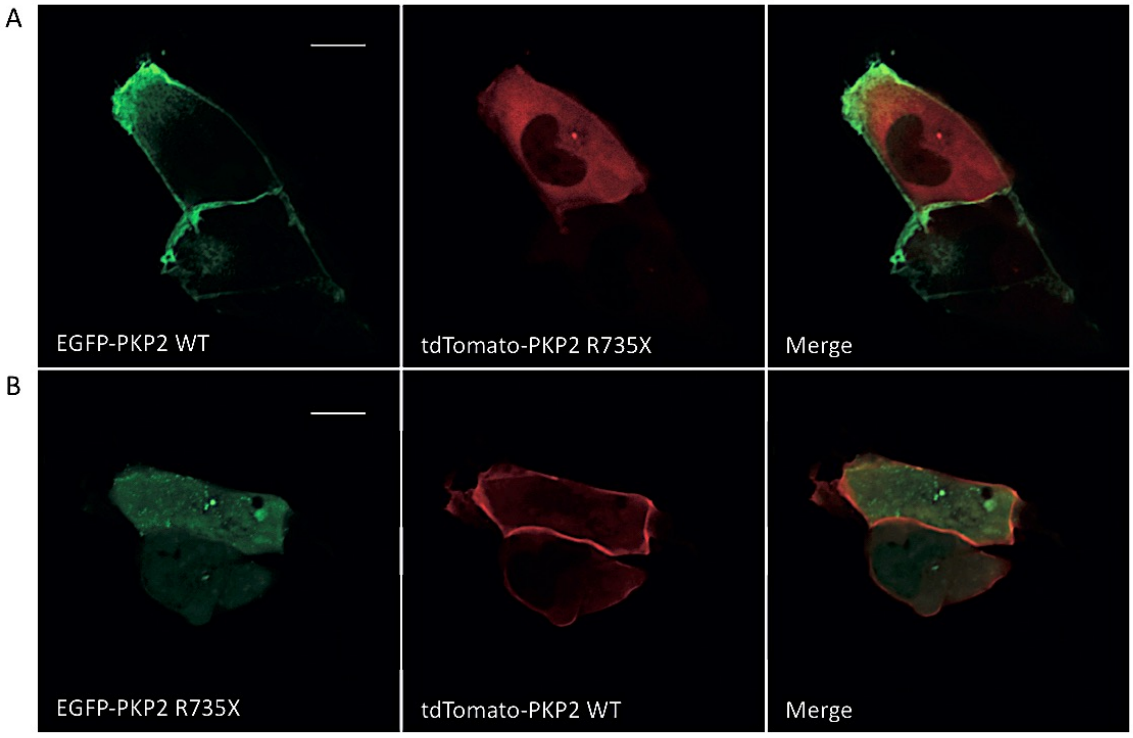

Figure 11. R735X does not alter PKP2 localization. A. Z-stacks projections of HL-1 cells co-transfected with *pEGFP-PKP2* (left panel) and *ptdTomato-R735X* (central panel). Merge showed at right panel. B. Z-stack projections of HL-1 cells co-transfected with *pEGFP-R735X* (left panel) and *ptdTomato-PKP2* (central panel). Merge showed at sight panel. Scale bar = 10 µm.

To confirm that the tag is not affecting the subcellular distribution of PKP2 proteins, we transfected HEK293T cells with *pCAG-PKP2* and *pCAG-R735X* without tags and we isolated proteins from cytoplasmic and plasma membrane fractions. The amount of PKP2 in the cytoplasmic fraction was approximately 0.6 times the amount of R735X found in the same fraction. In contrast, R735X was only detectable when overexposing the membrane (Figure 12). Subcellular fractionation in HEK293T cells corroborates the results obtained by microscopy analysis of fluorescent-tagged PKP2 proteins in HL-1 cells, indicating altogether that R735X is mislocalized from the desmosome in the inner face of the plasma membrane to the cytoplasm.

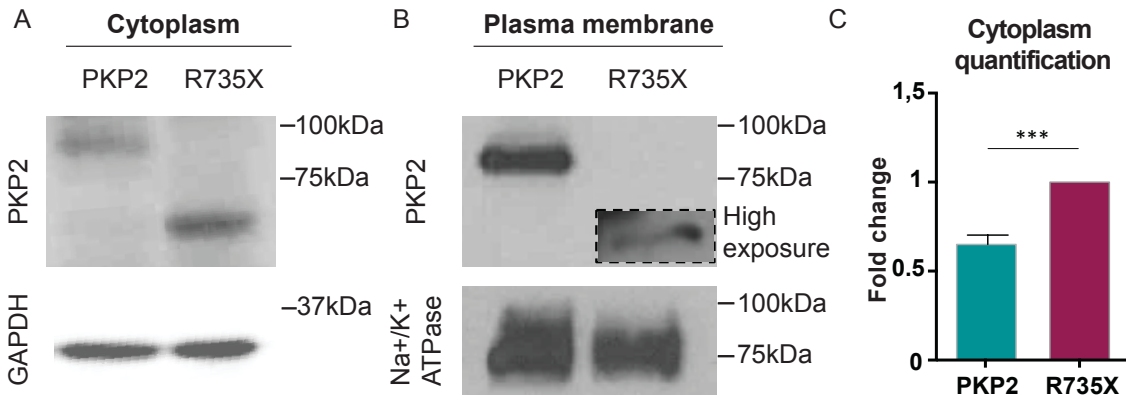

Figure 12. Subcellular fractionation of PKP2 and R735X in HEK293T cells. A. Western Blot showing PKP2 and R735X (upper panel) and GAPDH (bottom panel) in the cytoplasm fraction. B. Western Blot showing PKP2 and R735X (upper panel) and N-Cadherin (bottom panel) in the plasma membrane fraction. C. Fold change quantification of PKP2 and R735X in the cytoplasm fraction normalized to GAPDH. N=3. Data are represented as means ± s.d. ***p<0.0001 by Student's t-test.

1.2. Mobility of R735X

We have shown that the amount of R735X located at the plasma membrane is decreased in comparison with PKP2. Thus, we hypothesized that the mobility of R735X along the membrane could also be affected. To study the mobility of PKP2 proteins, we transfected HL-1 cells with *pEGFP-PKP2* and *pEGFP-R735X*, and performed a Fluorescence Recovery After Photobleaching (FRAP) experiment. After photobleaching a region of interest (ROI, diameter = 1.7 µm) at the plasma membrane with a high level of light, we measured the rate of fluorescence recovery during 120 seconds (Figure 13).

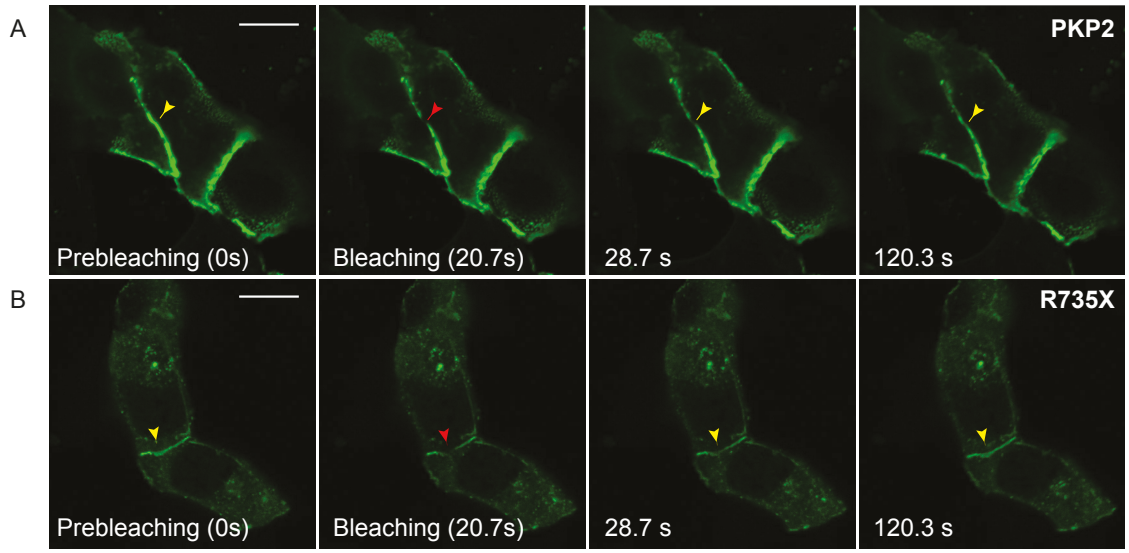

Figure 13. Representative images from FRAP experiments of EGFP-PKP2 and EGFP-R735X in HL-1 cells. A. Stills from FRAP movies of HL-1 cells transfected with *pEGFP-PKP2*. B. Stills from FRAP movies of HL-1 cells transfected with *pEGFP-R735X*. Arrows indicate region of interest ROI. White arrows indicate prebleaching ROI. Red arrows indicate bleaching ROI. Yellow arrows indicate recovery after bleaching ROI at different times. Time is indicated in each panel. Scale bar = 10 µm.

Levels of initial fluorescence in areas selected for bleaching were not significantly different between the two groups (PKP2= 937.9 ± 230.0 AU and R735X = 519.0 ± 89.33 AU) (Figure 14A). After bleaching a region of the cell-cell contact, both EGFP-PKP2 and EGFP-R735X proteins were able to recover approximately 60% of the initial fluorescence after 120 seconds (Figure 14B). This indicates that EGFP-PKP2 protein population is composed by 60% of mobile proteins (mobile fraction, MF) and 40% of immobile proteins (immobile fraction, IF). This would mean that 40% of the initial signal is coming from proteins that are stably anchored to the membrane to not be moving during the recording time. On the other hand, 60% of the initial signal is coming from proteins that are able to move during the time of measurement. Despite representing the same percentage, EGFP-PKP2 and EGFP-R735X mobile fraction showed a different recovery curve . Indeed, half-time of recovery (time necessary to achieve half of the final fluorescence, $T_{1/2}$) was 2.5 times shorter for EGFP-R735X (EGFP-PKP2 $T_{1/2}$= 24.29 ± 2.33 s and EGFP-R735X $T_{1/2}$= 9.31 ± 2.40 s) (Figure 14C). Moreover, the percentage of bleaching that we were able to achieve in the mutant was lower than in the PKP2 (PKP2= 78.95 ± 3.61% and R735X = 47.72 ± 3.56%) (Figure 14D). This would agree with the observed differences in the mobility of both proteins; the percentage of bleaching of the mutant might be masked by the rapid diffusion of the protein. Thus, FRAP results would indicate that EGFP-R735X moves 2.5 times faster along the plasma membrane than EGFP-PKP2 protein.

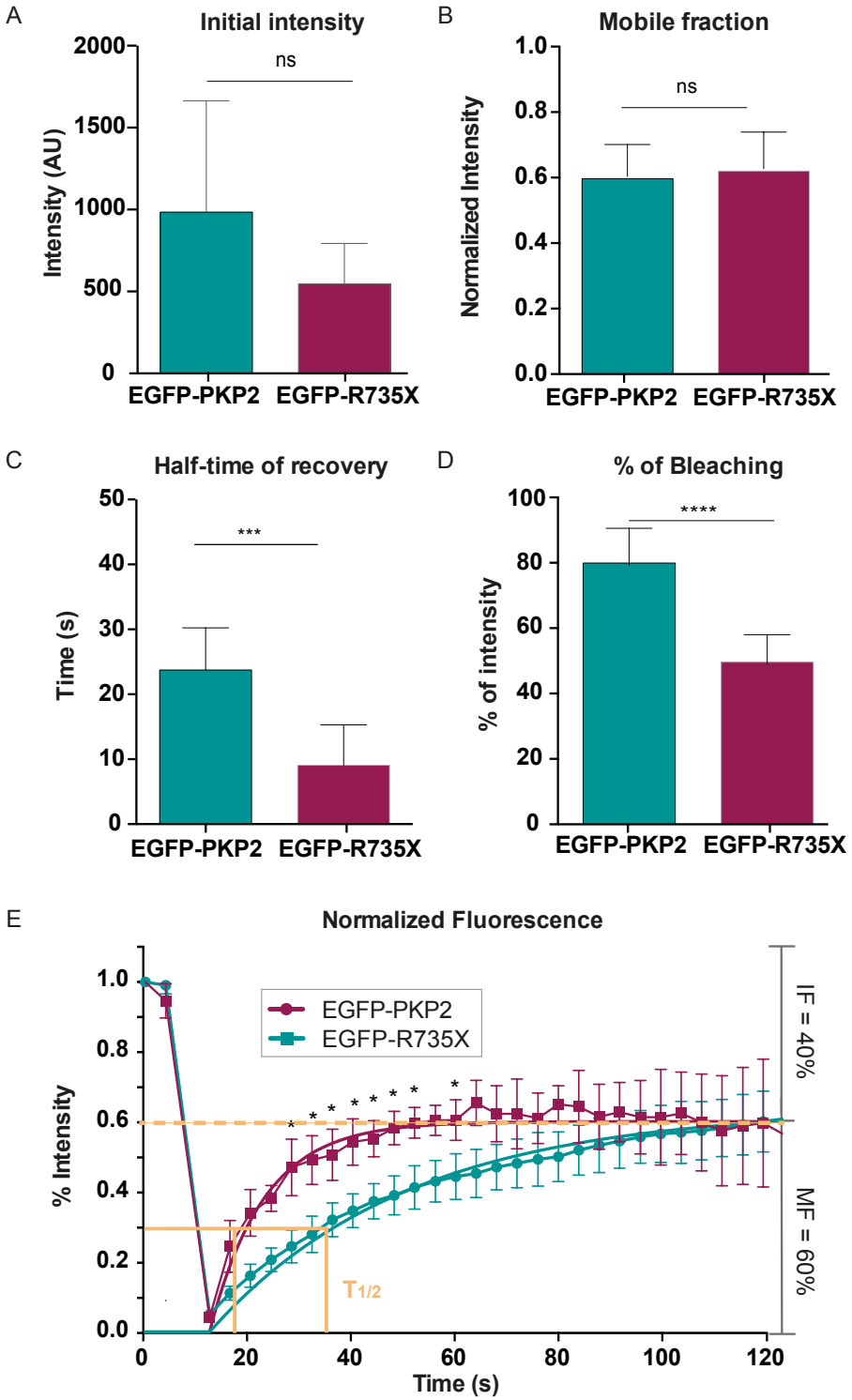

Figure 14. PKP2 C-terminal deletion alters plasma membrane mobility. FRAP of EGFP-PKP2 and EGFP-R735X in HL-1 cells. A. Intensity of the stimulation ROI at 0 seconds. ns>0.05 by Student's t-test. B. Quantification of the Mobile fraction (MF). ns>0.05 by Student's t-test. C. Quantification of the half-time of recovery after photobleaching ($T_{1/2}$). ***<0.001 by Student's t-test. D. Percentage of bleaching achieved after laser stimulation. ****p<0.0001 by Student's t-test. E. Normalized fluorescence intensity plotted (*y* axis) against time (*x* axis), fitted to a single component exponential (solid lines). Mobile fraction (MF) and Immobile fraction (IF) are delimited by orange dashed line. Half-time of recovery is indicated with solid orange lines. *p<0.01 in Time = 20.7, 24.8, 36.8, 44.9, 52.9 and 57.0 s; **p<0.0001 in Time = 32.8, 40.8, 48.9, 65.0 s; ***p<0.00001 in Time = 28.8s by two-way ANOVA. Data are represented as mean ± s.d. EGFP-PKP2 n=8 and EGFP-R735X n=7.

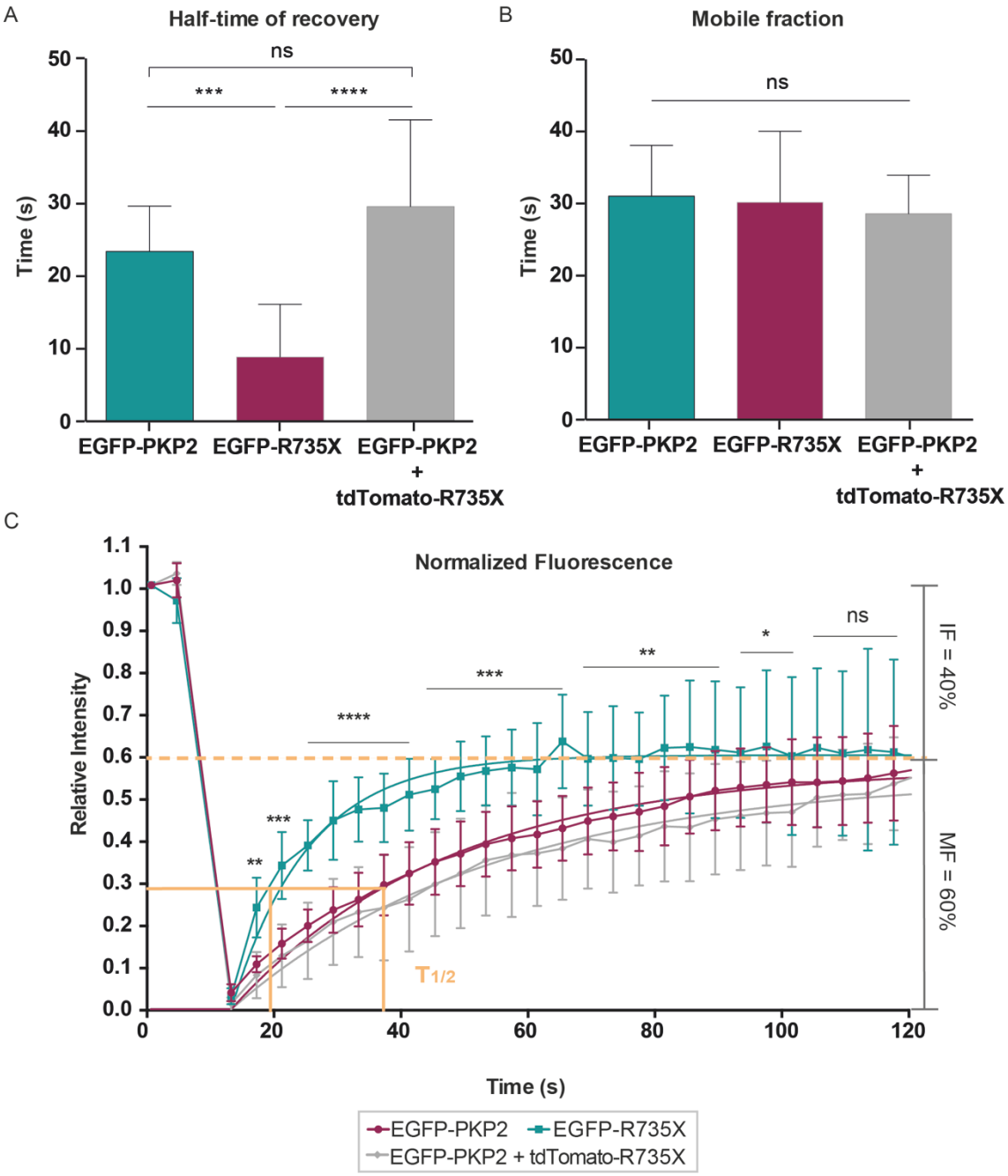

Figure 15. R735X does not alter PKP2 plasma membrane mobility. FRAP of EGFP-PKP2 in control HL-1 cells, EGFP-R735X in control HL-1 cells and EGFP-PKP2 in HL-1 cells co-transfected with tdTomato-R735X. A. Quantification of the half-time of recovery after photobleaching ($T_{1/2}$). ***p<0.001, **** p<0.0001 by one-way ANOVA. B. Quantification of the Mobile fraction (MF). ns>0.05 by one-way ANOVA. C. Normalized fluorescence intensity plotted (*y* axis) against time (*x* axis), fitted to a single component exponential (solid lines). Mobile fraction (MF) and Immobile fraction (IF) are delimited by orange dashed line. Half-time of recovery is indicated with solid orange lines. * p<0.05, **p<0.01, ***p<0.001, **** p<0.0001 by two-way ANOVA. Data are represented as means ± s.d. EGFP-PKP2 n=12, EGFP-R735X n=13 and EGFP-PKP2 + tdTomato-R735X =6.

To check if R735X might alter the mobility of PKP2, we performed FRAP on HL-1 cells co-transfected with *pEGFP-PKP2* and *ptdTomato-R735X*. EGFP-PKP2 alone or co-expressed with tdTomato-R735X showed a similar kinetics of fluorescence recovery after photobleaching. Initial fluorescence and percentage of bleaching achieved in EGFP-PKP2 were similar regardless of the co-expression of tdTomato-R735X. In both situations, EGFP-PKP2 showed a similar half-time of recovery (PKP2 $T_{1/2}$ = 33.28 ± 5.84 s and PKP2 (R735X) $T_{1/2}$ = 36.49 ± 7.47 s) (Figure 15). These results would indicate that the mobility of EGFP-PKP2 is not affected by the co-expression of tdTomato-R735X.

2. Effect of R735X on $Na_V1.5$

AC patients at early stages of the disease (the so-called "concealed phase") are normally asymptomatic, but risk suffering ventricular arrhythmias and sudden cardiac death. The mechanism leading to these ventricular arrhythmias is not well understood. Several studies have demonstrated that PKP2 mutations might alter proteins from the intercalated disc, such as $Na_V1.5$, and have proposed that this could contribute to ventricular arrhythmias during the concealed phase. Thus, we tested whether R735X affects $Na_V1.5$.

2.1. Subcellular localization of $Na_V1.5$ in R735X cells

2.1.1. Subcellular localization of $Na_V1.5$ in R735X HEK293T cells

It has been reported that protein levels of $Na_V1.5$ channel decreases a the plasma membrane in PKP2 mutant cells (Cerrone et al., 2014). To study whether R735X has an effect on the amount of $Na_V1.5$ that localizes at the plasma membrane, we co-transfected HEK293T cells with *pEGFP-$Na_V1.5$* and *pCAG-PKP2* or *pCAG-R735X*, and we analyzed the amount of $Na_V1.5$ at the total membrane (Figure 16A) and the plasma membrane fractions (Figure 16B). We found that $Na_V1.5$ protein levels were similar in both PKP2 and R735X total membrane fractions (Figure 16C) while the amount of $Na_V1.5$ detected at the plasma membrane of cells overexpressing R735X was almost five times smaller than the amount of $Na_V1.5$ detected in cells overexpressing PKP2 (Figure 16D). This result would indicate that R735X leads to a decrease in the amount of $Na_V1.5$ located at the plasma membrane in HEK293T cells.

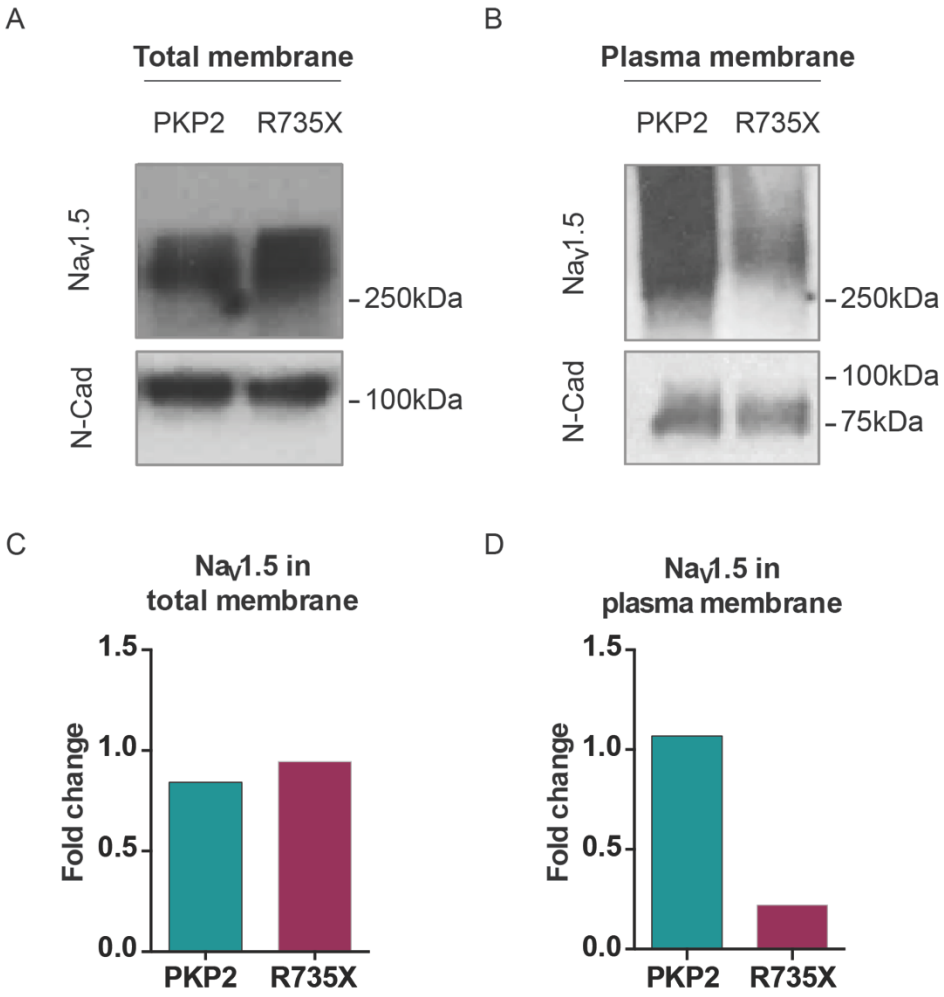

Figure 16. R735X leads to a decrease of Na$_V$1.5 at the plasma membrane. Subcellular fractionation of Na$_V$1.5 in HEK293T cells transiently expressing PKP2 and R735X proteins. A. Immunoblot of total membrane protein fraction incubated with anti-Na$_V$1.5 and anti-N-Cadherin antibody. B. Immunoblot of plasma membrane protein fraction incubated with anti-Na$_V$1.5 and anti-N-Cadherin antibody. C & D. Quantification of Na$_V$1.5 in total and plasma membrane protein fraction normalized to N-Cadherin.

2.1.2. Subcellular localization of Na$_V$1.5 in R735X HL-1 cells

We have shown that R735X leads to a decrease in the amount of Na$_V$1.5 located at the plasma membrane using transient transfections in HEK293T cells. To check whether R735X have the same effect on Na$_V$1.5 in the mouse cardiac derived HL-1 cells, we generated HL-1 cell lines stable for the expression of PKP2 and R735X. These cell lines will also allow us to validate the effect of R735X on Na$_V$1.5 independently of PKP2 and R735X transient transfections. We transfected PKP2 and R735X stable HL-1 cell lines with EGFP-Na$_V$1.5. EGFP tag was placed at the N-terminal region of Na$_V$1.5 since it has been described that it does not affect densities of currents generated by the channel (Clatot et al., 2012).

Overexpression of Nav1.5 channels is toxic in HL-1 cells (data not shown) (Moriya, 2015). Therefore, we selected cells with fluorescence intensity level below 500 AU and did not show any apoptotic features (Figure 17A). To increase resolution, to get a better contrast, and to improve signal-to-noise ratio, we took z-stack pictures and we deconvoluted the images. Analysis of deconvoluted z-projections (Figure 17B) showed that the ratio membrane-cytoplasm intensity was 1.769 ± 0.16 in PKP2 HL-1 cells and 0.8799 ± 0.08 in R735X HL-1 cells (Figure 17C). This data would suggest that R735X decrease the amount of EGFP-$Na_V1.5$ protein found in the plasma membrane of HL-1 cells.

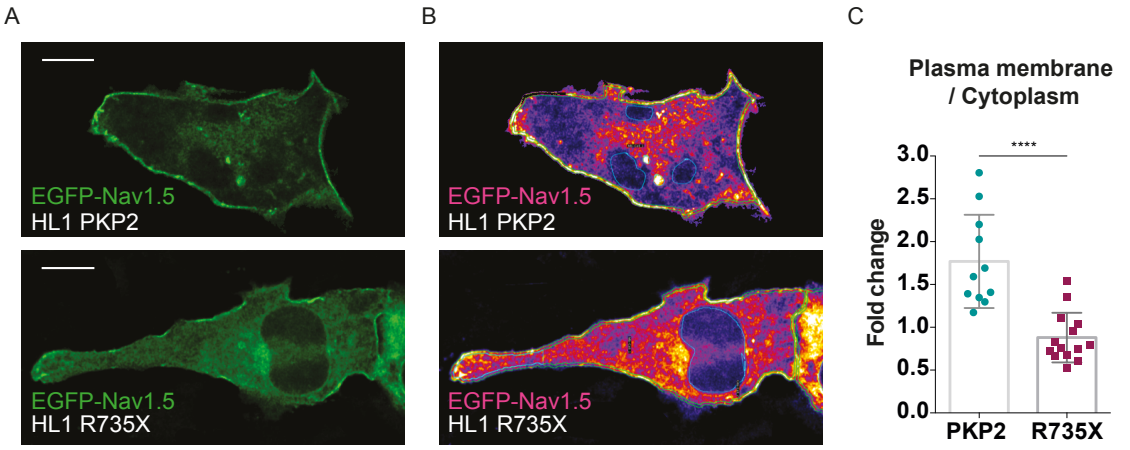

Figure 17. R735X changes distribution of EGFP-$Na_V1.5$ in HL-1 cells. A. Deconvoluted z-stacks projections of PKP2 (upper panel) and R735X (bottom panel) HL-1 cells transfected with EGFP-$Na_V1.5$. B. Example of image processing showing plasma membrane (green lines) and excluded (blue lines, nucleus and big vacuoles) regions in high contrasted images. Scale bar = 10 µm. C. Quantification of membrane intensity levels normalized to cytoplasm intensity. Data are represented as means ± s.d. **** $p<0.0001$ by Student's t-test. PKP2 n=11, R735X n=13.

To check whether R735X has an effect on endogenous $Na_V1.5$ levels in the plasma membrane, we performed a cell surface protein biotinylation assay. We incubated HL-1 monolayers with a biotinylation reagent that labels proteins on the outer face of the plasma membrane (Figure 18A). Biotin labeled proteins were pulled down and analyzed by Western Blot (Figure 18B). In an attempt to normalize for the amount of surface $Na_V1.5$ with respect to total surface proteins, each biotin labeled fraction of the $Na_V1.5$ band was compared to the Streptavidin intensity of the same lane. Since the Streptavidin intensity correlates with the total amount of surface protein that was pulled-down, we were able to calculate relative Nav1.5 amount for each group. $Na_V1.5$-Streptavidin ratio in R735X cells was 2.3 times lower than in the case of PKP2 cells (PKP2= 1415 ± 9.,76 and R735X=607.7 ± 163.6). It is also important to note that Control cells (non-

modified cells) showed a similar $Na_V1.5$-Streptavidin ratio (1478 ± 89.88) to PKP2 cells (Figure 18C).

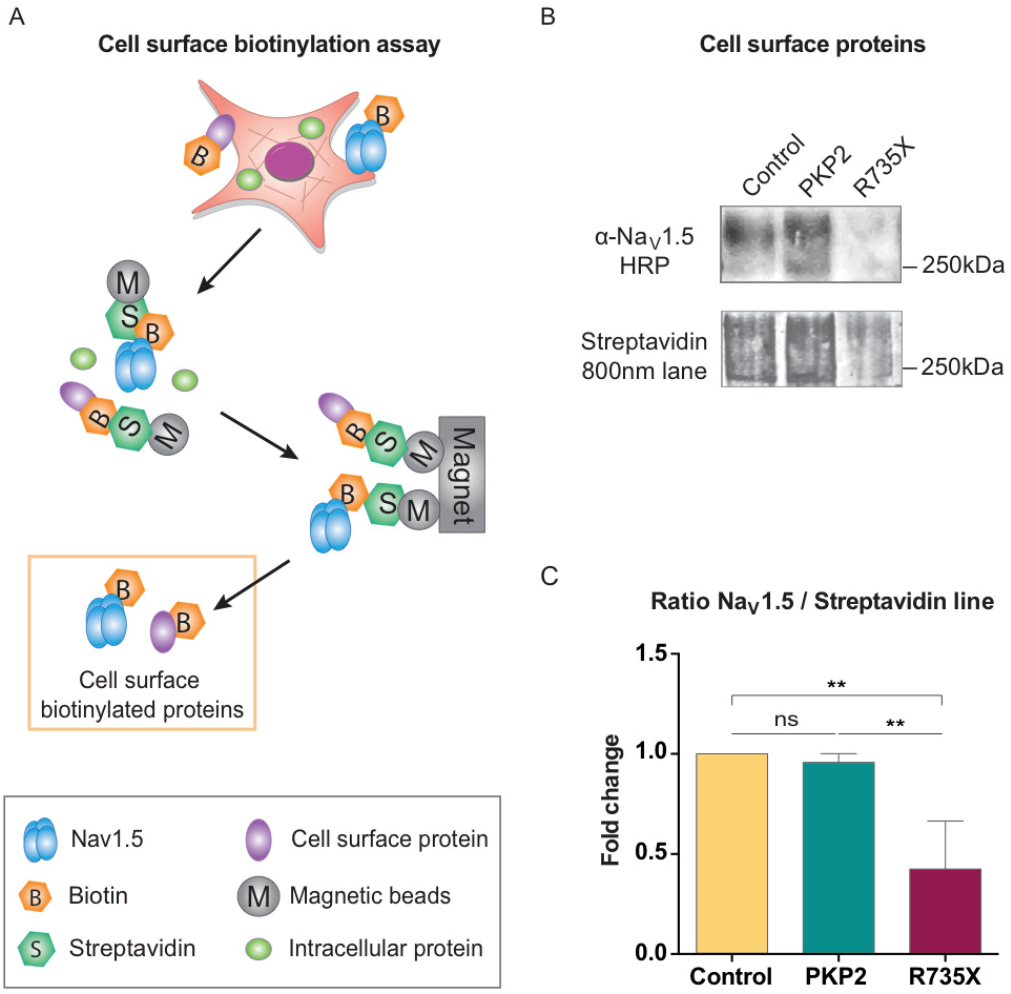

Figure 18. R735X drives to a decrease in plasma membrane $Na_V1.5$. Cell surface biotinylation in HL-1 cells. A. Diagram illustrating cell surface protein labeling with Biotin method (see Materials and Methods). A. Immunoblot of protein samples precipitated with streptavidin-coated magnetic beads incubated with anti-$Na_V1.5$ antibody (upper panel) and streptavidin-800nm (bottom panel). C. Quantification of precipitated $Na_V1.5$ normalized to Streptavidin signal in each line. Data are represented as means ± s.d**.** **p<0.001 by one-way ANOVA. N=3 for each group.

This result agrees with the distribution of the exogenous EGFP-$Na_V1.5$ in the cell, and altogether, this data indicates that R735X leads to a decrease in the amount of sodium channel $Na_V1.5$ located at the plasma membrane in HL-1 cells. Moreover, we did not observe an effect on $Na_V1.5$ plasma membrane levels on PKP2 HL-1 cells when compared with Control cells. This means that the level of PKP2 overexpression in HL-1 stable cell lines do not have an effect on $Na_V1.5$.

2.2. R735X and $Na_V1.5$ co-immunoprecipitation

It has been reported that the N-terminal region of PKP2 (amino acids 1-335) interacts with $Na_V1.5$ channels in adult heart lysate (Sato et al., 2009). To further investigate the role of the C-terminal region in the interaction with the channels, we performed an immunoprecipitation assay of $Na_V1.5$ and PKP2 or R735X. Briefly, HEK293T cells were co-transfected with *pEGFP-$Na_V1.5$* and *pCAG-PKP2* or *pCAG-R735X* constructs, and protein samples were precipitated with an α-GFP antibody-coated Protein A beads complex.

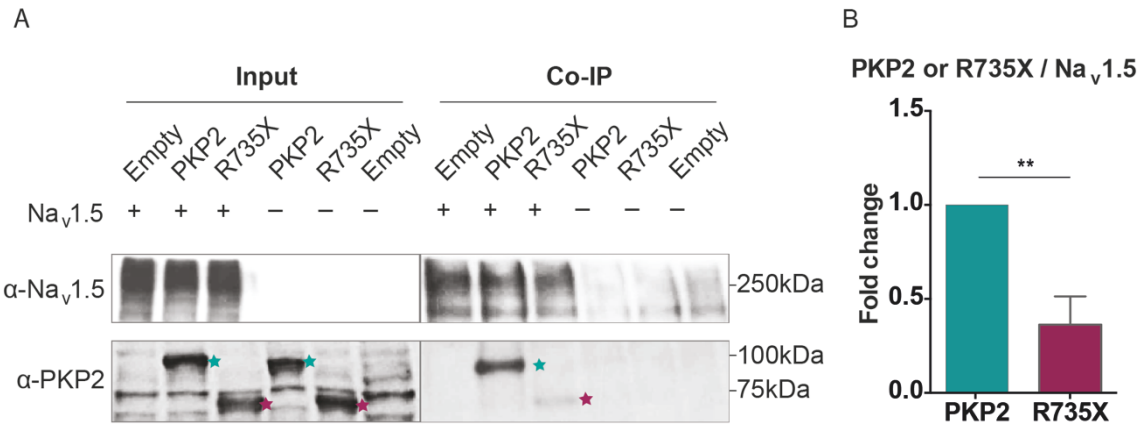

Figure 19. R735X co-immunoprecipitates with $Na_V1.5$. A. Symbols + and - indicate transfection or not with EGFP-$Na_V1.5$. Left panels: immunoblot for $Na_V1.5$ (top) and PKP2 (bottom) from input samples. Right panels: Immunoblot for $Na_V1.5$ (top) and PKP2 (bottom) from samples exposed to α-GFP antibody-coated Protein A beads. Samples no transfected EGFP-$Na_V1.5$ run as negative control. B. Quantification of PKP2 and R735X proteins precipitated with EGFP-$Na_V1.5$, normalized to precipitated EGFP-$Na_V1.5$ levels. Data are means ± s.d. **p<0.01 by Student's t-test.

Both PKP2 and R735X were able to precipitate with EGFP-$Na_V1.5$ (Figure 19A). However, R735X co-immunoprecipitation with EGFP-$Na_V1.5$ was reduced in a 60% (0.3629 ± 0.09 N=3) when compared with PKP2 (Figure 19B). The fact that EGFP- $Na_V1.5$ was able to precipitate with R735X agrees with what has been described: the common region between PKP2 and R735X is enough to establish an interaction with the channel. However, the lack of PKP2 C-terminal region leads to a decrease in the level of interaction between R735X and $Na_V1.5$.

2.3. R735X and $Na_V1.5$ co-localization

It has been reported that PKP2 and Nav1.5 co-localize at the intercalated disk of cardiomyocites (Sato et al., 2009). To determine whether R735X and $Na_V1.5$ interact at the cell membrane in a cardiac context, we co-transfected HL-1 cells with *pEGFP-$Na_V1.5$* and *ptdTomato-PKP2* or *ptdTomato-R73X* and analyzed z-stack by confocal microscopy. Z-projections were

deconvoluted to improve EGFP signal quality (Figure 20A). We identified peaks of fluorescence intensity at the plasma membrane and quantified the distances between red and green peaks (Figure 20B). We observed that in cells expressing tdTomato-PKP2, most of red and green picks were aligned while in cells expressing tdTomato-R735X, red and green picks were separated. (PKP2 = 0.03978 ± 0.005 µm and R735X= 0.2022 ± 0.021 µm) (Figure 20C). This result would suggest that the co-localization between R735X and $Na_V1.5$ is impaired at the plasma membrane in HL-1 cells.

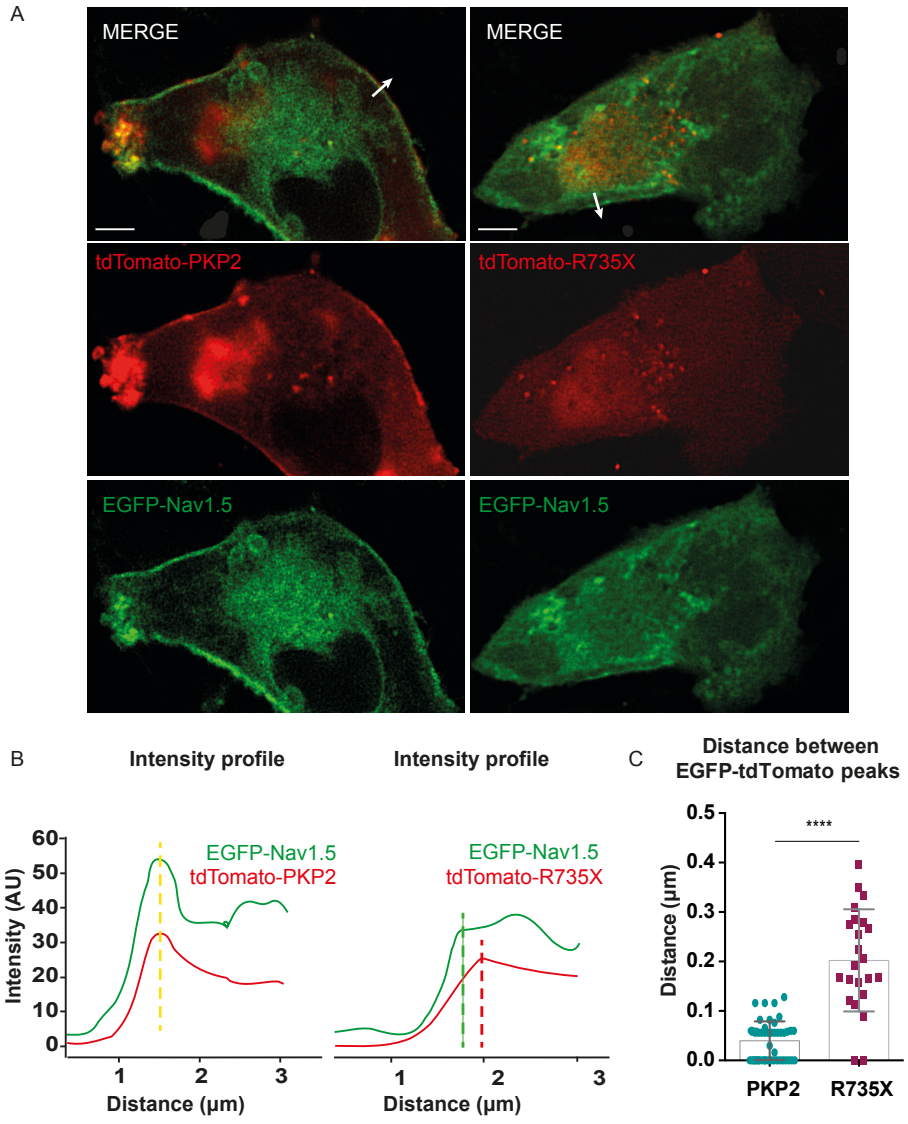

Figure 20. R735X and $Na_V1.5$ do not co-localize in HL-1 cells plasma membrane. A. HL-1 cells co-transfected with *pEGFP-$Na_V1.5$* and *ptdTomato-PKP2* (right panels) or *ptdTomato-R735X* (left panels). White arrow (3µm) indicating where the intensity profile of EGFP and tdTomato signal has been analyzed. Scale bar=5µm. B. EGFP and tdTomato intensity profiles along a 3µm line (white arrows in A upper panels). Left panel: EGFP-$Na_V1.5$ and tdTomato-PKP2 peaks. Yellow dashed line indicating peaks alignment. Right panel: EGFP-$Na_V1.5$ and tdTomato-R735X peaks. Green and red dashed lines indicating separation between peaks. C. Quantification of the distance between EGFP and tdTomato peaks at the plasma membrane. Data are means ± s.d. ****p<0.0001 by Student's t-test.

2.4. Mobility of $Na_V1.5$

As demonstrated previously, R735X shows a different pattern of mobility at the cell borders than PKP2 and is able to co-precipitate with $Na_V1.5$. We questioned whether R735X could lead to a decrease in $Na_V1.5$ at the plasma membrane by altering the channel mobility. To study $Na_V1.5$ mobility at the plasma membrane, we transfected PKP2 and R735X HL-1 stable cell lines with *pEGFP-$Na_V1.5$* and performed FRAP on 1.5 µm diameter ROIs at the plasma membrane. Curves of normalized fluorescence recovery after photobleaching were similar between cell lines (Figure 21A). EGFP-$Na_V1.5$ mobile fraction was approximately 70% in all groups analyzed (Control = 67.72 ± 5.87 % (N=11), PKP2 = 69.46 ± 4.36 % (N=8) and R735X = 73.52 ± 5.03 % (N=14)) (Figure 21B) and $T_{1/2}$ was not statistically different (Control = 10.65 ± 1.71 s, PKP2 = 11.23 ± 1.63 s and R735X = 13.34 ± 2.28 s) (Figure 21C). Therefore, this data indicates that R735X does not alter EGFP-$Na_V1.5$ mobility at the plasma membrane.

3. Arrhythmogenic effect of R735X on hiPSC-CM

Several studies have been done in mice or cell derived from mice to study the effect of PKP2 mutations on cardiac electrophysiology. However, it has been shown that human and murine cardiac electrophysiology differ in many aspects, and some mechanisms of arrhythmias in mice may differ from those in humans (Kaese and Verheule, 2012). Therefore, to further investigate the effect of PKP2 mutations on a human cardiac context, we generated an AC model based on human induced pluripotent stem cell-derived cardiomyocytes (hiPSC-CMs).

3.1. Somatic cell reprogramming and hiPSCs characterization

Available commercial human dermal fibroblasts (HDF) were reprogramed using CytoTune-iPS 2.0 Sendai Reprogramming technology. CytoTune system is a footprint-free reprogramming technology based on the transduction of somatic cells with Sendai virus derived RNA vectors codifying for reprograming factors (hOct3/4, hSox2, hKlf4 and hc-Myc). Colonies with hiPSC morphology were expanded and tested for the expression of endogenous pluripotency markers and the ability to differentiate into different lineages *in vitro*.

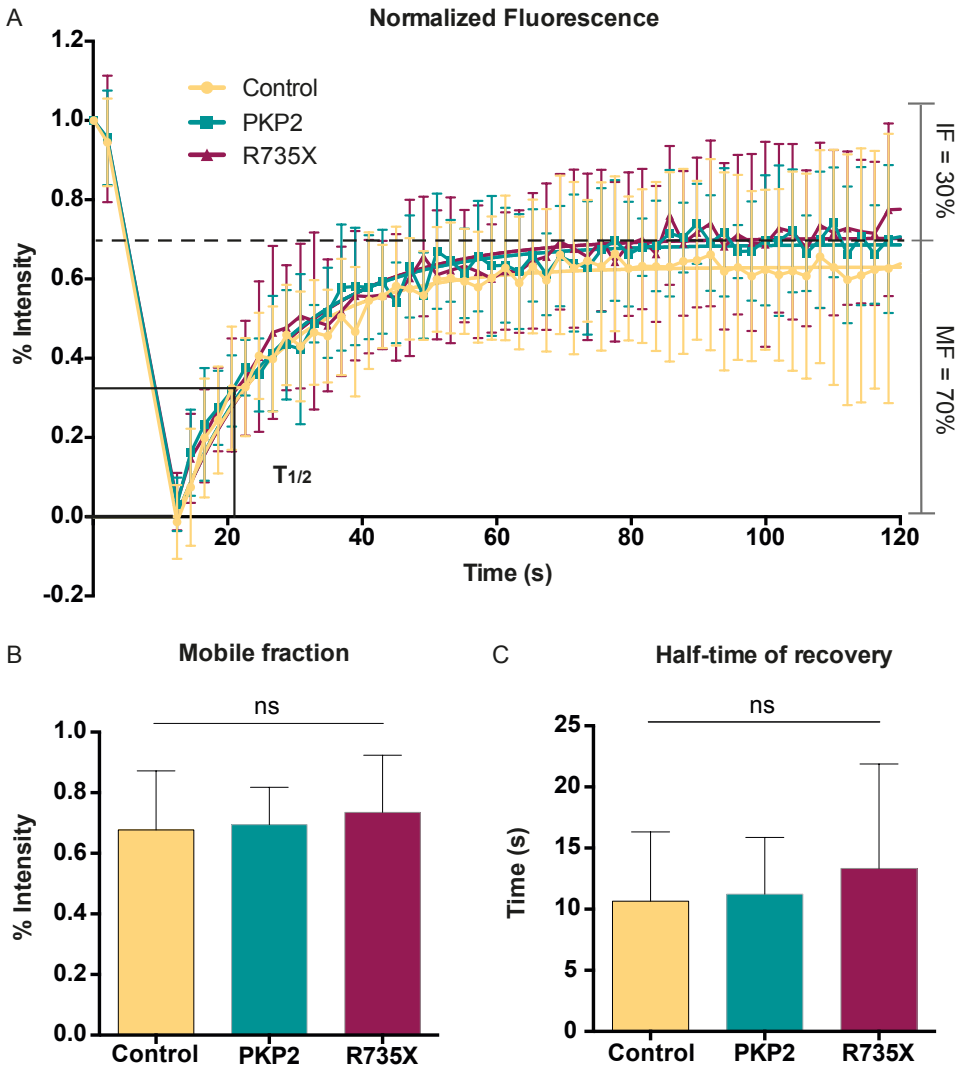

Figure 21. R735X does not affect $Na_V1.5$ mobility at the plasma membrane. FRAP of EGFP-$Na_V1.5$ in PKP2 and R735X stable HL-1 cells. A. Normalized fluorescence intensity plotted (*y* axis) against time (*x* axis), fitted to a single component exponential (solid lines). Mobile fraction (MF) and Immobile fraction (IF) are delimited by black dashed line. Half-time of recovery is indicated with solid black lines. No significant differences were observed normalized fluorescence intensity by two-way ANOVA analysis. B. Quantification of the Mobile fraction (MF). ns p>0.05 by one-way ANOVA. C. Quantification of the half-time of recovery after photobleaching ($T_{1/2}$). ns p>0.05 by one-way ANOVA. Data are means ± s.d. Control n=12, PKP2 n=9 and R735X n = 14.

3.1.1. Alkaline phosphatase test

Alkaline phosphatase (ALP) activity has been shown to be up-regulated in pluripotent stem cells (ref). After reprograming, emerging colonies were tested for ALP activity. We selected hiPSC colonies positive for ALP staining (Figure 22A).

3.1.2. Karyotype

The hiPS cell line was karyotyped using high resolution Giemsa banding. The Giemsa staining of chromosomes showed a normal chromosomal content of the hiPS cell line, in this case, a diploid female (Figure 22B).

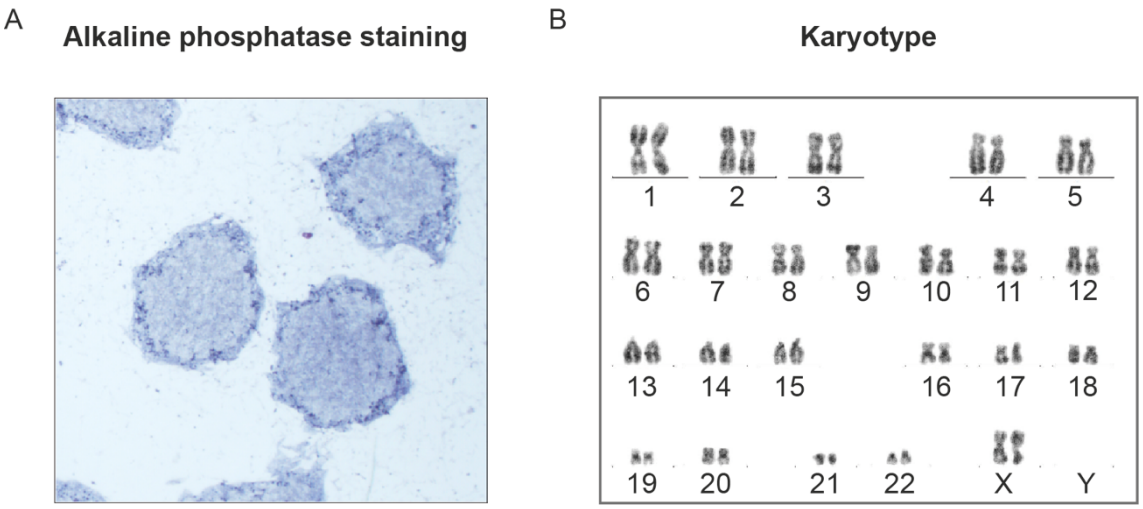

Figure 22. Alkaline phosphatase staining and karyotype in hiPSCs. A. Alkaline phosphatase staining in hiPSCs reprogrammed from HDF. B. Karyotype of hiPS cell line.

3.1.3. Detection of pluripotency markers by semicuantitaive PCR.

hiPSC colonies were examined for the expression of pluripotency markers, such as *OCT4*, *SOX2*, *KLF4*, and *c-MYC.* We extracted RNA from hiPSC and performed a reverse transcription PCR to detect the expression of these pluripotency markers. Human embryonic stem cell line (ES4) samples were used as a positive control. We observed that hiPSCs and ES4 cells showed similar expression of *OCT4*, *SOX2*, *KLF4*, and *c-MYC.* (Figure 23).

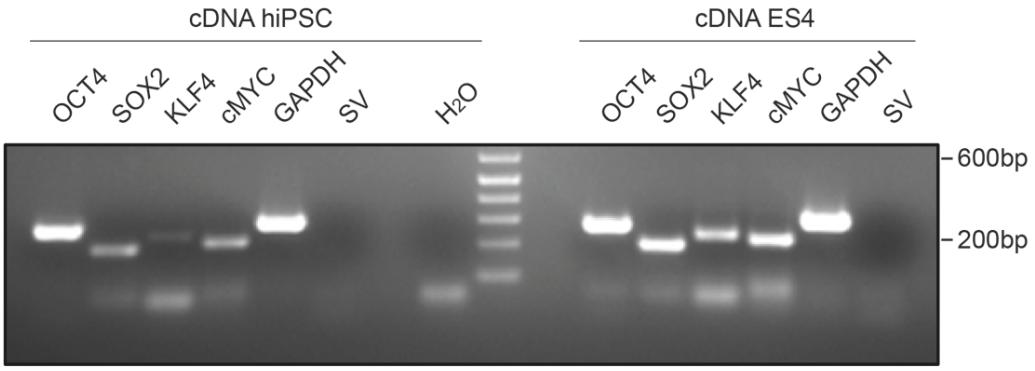

Figure 23. Expression of pluripotency markers (*OCT4*, *SOX2*, *KLF4*, and *c-MYC*) in hiPSCs. ES4 cDNA was used as a positive control of the expression of pluripotency markers. SV indicates a PCR product using primers that anneals at the Sendai Virus genome sequence. It indicates that the genome of Sendai Virus has been eliminated.

3.1.4. Detection of pluripotency markers by immunofluorescence

To double check the expression of pluripotency markers, we performed immufluorescence of OCT3/4, NANOG, SSEA4 and TRA1-80. hiPSC colonies showed expression of all tested pluripotency markers (Figure 24).

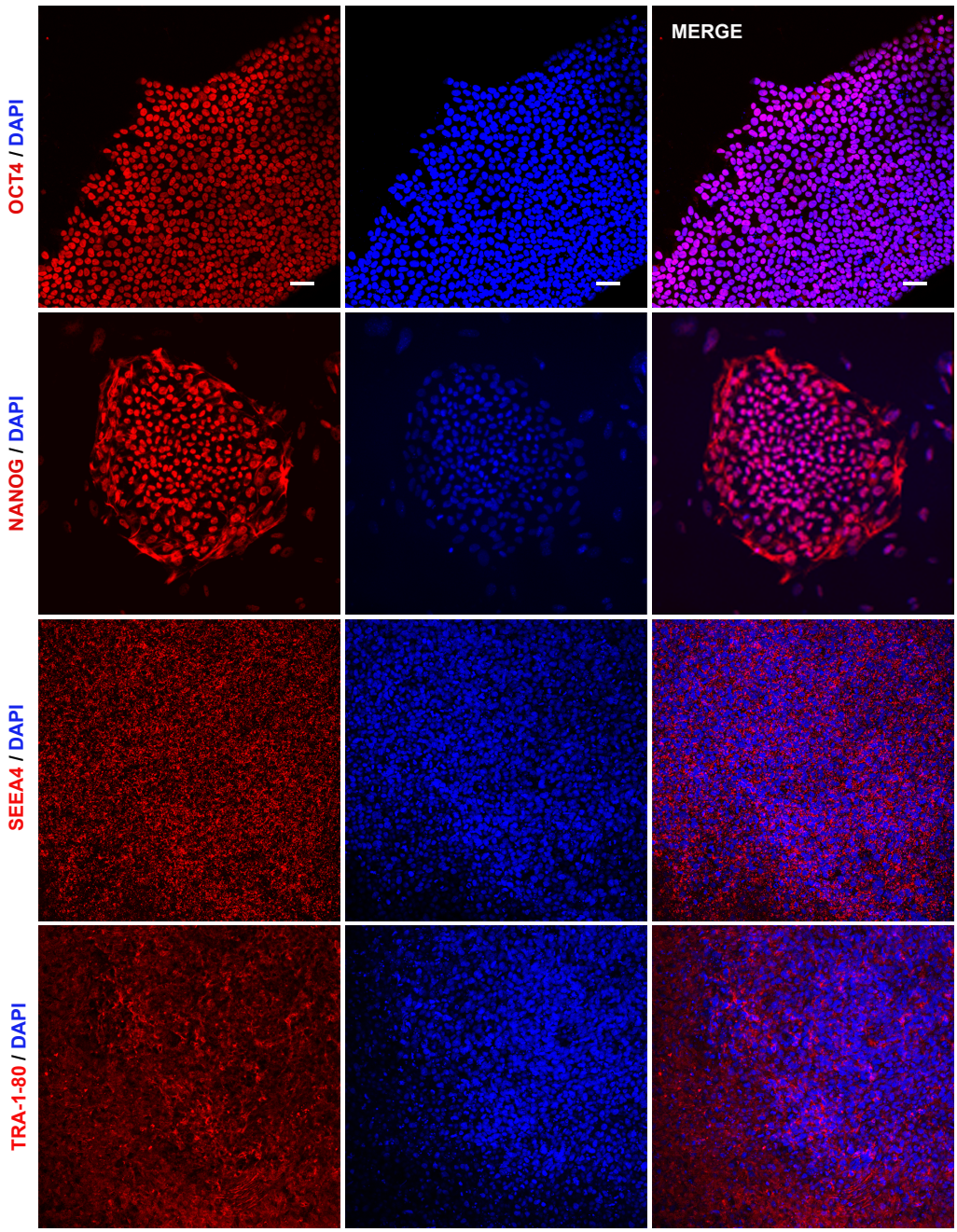

Figure 24. Immunofluorescence of OCT4, NANOG, SSEA4 and TRA 1-80 in hiPSC colonies. Scale bar = 50 µm.

3.1.4. *In vitro* differentiation test

We evaluated the capacity of hiPSCs to differentiate into the three germ layers: mesoderm, endoderm, and ectoderm. hiPSCs were cultured as embryoid bodies (EBs) and expression markers of each germ layer were detected by immunofluorescence. hiPSC showed expression for the markers smooth muscle actin (SMA) for mesoderm layer, α-fetoprotein (AFP) for endoderm layer, Glial Fibrillary Acidic Protein (GFAP) and neuron-specific class III beta-tubulin (Tuj1) for ectoderm layer (Figure 25).

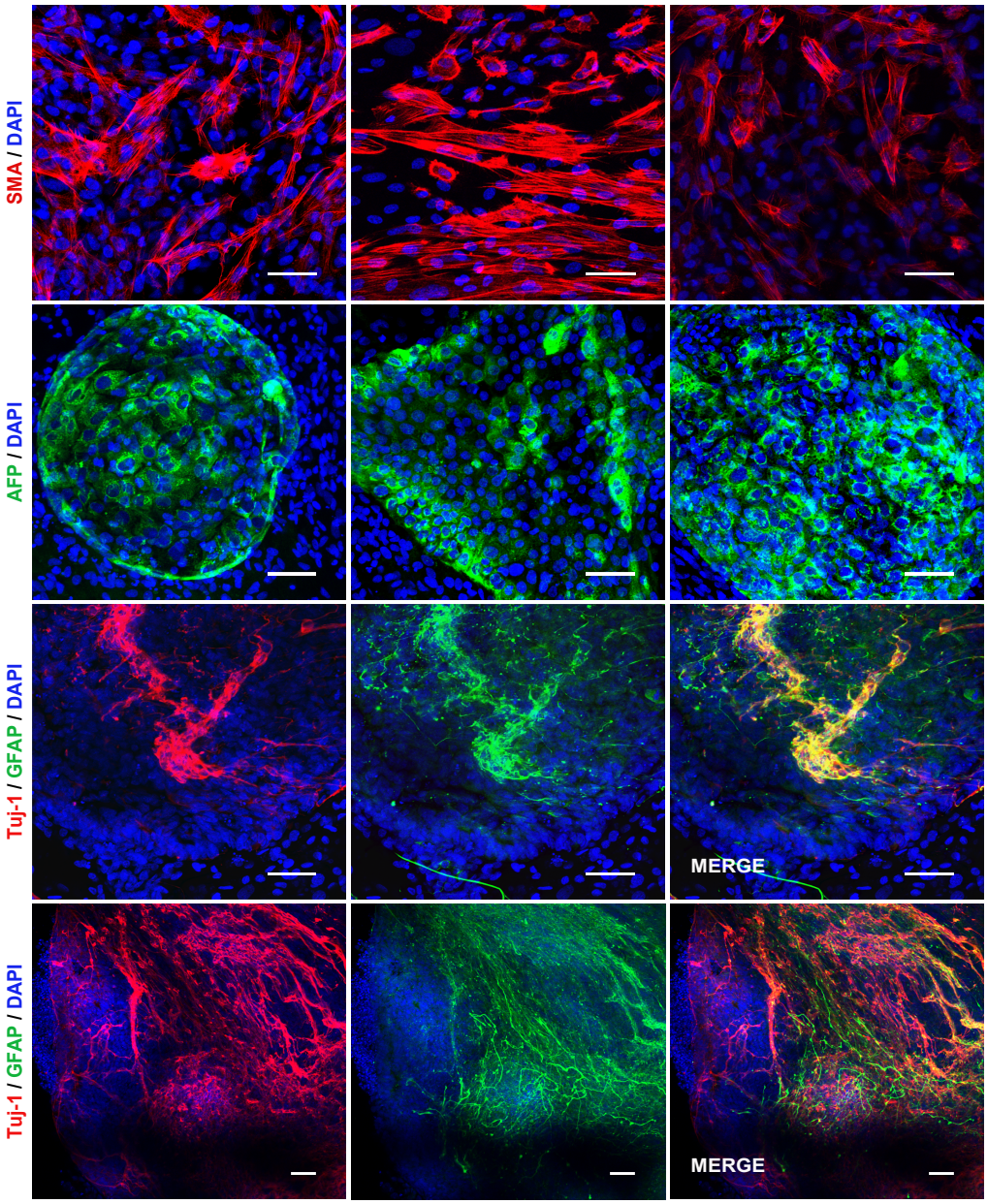

Figure 25. *In vitro* differentiation test of hiPSCs into the three germ layers. Immunofluorescence of smooth muscle actin (SMA) (mesoderm layer), α-fetoprotein (AFP) (endoderm layer), Glial Fibrillary Acidic Protein (GFAP) and neuron-specific class III beta-tubulin (Tuj1) (ectoderm layer). Scale bar=50µm.

3.2. Generation of PKP2 and R735X transgenic hiPS cell line

Once the hiPS cell line was characterized and established, we generated hiPS cell lines that stably expressed PKP2 or R735X. We transfected hiPSCs by electroporation with two plasmids containing the PB cassette (*pPB-CAG-PKP2* or *pPB-CAG-R735X*) and the PB transposase (*pCMV-Transposase*). After 10 days of treatment with Neomycin, individual colonies of resistant hiPSCs were picked and propagated as different clonal cell lines. Each clonal cell line will have a variable number of insertions (between 1-7 insertions) and these insertions will be in a random site of the genome. To confirm that the fragment of interest has been inserted into the genome, we genotyped different clones by extracting genomic DNA and running a PCR using primers that anneal in *PKP2/R735X* (Figure 26A) and *Neomycin resistance* gene (Figure 26B).

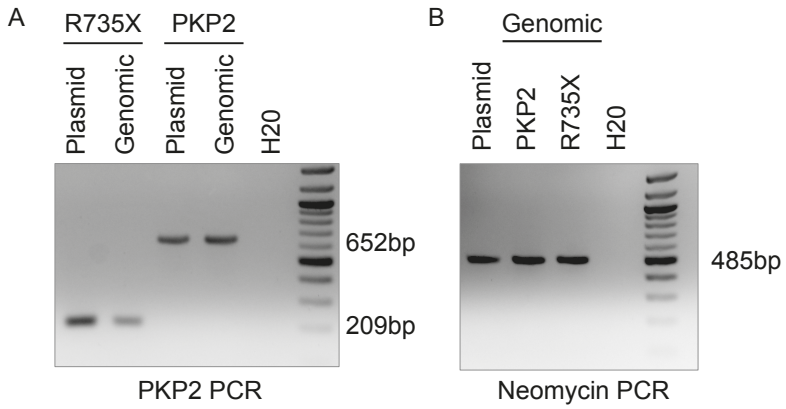

Figure 26. Transgenic hiPSC-CMs genotyping. A. PCR on PKP2 or R735X sequence. PCR product was 652bp long for hiPSC transfected with the construct *pPB-CAG-PKP2-PGK-Neo-PB* and 209bp long in cells transfected with the construct *pPB-CAG-R735X-PGK-Neo-PB*. B. PCR on Neomycin resistance gene. PCR product was 485bp long for cells transfected with both constructs.

Since the number of insertions in hiPSCs does not necessarily correlate with the final amount of exogenous protein present in hiPSC-CMs, we measured the actual PKP2 and R735X proteins levels on cardiomyocytes derived from hiPSC clones by Western Blot (Figure 27A). We observed a mild overexpression of PKP2 (98kDa band) in the PKP2 cell line compared to Control cell line (0.2890 ± 0,019 versus 0.2339 ± 0.005). However, PKP2 levels in mutant cell line (0.2661 ± 0.02) were not significantly different when compared to PKP2 or Control cells. On the other hand, R735X protein (~65 kDa band) is 63% fewer than the amount of PKP2 protein (98kDa band) in the mutant cell line (Figure 27B).

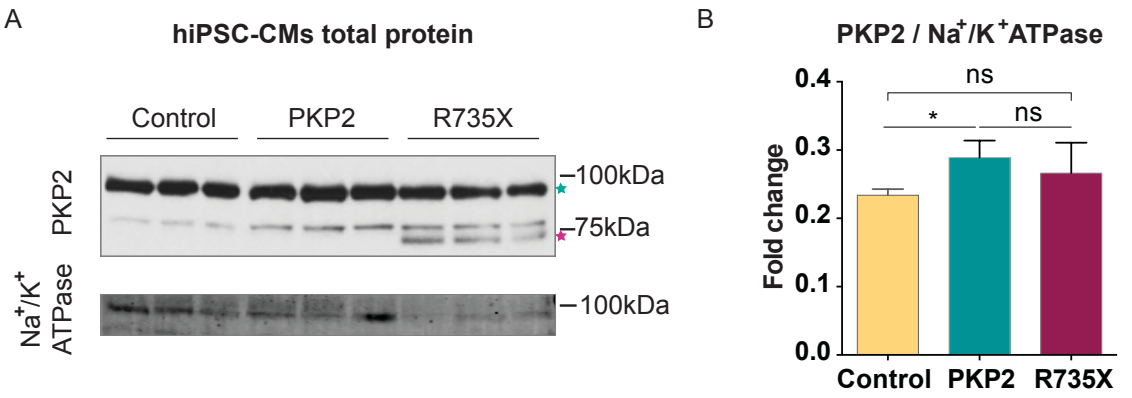

Figure 27. PKP2 and R735X protein expression in hiPSC-CM lines. Western Blot from hiPSC-CM total protein samples. A. Immunoblot incubated with anti-PKP2 antibody (upper panel) and immunoblot incubated with anti-Na^+/K^+ ATPase (bottom panel). Green star indicates PKP2 protein (98kDa) and pink star indicates R735X protein (~65 kDa). B. Quantification of the expression of PKP2 protein normalized to the expression of Na^+/K^+ ATPase. Data are means ± s.d. ns, $p>0.05$ by One-way ANOVA.

3.3. hiPSC-CMs maturation

Using hiPSC-CMs to model human cardiac disease has extraordinary and unique advantages. However, it is widely recognized that hiPSC-CMs remain immature in terms of structure and function, showing fetal gene expression, disorganized morphology, and electrophysiological properties that differ from those of adult cardiomyocytes. As such, using these cells to model adult human cardiac disease may be limited (Machiraju and Greenway, 2019). It has been described that hiPSC-CMs showed more mature features (increase of I_{Na} and I_{K1} levels, overexpression of Cx43, bigger cells, etc.) after being plated over a PDMS-Matrigel coated plate for 1 week (Herron et al., 2016). For this reason, in this thesis project, transgenic hiPSC-CMs were routinely maturated before performing any experiment by implementing the above-described protocol. Transgenic hiPSC-CMs were immunostained with α-actinin, revealing that PKP2 and R735X hiPSC-CMs did not show any evident abnormality (Figure 28).

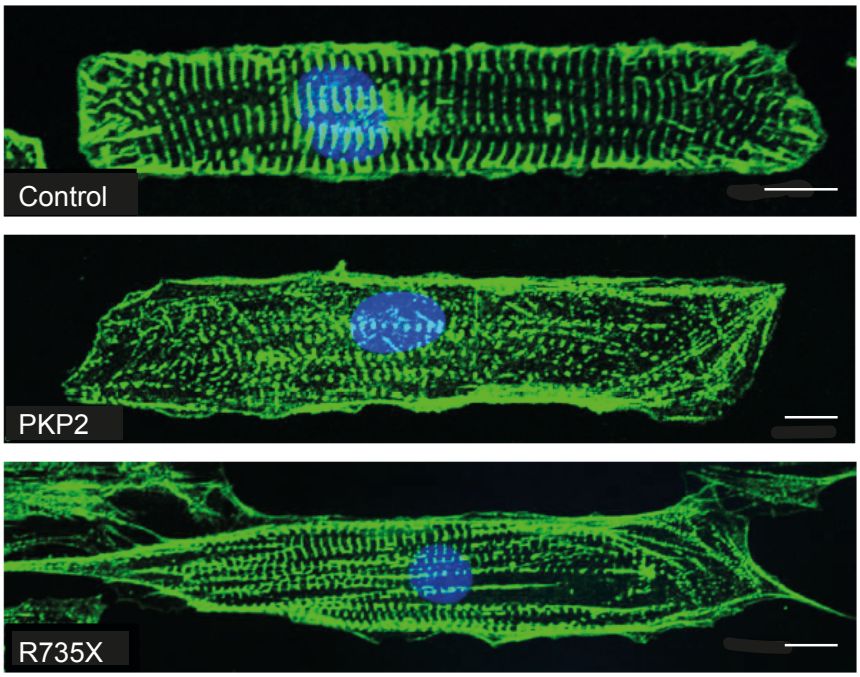

Figure 28. α-actinin immunostaining in trasgenic hiPSC-CMs after one week of PDMS maturation. Scale bar = 10 µm.

3.4. Electrical characterization of single transgenic hiPSC-CMs

To study the electrical changes that hiPSC-CMs overexpressing PKP2 or R735X could undergo, we measured the density of the main independent ion currents of single hiPSC-CMs by whole-cell patch-clamp recordings under the same ionic conditions. Before each experiment, purified hiPSC-CMs were plated as a monolayer over matrigel-PDMS coated plates for 7 days and subsequently, re-plated on matrigel-PDMS micropatterns for at least 4 days. Control, PKP2 and R735X cells presented the same I_{Ca} current density (Control = 10.09 ± 1.6 pA/pF, PKP2 = -8.669 ± 1.2 pA/pF, R735X = -9.01 ± 1.35 pA/pF at Vm = 5mV) along a range of voltage pulses from -40 mV up to +80 mV (Figure 29A-B). Also, three hiPSC-CM lines showed no significant differences in I_{K1} density (Control = -2.22 ± 0.35 pA/pF, PKP2 = -2.77 ± 0.63 pA/pF, R735X = -2.81 ± 0.50 pA/pF at Vm = -120mV) (Figure 29C-D).

However, R735X cells showed a strong and substantial reduction in mean sodium current density by ~ 70% when compared with Control and PKP2 cells (Figure 30A-C). Reduction in the sodium current density was accompanied by a lower conductance without changes in the electrophysiological properties of the sodium channel (Figure 30D). Reproducible data from three independent differentiations experiments where collected. Figure 30E shows sodium

current density at -20mV obtained from Figure33C and conductance parameters ($V_{1/2}$ and slope) calculated from Figure33D. Thus, patch-clamp experiments indicate that I_{K1} and I_{Ca} are not affected by PKP2 and R735X transgenes in hiPSC-CM. They also revealed that R735X expression in hiPSC-CM leads to a decrease of total cell I_{Na} density and in sodium channel conductance.

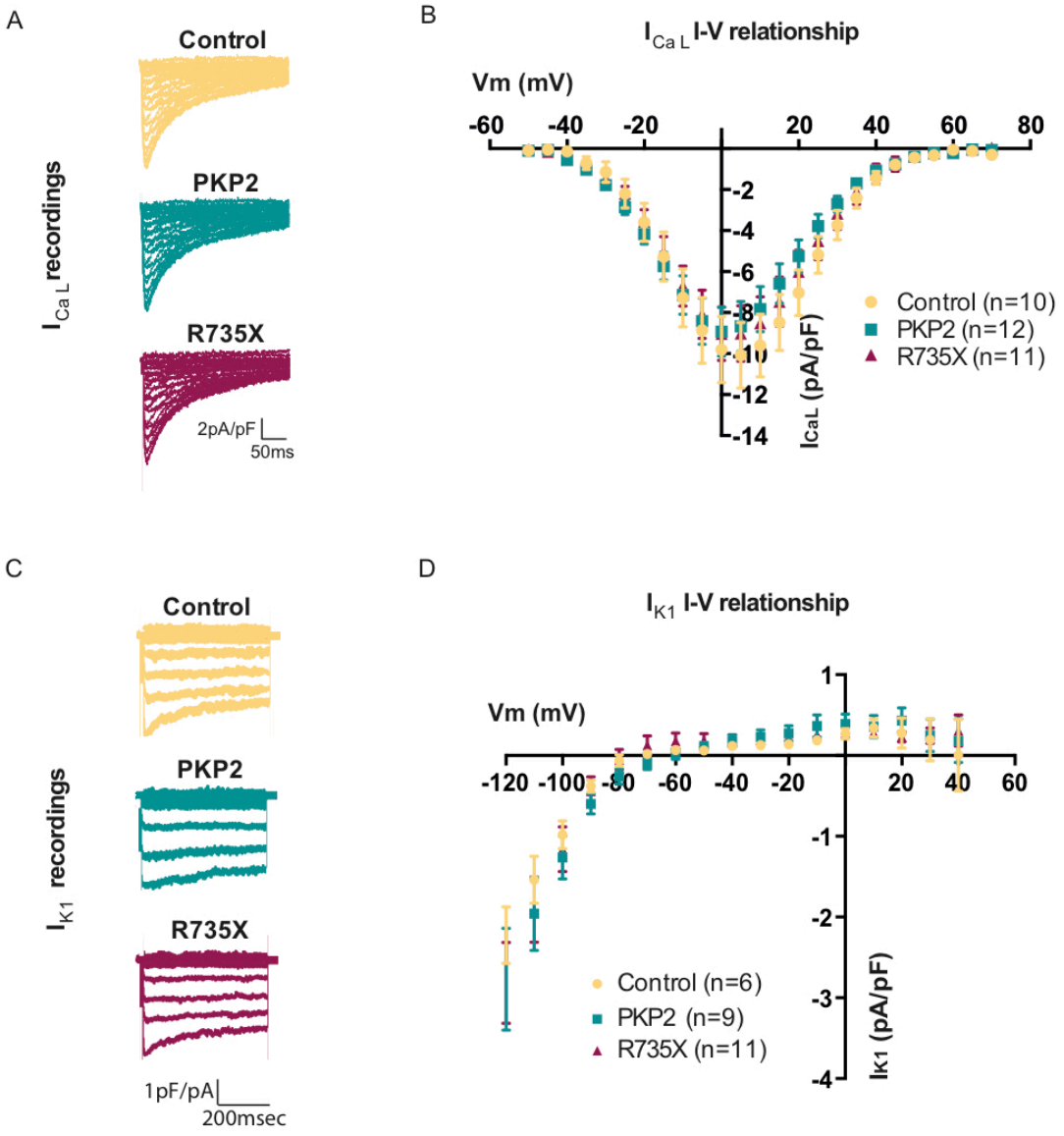

Figure 29. R735X does not have an effect on I_{CaL} and I_{K1} currents. Whole-cell patch-clamp measurements of Ca^{2+} current (I_{Ca}) and inward-rectifier K^+ current in Control, PKP2 and R735X hiPSC-CMs. A. I_{Ca} traces. B. I_{Ca} voltage-current relationship. C. I_{K1} traces. D. I_{K1} voltage-current relationship. Data are means ± s.e.m. hiPSC-CMs showed no significant differences in I_{Ca} and I_{K1} between groups (Two-way ANOVA). Number of observations are indicated in the figure.

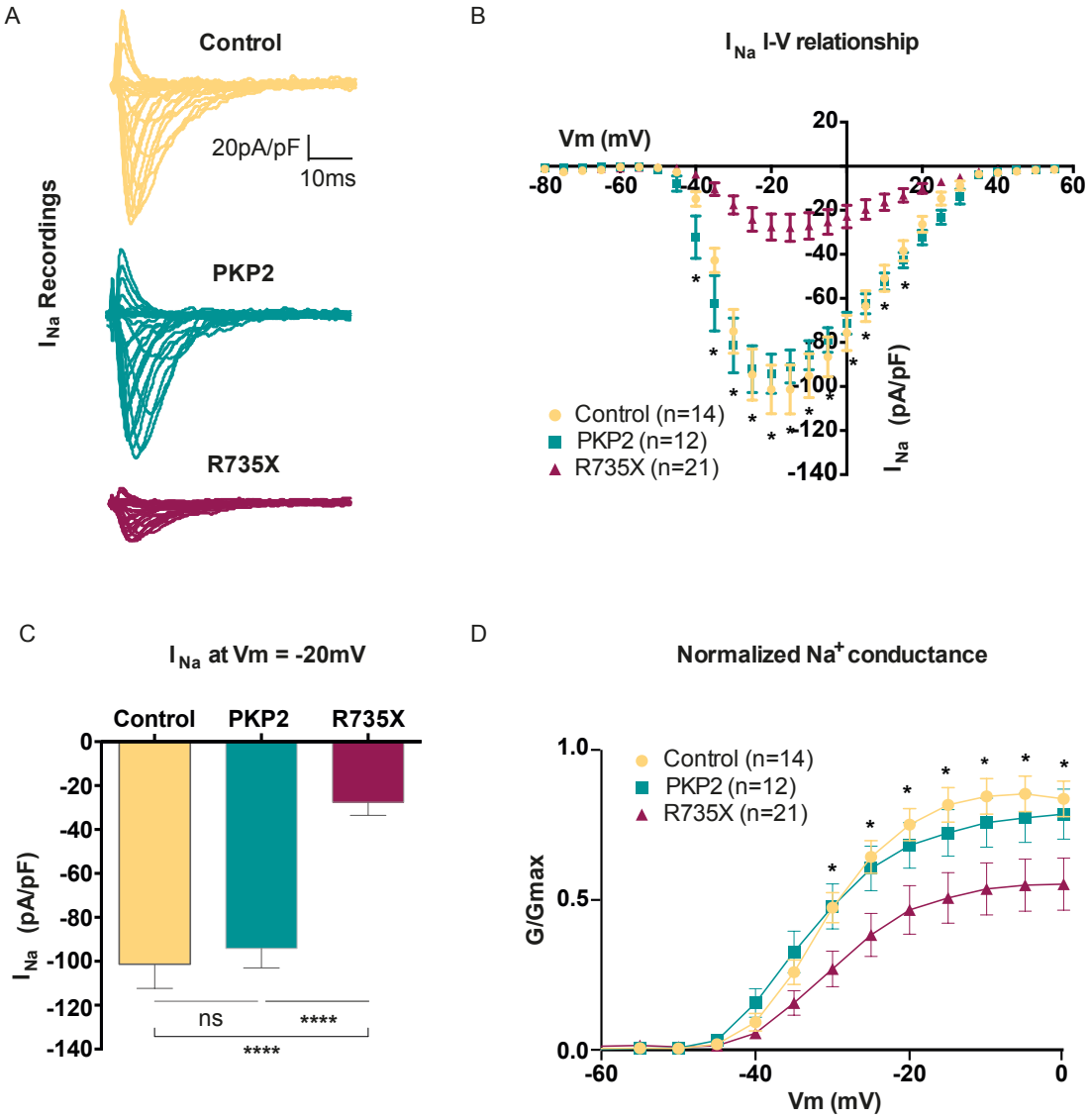

E

	Current density (pA/pF)	$V_{1/2}$ (mV)	Slope
Control	-101.3 ± 11.06	-24.39 ± 3.35	0.07993 ± 0.01042
PKP2	-94.16 ± 8.87	-20.51 ± 5.52	0.07175 ± 0.01268
R735X	27.59 ± 5.95	-18.45 ± 4.52	0.06198 ± 0.009303

Figure 30. R735X leads to a decrease in I_{Na} current. Whole-cell patch-clamp measurements of Na^+ current (I_{Na}) in Control, PKP2 and R735X hiPSC-CMs. A. I_{Na} traces. B. I_{Na} voltage-current relationship. R735X cells showed significant reduction in I_{Na} amplitude (between -40 and +15 mV, *< 0.0001 by Two-way ANOVA). Vm, membrane voltage. C. Detail of maximum I_{Na} at -20mV (**** < 0.0001 by One-way ANOVA). D. Voltage dependence of channel activation or channel conductance (G), estimated by dividing I_{Na} at each test potential by the electrochemical driving force for Na^+, normalized to the maximum Na^+ conductance (G_{max}). R735X cells showed significant reduction in Na^+ conductance (between -20 and 0 mV, ***< 0.001, Two-way ANOVA). E. Values of sodium current density, $V_{1/2}$ and Slope of all groups. Data are means ± s.e.m. Number of observations are indicated in the figure.

3.5. Analysis of transgenic hiPSC-CM monolayers

Since we have demonstrated that R735X leads to a 4 times decrease in sodium current density, we questioned whether this sodium current reduction could have arrhythmogenic effects. In order to study the arrhythmogenic effect of R735X mutation, we performed optical mapping on hiPSC-CMs monolayers. We cultured the transgenic hiPSC-CMs in circular monolayers and let them mature for 7 days on PDMS. Two or three days after being plated in monolayers, hiPSC-CMs reestablished intercellular attachments and some of them take the role of pacemaker. In physiological situations, electrical impulse originated at the pacemaker propagates through the surrounding cells towards the well edges; generating a spontaneous, rhythmic beating activity.

Transgenic hiPSC-CM monolayers were loaded with a voltage sensitive fluorescent probe that responds to changes in membrane potential (FluoVolt), and we recorded their electrical activity with a high speed CCD camera. Analysis of spontaneous activity revealed that the amplitude of action potentials in PKP2 monolayers was higher than in R735X monolayers (PKP2= 205.0 ± 20.62 AU and R735X= 110.0 ± 6.32 AU) (Figure 31A). Spontaneous pacemaker activity from PKP2 monolayers showed higher frequency than the ones from R735X monolayers (PKP2= 0.7250 ± 0.09 Hz and R735X= 0.3200 ± 0.03 Hz) (Figure 31C). However, the most remarkable feature of their spontaneous activity was the irregularly timed peaks seen in all R735X monolayers. Meanwhile, all PKP2 monolayers presented a regular activity, showing consistent intervals between peaks during the same recorded time (Figure 31C & D).

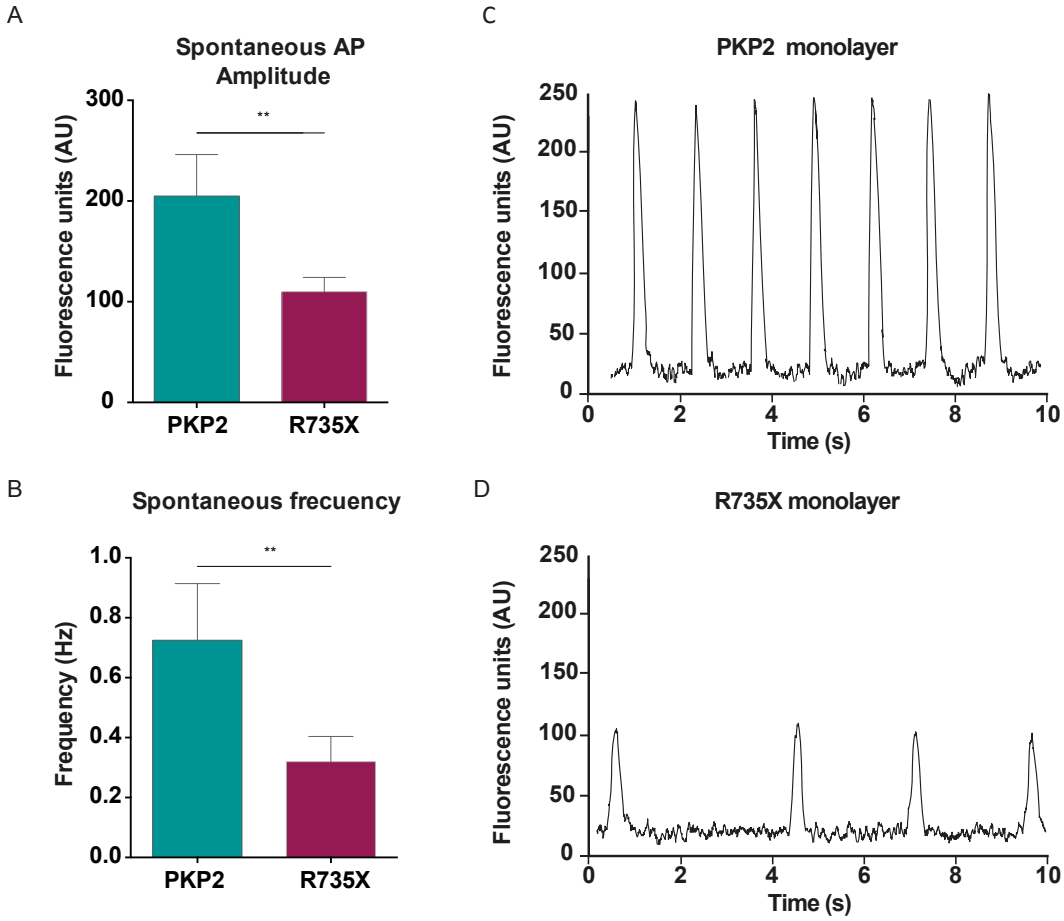

Figure 31. R735X monolayers exhibit arrhythmogenic activity. Spontaneous activity of PKP2 and R735X hiPSC-CMs recorded by optical mapping. A. Spontaneous AP amplitude. B. Spontaneous beating frequency. Data are represented as means ± s.d. **p<0.001 by Student's t-test. N=5 for each group. C. Single pixel recordings from spontaneous activity of a PKP2 monolayer (upper panel) and a R735X monolayer (bottom panel).

Optical mapping allowed us to quantify the duration of the action potential that occurs in an image pixel (where several cells can be found) and the conduction velocity (CV) of the electrical impulse along the well. To compare these parameters between monolayers, we synchronized them by applying point stimulation in each monolayer using a custom made electrical pacing frame. PKP2 monolayers were able to follow a wider range of frequencies than R735X monolayers (Figure 32A). The amplitude of the action potential was higher in PKP2 monolayers than in mutant monolayers (PKP2 amplitude = 140.0 ± 7.07 AU; R735X amplitude = 100.0 ± 4.08 AU) (Figure 32B-D).

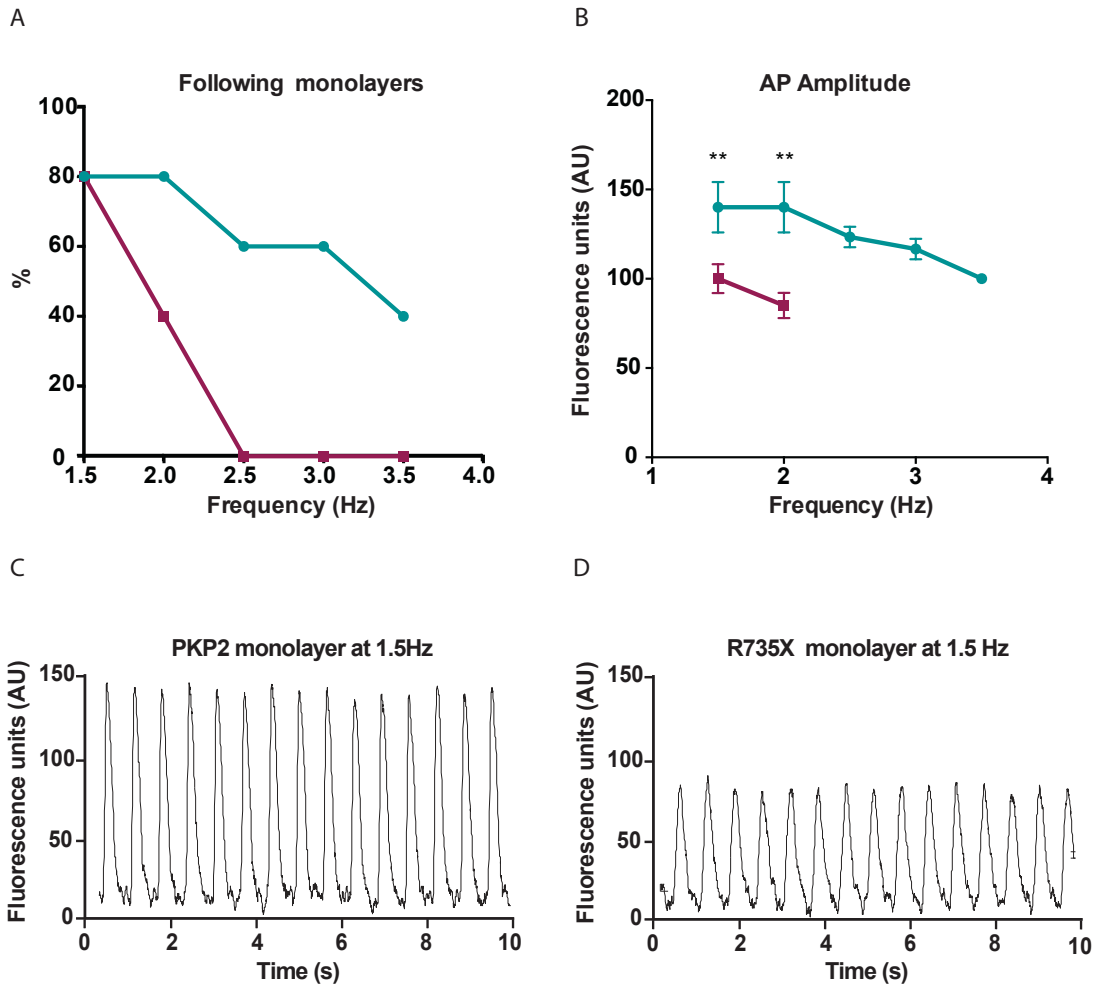

Figure 32. PKP2 monolayer follow a wider range of pacing frequencies. Optical mapping of PKP2 and R735X hiPSC-CMs paced at different frequencies. A. Percentage of monolayers that were able to follow the pacing at different frequencies. B. Quantification of AP amplitude at different frequencies. **p<0.001 by Student's t-test. Data are represented as means ± s.d. N=4 for each group at pacing=1.5Hz. N=3 for each group at pacing=2Hz. No R735X monolayer followed the pacing beyond 2Hz. C & D. Single pixel recordings from a PKP2 monolayer (right panel) and R735X monolayer (left panel) paced at 1.5Hz.

APD_{80} (action potential duration at 80% of repolarization) was 1.5 times longer in R735X monolayers than in PKP2 monolayers (PKP2 APD80= 267.5 ± 4.78 ms, R735X APD80=407.5 ± 4.78 ms, monolayers paced at 1.5Hz)(Figure 33A). Pixel action potentials obtained from optical mapping have to predominant phases: depolarization and repolarization (Figure 33B). Quantification of the ratio APD_{20}/APD_{90} (ratio between the APD at 20% of repolarization and the APD at 90% of repolarization) showed no differences between the repolarization phases of PKP2 and R735X monolayers (Figure 33C). However, quantification of the slope of the depolarization phase revealed that the depolarization of PKP2 monolayers is two times faster than the depolarization of R735X monolayers (PKP2 slope=3.44 ± 0.18 AU, R735X slope = 6.18 ± 0.82 AU

paced at 1.5Hz) (Figure 33D). These data indicate that R735X leads to a prolongation of the action potential duration due to a slower depolarization phase. Thus, the observed decrease in the inward sodium current density is leading to a slow depolarization phase and, as a consequence, to a prolongation of the APD in R735X monolayers.

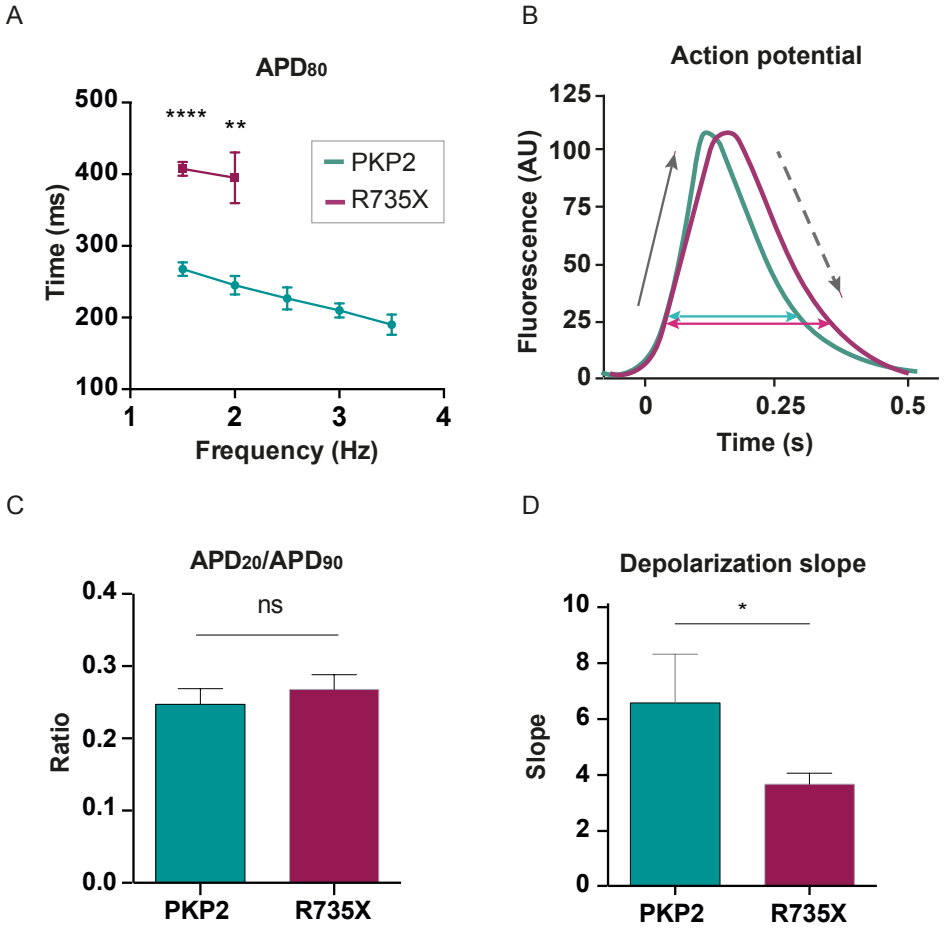

Figure 33. R735X monolayers showed an elongated APD. A. Quantification of action potential duration at 80% of repolarization (APD_{80}) at different frequencies. N=4 for each group at pacing=1.5Hz. N=3 for each group at pacing=2Hz. No R735X monolayer followed the pacing beyond 2Hz. B. Detail of an action potential of a PKP2 and R735X monolayer paced at 1.5Hz. Action potential lines have been escalated up to the same amplitude. Green (PKP2) and pink (R735X) solid arrows indicate AP width. Grey solid arrow indicates depolarization phase and grey dashed arrow indicates repolarization phase. C. Ratio between action potential duration at 20% of repolarization (APD_{20}) and action potential duration at 90% of repolarization (APD_{90}) at 1.5Hz. N=4 for each group. D. Quantification of the depolarization slope at 1.5Hz. N=4 for each group. Data are represented as means ± s.d. Ns $p>0.05$, *$p<0.01$, ** $p<0.001$ and *** $p<0.0001$ by Student's t-test.

Analysis of the activation maps revealed how the impulse propagation is slower in R735X monolayers (Figure 34A). In fact, CV was 3.6 times slower in R735X monolayers when compared with PKP2 monolayers (PKP2 CV=9.25 ± 0.52 cm/s, R735X CV= 2.57 ± 0.09 cm/s paced at 1.5Hz) (Figure 34B).

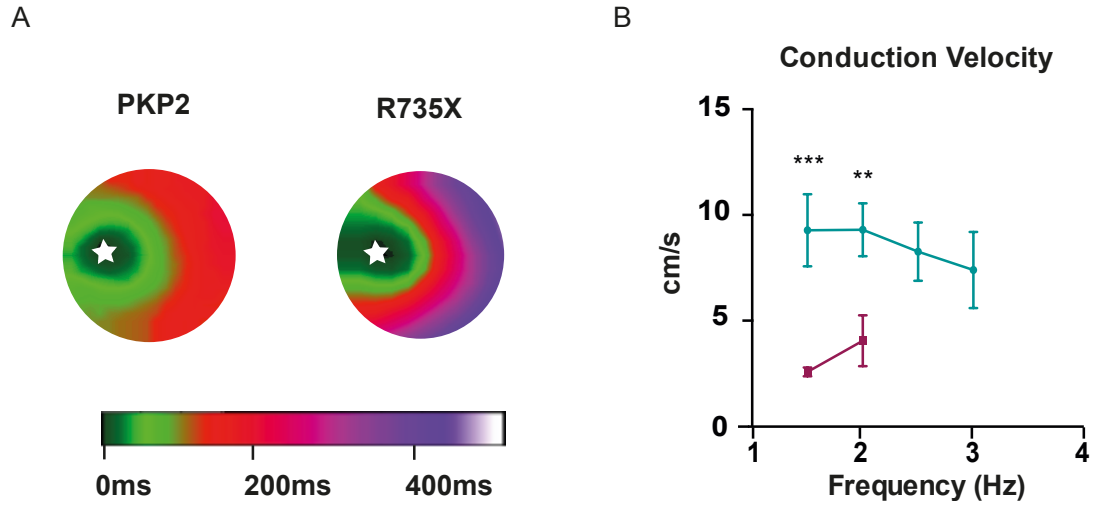

Figure 34. R735X monolayers showed a prolonged CV. A. Activation maps during 1.5Hz pacing. Colors represent the time (milliseconds) the impulse takes from the pacemaker place (white star) to the rest of the well. B. Quantification of conduction velocities at different frequencies. N=4 for each group at pacing=1.5Hz. Data are represented as means ± s.d. N=3 for each group at pacing=2Hz. No R735X monolayer followed the pacing beyond 2Hz. ** $p<0.001$ and *** $p<0.0001$ by Student's t-test.

The study of the rhythmicity of transgenic monolayers also revealed that the increase of the pacing frequency exacerbates the arrhythmic activity in most of mutant monolayers (Figure 35A). Under high frequency pacing (2-3Hz), R735X monolayers underwent arrhythmic events similar to early afterdepolarization (EAD) events (Figure 35B) and triggered arrhythmias (Figure 35C).

In conclusion, optical mapping results indicate that the reduction of both sodium current density and conductance in hiPSC-CMs slows the depolarization time and reduces impulse propagation velocity. This phenomenon leads to arrhythmic electrical behavior, such as EAD-like events. Thus, this experiment highlights the arrhythmogenic effect of R735X in hiPSC-CMs and suggests that EAD-like events could be the mechanism underlying R735X arrhythmias in AC patients.

A

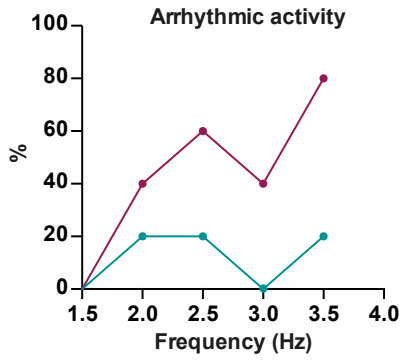

B

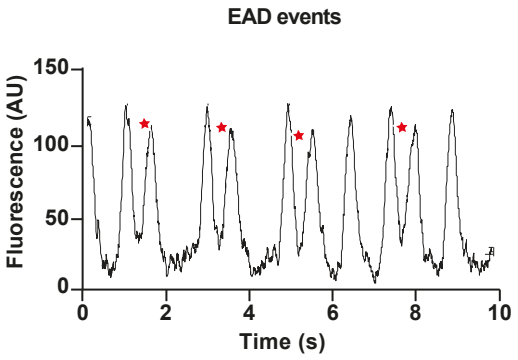

C

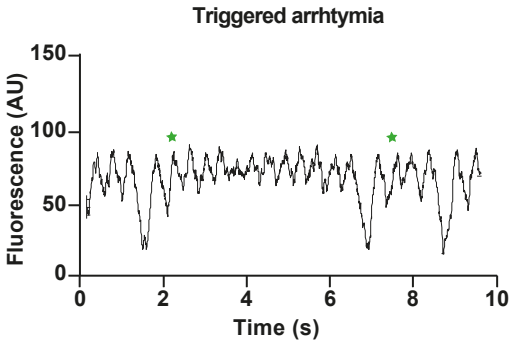

Figure 35. R735X leads to arrhythmic activity in hiPSC-CMs monolayers. A. Percentage of monolayers showing arrhythmic activity at different frequencies. B. Example of R735X monolayers undergoing EAD events. Red stars indicate EAD events. C. Example of R735X monolayers undergoing triggered arrhythmia. Green stars indicate triggered arrhythmia.

DISCUSSION

DISCUSSION

Transgenic hiPSC-CM platform to model arrhythmic diseases

While others derive patient specific hiPSC for modeling inherited arrhythmias (El-Battrawy et al., 2018)(Itzhaki et al., 2011), we applied a genetic background independent approach to investigate the effect of the R735X mutation. This experimental design avoids heterogeneity related to patient's polymorphisms and allowed us to work with isogenic hiPS cell lines. In the future, we could also compare the effect of the overexpression of different mutations over the same genetic background. Moreover, overexpressing the mutant version of a protein over a wild-type background would help us to distinguish between dominant negative or haploinsufficient related phenotypes. However, both approaches are interesting and complementary, and its combination would help to identify compensatory mechanism or modulators of the disease.

Modeling inherit cardiac diseases in hiPSC-CMs presents a major concern: immaturity of cells (Goversen et al., 2018). Many strategies have been reported to improve maturity of hiPSC-CMs (Machiraju and Greenway, 2019). In this project, we have used the extracellular matrix mediated maturation method described by Herron et al. which consists on plating the cells over a soft surface made up of a matrigel-coated PDMS sheet. This system has proven to maturate the hiPSC-CMs electrophysiological features needed to model arrhythmic diseases (Herron et al., 2016).

Currently, there is a lack of use of hiPSC-CM model for personalized drug therapy. Among other mayor reasons, generating and studying patient's derived hiPSC-CM is very expensive and time-consuming technique (Knollmann, 2013). Here, we have carried out the proof of concept of a potential platform that could quickly generate hiPS cell lines that overexpress inherited arrhythmic disease-related mutations without having to perform skin biopsies, reprogrammation of cells and characterization of patient derived hiPS cell lines. Such platform would allow for the study of the molecular mechanism underlying the arrhythmic disease while the same time performing personalized drug therapy studies. Since the maturity status of hiPSC-CMs interferes in the drug compound responsiveness (da Rocha et al., 2017), the PDMS maturation that we have implemented on these cells may add value to this model as a drug testing platform.

R735X arrhythmogenic effect on hiPSC-CMs

The expression of R735X hiPSC-CMs leads to a consistent reduction (by 70%) in the sodium current density. Cell surface biotinylation assay (data not shown) revealed a clear tendency of $Na_V1.5$ to be decreased at the plasma membrane of R735X hiPSC-CM, which would explain the reduction in the sodium current density. As reported in other hiPSC-CMs with defect in I_{Na} density (Ma et al., 2018) (Roche et al., 2019), such decrease slows down cell depolarization. Indeed, analysis of pixel's APs obtained from 2D hiPSC-CM optical mapping experiments showed that the depolarization phase was two times slower in R735X monolayers, leading to a prolongation of the APD. I_{Na} decrease was also reflected in the amplitude of the action potential that was reduced by half when spontaneous or paced activity was recorded. Despite the role played by Cx43, a decrease of 4 times in the sodium current would also be enough to cause the observed reduction in conduction velocity.

Analysis of spontaneous activity revealed that R735X monolayers showed spontaneous arrhythmic activity while electrical activity of PKP2 monolayers were regular and rhythmic. Also, the frequency of spontaneous AP driven by R735X was significantly smaller. We observed that the increase of the pacing frequency exacerbates the arrhythmic behavior of mutant monolayers, showing arrhythmogenic events such as early afterdepolarizations (EAD)-like events. Thus, optical mapping data indicate that such a defect in the cell depolarization would make the cardiomyocytes unable to follow higher pacing frequencies. With our data, we propose that the mutant R735X leads to a decrease in the sodium current generated by the voltage-gated sodium channel. This decrease slows down cell depolarization, action potential duration and, subsequently, conduction velocity of the electrical impulses through the cardiomyocytes, which could lead to life-threatening arrhythmogenic events at early stages of AC patients.

To date, several studies have been trying to characterize AC hiPSC lines carrying different PKP2 mutations, but they have focus their investigation in the metabolic alterations –adipogenesis, lipid accumulation - may happen during the disease (Ma et al., 2013)(Caspi Oren et al., 2013)(Kim et al., 2013). However, none of these papers have characterized the electrophysiological alterations PKP2 mutation may cause in these hiPSC-CMs. Just one study has shown evidence of a decrease in the sodium current in hiPSC-CM from a AC patient carrying a mutation in PKP2. In this study, they used hESC and patient derived hiPSC-CM infected with the wild-type PKP2 as a control when recording sodium current densities (Cerrone et al., 2014). In contrast, we have

compared R735X hiPSC-CMs patch-clamp recordings with the recordings obtained from both Control and PKP2 hiPSC-CM isogenic lines under the same experimental conditions, thereby avoiding the heterogeneity intrinsic to cardiomyocytes coming from different cells types. It also has been reported that patch-clamp measurements could not be completely accurate given the challenge of proper voltage control resulting from the large cell size of hiPSC-CMs and their short survival during the experiment (Roche et al., 2019)(Cerrone et al., 2014). Patch-clamp data showed in this project are robust because we only included recordings where the voltage was systematically controlled as reflected in the Intensity-Voltage curves.

To date, there is one study where an AC patient derived hiPSC-CMs 2D monolayer electrical performance was measured. They generated hiPSC-CMs from a patient with the mutation A324fs335X in PKP2 and plated them on a MEA device (Multi Channel Systems MCS GmbH, 2019). They demonstrated a prolonged field potential rise time in the AC hiPSC-CMs (Caspi Oren et al., 2013) but they could not directly measure the excitability, the conduction velocity or identify arrhythmic events with this technique. Therefore, we are presenting for the first time a thorough study of the electrical performance of AC hiPSC-CM 2D monolayers.

AC and BrS: two different diseases?

After the initial description of BrS, it has been suggested that this syndrome could share several clinical features with AC, implying that these were not completely distinct diseases (Corrado et al., 2001; Corrado et al., 1999). Indeed, the screening of 200 patients diagnosed with BrS, no symptoms of AC and no mutations in genes related with BrS (*SCN5A, CACNa1c, GPD1L* and *MOG1*) revealed that 5 of the patients had single amino acid substitutions in PKP2. They also showed that this BrS related PKP2 mutants lead to a significant reduction of the sodium current in HL-1 cells, when compared with cells transfected with wild type PKP2 (Cerrone et al., 2014). I_{Na} decrease has been widely accepted as a hallmark of BrS. Thus, in this project we have described a PKP2 mutation identified in AC patients that could present with BrS clinical manifestations at the early stages of the diseases.

R735X molecular mechanism?

PKP2 integrates into the desmosomal complex at the inner face of the plasma membrane (Godsel et al., 2004). It has been previously described that early truncated mutant versions of

PKP2 such as R79X and 179fs proteins fail to localize at the cell borders and are detected at the intracellular space (Joshi-Mukherjee et al., 2008b). However, these are very early truncates resulting in less than 30kDa proteins, and may not be representative of the subcellular distribution of larger truncates. In this thesis, we have described that R735X –a PKP2 truncated protein of ~65kDa- is primarily found diffusely at the intracellular space of cells and is only found in some discontinuous spots at cell borders. Thus, we provide an example of the subcellular mislocalization of a larger PKP2 truncated protein, which could have a consequence in the sodium channel function.

Data obtained from FRAP assay of PKP2 proteins tagged with EGFP indicates that EGFP-R735X mobility at the cell-cell contacts is higher than EGFP-PKP2 mobility. Although, their mobile fraction after 120 seconds of bleaching is similar, EGFP-R735X is able to recover half of the final fluorescence 2.5 times faster. Mobile fraction can be composed of free diffusing proteins or transiently immobile proteins that interact in a steady-state with immobile partners (Houtsmuller, 2005). Free diffusing proteins contribute to a fast recovery of the signal and transiently immobile proteins contribute to a slow and more linear recovery of the signal. Therefore, EGFP-R735X recovery kinetics would suggest that the recovery is mostly due to diffusion of mobile molecules along the ROI of stimulation. Meanwhile, EGFP-PKP2 kinetics of recovery has a stronger lineal component which would suggest that the recovery is partially due to redistribution of mobile molecules but also due to the movement of transiently immobile molecules that are being released. FRAP experiments would indicate that PKP2 protein is less mobile because it is interacting with its partners and is being integrated into superior complexes, while the lack of the C-terminal in R735X protein would be avoiding these interactions and impairing its integration into macromolecular structures.

Our data shows that R735X does not disrupt PKP2 localization or mobility pattern, as have been described for other PKP2 mutants (Sato et al., 2009). In fact, the desmosomal structures in the R735X mouse model were not affected when analyzed by transmission electron microscopy and immunofluorescence (Cruz et al., 2015). Moreover, post mortem biopsy of AC patients with mutations in *PKP2* gene showed normal immunoreactive signals for PKP2 (Noorman et al., 2013). Thus, localization and mobility data shows that R735X do not have a direct dominant negative effect over PKP2, which suggest that R735X may be playing a new role in the cardiomyocyte physiology.

Here we have shown that R735X decreases the amount of exogenous $Na_V1.5$ located on the plasma membrane of HEK293 and HL-1 cells transiently expressing PKP2 or R735X proteins. Cell surface biotinylation assay also showed that R735X decreases levels of endogenous $Na_V1.5$ proteins in HL-1 cells and in hiPSC-CMs stably expressing R735X. It has been described that PKP2 and $Na_V1.5$ co-exist at the same molecular complex since both proteins co-precipitate together in heart lysates and their immunoreactive signals co-localize on the cell borders of isolated adult cardiomyocytes (Sato et al., 2009). However, we observed that tdTomato-R735X failed to co-localize with EGFP-$Na_V1.5$ in most of the cell border regions, and we did not detect a change in $Na_V1.5$ mobility pattern in HL-1 cells expressing R735X. Altogether, our data indicates that the effect of R735X on voltage-gated sodium channels is not happening at the plasma membrane level. Nonetheless, we have observed that R735X and $Na_V1.5$ are able to co-precipitate together. Therefore, we believe that the interaction between R735X and the sodium channel must be taken place away from the cell border, in the intracellular space. Thus, we could hypostatized that this interaction could be affecting the life cycle of the sodium channel, which opens up a new filed of investigation.

We have observed that $Na_V1.5$ levels of total membrane fractions (including plasma membrane, Golgi, ER and mitochondria) from HEK293 cells did not differ between cells transfected with PKP2 or R735X. However, isolated proteins from the plasma membrane fraction showed a significant reduction of $Na_V1.5$. The data would indicate that R735X is not having a transcriptional or translational effect on $Na_V1.5$ in this system, but suggest that R735X could be impairing the proper trafficking of the channel to their appropriate plasma membrane subdomain.

The canonical anterograde $Na_V1.5$ trafficking has been described as an active transport of $Na_V1.5$ containing vesicles from the ER/Golgi apparatus through the cell along microtubule tracks (Mercier et al., 2017). Indeed, enhanced tubulin polymerization by the anticancer agent Taxol (TXL) have been shown to decrease $Na_V1.5$ membrane expression, leading to a two-fold reduction in I_{Na} amplitude, as well as modifying its gating properties. Targeting cardiac $Na_V1.5$ to specific membrane areas, such as the intercalated disc, involves the anchoring protein Ankyring-G and interacting proteins such as SAP97, N-cadherin and connexin 43, as well as plakophilin-2 and desmoglein-2(Makara et al., 2014) (Séverine et al., 2011) (Malhotra et al., 2004) (Rhett et al., 2012) (Sato et al., 2009) (Rizzo et al., 2012). At the lateral membrane of cardiomyocytes,

$Na_V1.5$ targeting depends on different macromolecular complexes related to syntrophin/dystrophin expression (Gavillet et al. 2006; Petitprez et al. 2011). In fact, Cerrone et al. showed that PKP2 deficiency led to increased distance between EB-1 clusters (as a marker of microtubules plus-ends), and the N-cadherin plaque midline. This finding indicates that PKP2 haploinsufficiency (directly or indirectly) affects the ability of microtubules to reach the intercalated disc, which could impair delivery of proteins relevant for sodium channel function (Cerrone et al., 2014). How R735X could affect $Na_V1.5$ trafficking via microtubule or microtubule related proteins needs to be further investigated. It has been recently published that a common early anterograde trafficking mechanism is involved in the transport of $Na_V1.5$ and Kir2.1 channels to the plasma membrane (Ponce-Balbuena et al., 2018). However, we observed no differences in I_{K1} current density in the I_{Na} deficient R735X hiPSC-CMs. It has been postulated that several pools of $Na_V1.5$ channels exists and that they are able to reach the plasma membrane from different origins (Golgi apparatus, unconventional Golgi pathway or storage pools)(Mercier et al., 2015). Therefore, if R735X would be interfering in $Na_V1.5$ trafficking pathway it seems likely to be affecting a different pool of channels that do not associate with Kir2.1 during their trafficking.

In a parallel project developed in our lab, we have observed that HL-1 cells stably expressing R735X have a defect in actin cytoskeleton organization. Concretely, actin microfilaments do not organize above the nucleus of R735X cells as it happens in PKP2 cells, and the ratio F-actin (filamentous) /G-actin (globular, monomeric) is lower in R735X cells (Marquez-Lopez et al. 2019, submitted). To date, several studies have highlighted the importance of the cytoskeleton in the regulation and functioning of the voltage-dependent Na^+ channel. It has been showed that treatment of rat and rabbit ventricular cardiomyocytes with cytochalasin-D (Cyto-D), an agent that interferes with actin polymerization, reduced whole cell peak Na^+ current by 20% (Undrovinas et al., 1995). Cyto-D and gelsolin (used to disrupt the actin cytoskeleton) abolished the perfusion-induced increase in Na^+ current of human jejunal circular smooth muscle cells (Strege et al., 2003). Altogether, such data could suggest that actin disorganization in R735X might be modulating $Na_V1.5$.

Besides its structural role, PKP2 has been pointed out to participate in different signaling pathways (Bass-Zubek et al., 2009). Its has been suggested that PKP2 may functionally link RhoA-dependent pathways to drive actin reorganization and regulate DP–IF interactions required for normal desmosome assembly (Godsel et al., 2010). Moreover, PKP2 has been proposed to serve

as a scaffold that recruits PKC (protein kinase C) locally to control the proper assembly and behavior of DP precursors to translocate to nascent desmosomes and properly organize IF. It has been shown that the absence of PKP2 is accompanied by increased phosphorylation of PKC substrate. Therefore, it has been proposed that, in PKP2 KO cells, PKC would be no longer recruited at DP complexes and would be free to phosphorylate other substrates (Bass-Zubek et al., 2008). $Na_V1.5$ is integrated into a macromolecular complex interacting with partner proteins that modulate its expression levels, localization, and gating. Such protein complex is the target of extensive post-translational modifications that modulates all these properties. Among many others, PKC phosphorylation of S1503 (human) in the $Na_V1.5$ III–IV inactivation loop has been described as a modulatory element of the sodium current (Qu, 1996) (Valdivia et al., 2009). PKC activity decreases cardiac I_{Na} in chinese hamster lung cells and in neonatal rat cardiomyocytes (Qu et al., 1994). In some systems, PKC effect on I_{Na} has been related to a decrease in the number of functional channels at the membrane. Hallaq H. et al. has demonstrated that PKC activation regulates the intracellular distribution of the cardiac Na^+ channels by preferentially trafficking away $Na_V1.5$ from the plasma membrane in HEK293 cells (Hallaq et al., 2012). We have demonstrate that R735X co-precipitates with $Na_V1.5$, likely at the intracellular space, and Bass-Zubek et al., (2008) have shown that PKP2 interacts with PKC by its N-terminal region. Thus, we could hypothesize that R735X may act as an alternative scaffold to PCK, delocalizing and altering PKC activity. As a consequence, PCK-dependent $Na_V1.5$ phosphorylation could be altered, leading to a decrease in $Na_V1.5$ at the membrane. To test whether R735X could be trafficking away $Na_V1.5$ from the plasma membrane and decreasing I_{Na} through PKC, the simplest experiment would be to co-transfect HEK293 cells with SCN5A-S1503A (a PKC resistant mutant) and R735X, and analyze if the amount of $Na_V1.5$ at the plasma membrane is restored.

In conclusion, we present a hiPSC-CM model of AC with a significant potential in the filed of cardiac arrhythmias. We believe this model opens up the possibility to study different mutation-dependent mechanisms and test new therapies in an advantageous way. Moreover, in this thesis project we have provide evidences of the negative effect that the PKP2 AC patient-related mutation R735X have over the voltage-gated sodium channel performance and how that could be responsible for the life-threatening arrhythmias during the concealed phase of AC patients.

CONCLUSIONS

CONCLUSIONS

1. The truncated version of Plakophilin-2 (PKP2) protein (R735X) loses its localization at the cell-cell contact, and is mainly found in the cytoplasm, but does not affect the localization of PKP2 protein.
2. R735X protein has a different mobility pattern than PKP2 protein at the plasma membrane, but does not affect PKP2 protein mobility.
3. R735X protein leads to a decrease of $Na_V1.5$ at the plasma membrane in HEK293T cells as well as in HL-1 cells.
4. R735X protein does not co-localize with $Na_V1.5$ at the plasma membrane of HL-1 cells but they are able to co-precipitate together.
5. R735X protein does not alter $Na_V1.5$ mobility at the plasma membrane of HL-1 cells.
6. Calcium and inward-rectifier potassium currents are not affected in R735X hiPSC-CMs. However, R735X protein leads to a significant decrease in sodium currents in hiPSC-CMs.
7. R735X protein causes an increase in action potential duration by slowing down the depolarization time in hiPSC-CM monolayers, but does not alter their repolarization time. R735X protein leads to a reduction of the conduction velocity in hiPSC-CM monolayers.
8. hiPSC-CM monolayers expressing R735X protein have spontaneous arrhythmic activity, and high frequency pacing exacerbates this arrhythmogenic activity.

CONCLUSIONES

CONCLUSIONES

1. La versión truncada de la proteína Placofilina-2 (proteína R735X) pierde su localización en la membrana plasmática celular, y se encuentra principalmente en el citoplasma, pero no afecta a la localización de Placofilina-2 (PKP2).
2. La proteína R735X tiene un patrón de movilidad diferente al de la proteína PKP2 en la membrana plasmática, pero no afecta a la movilidad de la proteína PKP2.
3. La proteína R735X provoca la disminución de $Na_V1.5$ en la membrana plasmática tanto en células HEK293T como en células HL-1.
4. La proteína R735X no co-localiza con $Na_V1.5$ en la membrana plasmática de células HL-1 pero ambas proteínas co-precipitan juntas.
5. La proteína R735X no altera la movilidad de $Na_V1.5$ en la membrana plasmática de células HL-1.
6. La corriente de calcio y la corriente rectificadora de potasio no están afectadas en cardiomiocitos mutantes derivados de células madre pluripotentes humanas (hiPSC-CMs). Sin embargo, la proteína R735X provoca una reducción significativa en la corriente de sodio en hiPSC-CMs.
7. La proteína R735X causa un incremento de la duración del potencial de acción, prolongando la fase de despolarización sin alterar el tiempo de repolarización. La proteína R735X provoca la disminución de la velocidad de conducción en monocapas de hiPSC-CM.
8. Monocapas de hiPSC-CM que expresan la mutación R735X presentan actividad arrítmica espontánea, y el incremento de la frecuencia exacerba dicha actividad arrítmica.

BIBLIOGRAPHY

BIBLIOGRAPHY

Agullo-Pascual, E., Cerrone, M., Delmar, M., 2014. Arrhythmogenic Cardiomyopathy and Brugada Syndrome: Diseases of the connexome. FEBS Lett 588, 1322–1330. https://doi.org/10.1016/j.febslet.2014.02.008

Alcalde, M., Campuzano, O., Berne, P., García-Pavía, P., Doltra, A., Arbelo, E., Sarquella-Brugada, G., Iglesias, A., Alonso-Pulpon, L., Brugada, J., Brugada, R., 2014. Stop-gain mutations in PKP2 are associated with a later age of onset of arrhythmogenic right ventricular cardiomyopathy. PLoS ONE 9, e100560. https://doi.org/10.1371/journal.pone.0100560

Allan Bradley, J.C., 2007. Generation of an inducible and optimized piggyBac transposon system. Nucleic Acids Res. 35(12): e87. https://doi.org/10.1093/nar/gkm446

Bao Jingru, Wang Jizheng, Yao Yan, Wang Yilu, Fan Xiaohan, Sun Kai, He Ding Sheng, Marcus Frank I., Zhang Shu, Hui Rutai, Song Lei, 2013. Correlation of Ventricular Arrhythmias With Genotype in Arrhythmogenic Right Ventricular Cardiomyopathy. Circulation: Cardiovascular Genetics 6, 552–556. https://doi.org/10.1161/CIRCGENETICS.113.000122

Bass-Zubek, A.E., Godsel, L.M., Delmar, M., Green, K.J., 2009. Plakophilins: multifunctional scaffolds for adhesion and signaling. Curr Opin Cell Biol 21, 708–716. https://doi.org/10.1016/j.ceb.2009.07.002

Bass-Zubek, A.E., Hobbs, R.P., Amargo, E.V., Garcia, N.J., Hsieh, S.N., Chen, X., Wahl, J.K., Denning, M.F., Green, K.J., 2008. Plakophilin 2: a critical scaffold for PKCα that regulates intercellular junction assembly. The Journal of Cell Biology 181, 605–613. https://doi.org/10.1083/jcb.200712133

Beckmann, B.-M., Pfeufer, A., Kääb, S., 2011. Inherited Cardiac Arrhythmias. Dtsch Arztebl Int 108, 623–634. https://doi.org/10.3238/arztebl.2011.0623

Biggs, D.S.C., 2010. 3D Deconvolution Microscopy. Current Protocols in Cytometry 52, 12.19.1-12.19.20. https://doi.org/10.1002/0471142956.cy1219s52

Caspi Oren, Huber Irit, Gepstein Amira, Arbel Gil, Maizels Leonid, Boulos Monther, Gepstein Lior, 2013. Modeling of Arrhythmogenic Right Ventricular Cardiomyopathy With Human Induced Pluripotent Stem Cells. Circulation: Cardiovascular Genetics 6, 557–568. https://doi.org/10.1161/CIRCGENETICS.113.000188

Cerrone, M., Lin, X., Zhang, M., Agullo-Pascual, E., Pfenniger, A., Gusky, H.C., Novelli, V., Kim, C., Tirasawasdichai, T., Judge, D.P., Rothenberg, E., Chen, H.-S.V., Napolitano, C., Priori, S., Delmar, M., 2014. Missense Mutations in Plakophilin-2 Cause Sodium Current Deficit and Associate with a Brugada Syndrome Phenotype. Circulation 129, 1092–1103. https://doi.org/10.1161/CIRCULATIONAHA.113.003077

Cerrone, M., Noorman, M., Lin, X., Chkourko, H., Liang, F.-X., van der Nagel, R., Hund, T., Birchmeier, W., Mohler, P., van Veen, T.A., van Rijen, H.V., Delmar, M., 2012. Sodium current deficit and arrhythmogenesis in a murine model of plakophilin-2 haploinsufficiency. Cardiovasc. Res. 95, 460–468. https://doi.org/10.1093/cvr/cvs218

Clatot, J., Ziyadeh-Isleem, A., Maugenre, S., Denjoy, I., Liu, H., Dilanian, G., Hatem, S.N., Deschênes, I., Coulombe, A., Guicheney, P., Neyroud, N., 2012. Dominant-negative effect of SCN5A N-terminal mutations through the interaction of Nav1.5 α-subunits. Cardiovasc Res 96, 53–63. https://doi.org/10.1093/cvr/cvs211

Claycomb, W.C., Lanson, N.A., Stallworth, B.S., Egeland, D.B., Delcarpio, J.B., Bahinski, A., Izzo, N.J., 1998. HL-1 cells: A cardiac muscle cell line that contracts and retains phenotypic characteristics of the adult cardiomyocyte. Proc Natl Acad Sci U S A 95, 2979–2984.

Cox, M., van der Zwaag, P.A., Hauer, R.N.W., 2011. Arrhythmogenic Right Ventricular Dysplasia/Cardiomyopathy. Circulation 123, 11.

Cruz, F.M., Sanz-Rosa, D., Roche-Molina, M., García-Prieto, J., García-Ruiz, J.M., Pizarro, G., Jiménez-Borreguero, L.J., Torres, M., Bernad, A., Ruíz-Cabello, J., Fuster, V., Ibáñez, B., Bernal, J.A., 2015. Exercise triggers ARVC phenotype in mice expressing a disease-causing mutated version of human plakophilin-2. J. Am. Coll. Cardiol. 65, 1438–1450. https://doi.org/10.1016/j.jacc.2015.01.045

da Rocha, A.M., Campbell, K., Mironov, S., Jiang, J., Mundada, L., Guerrero-Serna, G., Jalife, J., Herron, T.J., 2017. hiPSC-CM Monolayer Maturation State Determines Drug Responsiveness in High Throughput Pro-Arrhythmia Screen. Scientific Reports 7. https://doi.org/10.1038/s41598-017-13590-y

Delpón, E., 2019. Proyecto ITACA [WWW Document]. ITACA. URL https://www.itaca.edu.es/cardiac-action-potential.htm#potential2 (accessed 6.18.19).

El-Battrawy, I., Zhao, Z., Lan, H., Cyganek, L., Tombers, C., Li, X., Buljubasic, F., Lang, S., Tiburcy, M., Zimmermann, W.-H., Utikal, J., Wieland, T., Borggrefe, M., Zhou, X.-B., Akin, I., 2018. Electrical dysfunctions in human-induced pluripotent stem cell-derived cardiomyocytes from a patient with an arrhythmogenic right ventricular cardiomyopathy. Europace 20, f46–f56. https://doi.org/10.1093/europace/euy042

Fressart, V., Duthoit, G., Donal, E., Probst, V., Deharo, J.-C., Chevalier, P., Klug, D., Dubourg, O., Delacretaz, E., Cosnay, P., Scanu, P., Extramiana, F., Keller, D., Hidden-Lucet, F., Simon, F., Bessirard, V., Roux-Buisson, N., Hebert, J.-L., Azarine, A., Casset-Senon, D., Rouzet, F., Lecarpentier, Y., Fontaine, G., Coirault, C., Frank, R., Hainque, B., Charron, P., 2010. Desmosomal gene analysis in arrhythmogenic right ventricular dysplasia/cardiomyopathy: spectrum of mutations and clinical impact in practice. Europace 12, 861–868. https://doi.org/10.1093/europace/euq104

Gandjbakhch, E., Redheuil, A., Pousset, F., Charron, P., Frank, R., 2018. Clinical Diagnosis, Imaging, and Genetics of Arrhythmogenic Right Ventricular Cardiomyopathy/Dysplasia: JACC State-of-the-Art Review. J. Am. Coll. Cardiol. 72, 784–804. https://doi.org/10.1016/j.jacc.2018.05.065

Gerull, B., Heuser, A., Wichter, T., Paul, M., Basson, C.T., McDermott, D.A., Lerman, B.B., Markowitz, S.M., Ellinor, P.T., MacRae, C.A., Peters, S., Grossmann, K.S., Michely, B., Sasse-Klaassen, S., Birchmeier, W., Dietz, R., Breithardt, G., Schulze-Bahr, E., Thierfelder, L., 2004. Mutations in the desmosomal protein plakophilin-2 are common in arrhythmogenic right ventricular cardiomyopathy. Nature Genetics 36, 1162. https://doi.org/10.1038/ng1461

Godsel, L.M., Dubash, A.D., Bass-Zubek, A.E., Amargo, E.V., Klessner, J.L., Hobbs, R.P., Chen, X., Green, K.J., 2010. Plakophilin 2 couples actomyosin remodeling to desmosomal plaque assembly via RhoA. Mol. Biol. Cell 21, 2844–2859. https://doi.org/10.1091/mbc.E10-02-0131

Godsel, L.M., Getsios, S., Huen, A.C., Green, K.J., 2004. The Molecular Composition and Function of Desmosomes. Cell Adhesion 165, 137–193. https://doi.org/10.1007/978-3-540-68170-0_6

Goversen, B., van der Heyden, M.A.G., van Veen, T.A.B., de Boer, T.P., 2018. The immature electrophysiological phenotype of iPSC-CMs still hampers in vitro drug screening: Special focus on IK1. Pharmacology & Therapeutics 183, 127–136. https://doi.org/10.1016/j.pharmthera.2017.10.001

Gray, B., Behr, E.R., 2016. New Insights Into the Genetic Basis of Inherited Arrhythmia Syndromes. Circulation: Cardiovascular Genetics 9, 569–577. https://doi.org/10.1161/CIRCGENETICS.116.001571

Groeneweg Judith A., Bhonsale Aditya, James Cynthia A., te Riele Anneline S., Dooijes Dennis, Tichnell Crystal, Murray Brittney, Wiesfeld Ans C.P., Sawant Abhishek C., Kassamali Bina, Atsma Douwe E., Volders Paul G., de Groot Natasja M., de Boer Karin, Zimmerman Stefan L., Kamel Ihab R., van der Heijden Jeroen F., Russell Stuart D., Jan Cramer Maarten, Tedford Ryan J., Doevendans Pieter A., van Veen Toon A., Tandri Harikrishna, Wilde Arthur A., Judge Daniel P., van Tintelen J. Peter, Hauer Richard N., Calkins Hugh, 2015. Clinical Presentation, Long-Term Follow-Up, and Outcomes of 1001 Arrhythmogenic Right Ventricular Dysplasia/Cardiomyopathy Patients and Family Members. Circulation: Cardiovascular Genetics 8, 437–446. https://doi.org/10.1161/CIRCGENETICS.114.001003

Hallaq, H., Wang, D.W., Kunic, J.D., George, A.L., Wells, K.S., Murray, K.T., 2012. Activation of protein kinase C alters the intracellular distribution and mobility of cardiac Na^+ channels. American Journal of Physiology-Heart and Circulatory Physiology 302, H782–H789. https://doi.org/10.1152/ajpheart.00817.2010

Haugaa, K.H., Haland, T.F., Leren, I.S., Saberniak, J., Edvardsen, T., 2016. Arrhythmogenic right ventricular cardiomyopathy, clinical manifestations, and diagnosis. Europace 18, 965–972. https://doi.org/10.1093/europace/euv340

Herron, T.J., Rocha, A.M.D., Campbell, K.F., Ponce-Balbuena, D., Willis, B.C., Guerrero-Serna, G., Liu, Q., Klos, M., Musa, H., Zarzoso, M., Bizy, A., Furness, J., Anumonwo, J., Mironov, S., Jalife, J., 2016. Extracellular Matrix–Mediated Maturation of Human Pluripotent Stem Cell–Derived Cardiac Monolayer Structure and Electrophysiological Function. Circulation: Arrhythmia and Electrophysiology 9. https://doi.org/10.1161/CIRCEP.113.003638

Houtsmuller, A.B., 2005. Fluorescence Recovery after Photobleaching: Application to Nuclear Proteins, in: Rietdorf, J. (Ed.), Microscopy Techniques. Springer Berlin Heidelberg, Berlin, Heidelberg, pp. 177–199. https://doi.org/10.1007/b102214

Idris, A., Shah, S.R., Park, K., 2018. Right ventricular dysplasia: management and treatment in light of current evidence. Journal of Community Hospital Internal Medicine Perspectives 8, 101–106. https://doi.org/10.1080/20009666.2018.1472513

Itzhaki, I., Maizels, L., Huber, I., Zwi-Dantsis, L., Caspi, O., Winterstern, A., Feldman, O., Gepstein, A., Arbel, G., Hammerman, H., Boulos, M., Gepstein, L., 2011. Modelling the long QT syndrome with induced pluripotent stem cells. Nature 471, 225–229. https://doi.org/10.1038/nature09747

Joshi-Mukherjee, R., Coombs, W., Musa, H., Oxford, E., Taffet, S., Delmar, M., 2008a. Characterization of the molecular phenotype of two arrhythmogenic right ventricular cardiomyopathy (ARVC)-related plakophilin-2 (PKP2) mutations. Heart Rhythm 5, 1715–1723. https://doi.org/10.1016/j.hrthm.2008.09.009

Joshi-Mukherjee, R., Coombs, W., Musa, H., Oxford, E., Taffet, S., Delmar, M., 2008b. Characterization of the molecular phenotype of two arrhythmogenic right ventricular cardiomyopathy (ARVC)-related plakophilin-2 (PKP2) mutations. Heart Rhythm 5, 1715–1723. https://doi.org/10.1016/j.hrthm.2008.09.009

Kaese, S., Verheule, S., 2012. Cardiac electrophysiology in mice: a matter of size. Front Physiol 3. https://doi.org/10.3389/fphys.2012.00345

Kim, C., Wong, J., Wen, J., Wang, S., Wang, C., Spiering, S., Kan, N.G., Forcales, S., Puri, P.L., Leone, T.C., Marine, J.E., Calkins, H., Kelly, D.P., Judge, D.P., Chen, H.-S.V., 2013. Studying arrhythmogenic right ventricular dysplasia with patient-specific iPSCs. Nature 494, 105–110. https://doi.org/10.1038/nature11799

Kim, S.-I., Oceguera-Yanez, F., Sakurai, C., Nakagawa, M., Yamanaka, S., Woltjen, K., 2016. Inducible Transgene Expression in Human iPS Cells Using Versatile All-in-One piggyBac Transposons. Methods Mol. Biol. 1357, 111–131. https://doi.org/10.1007/7651_2015_251

Knollmann, B.C., 2013. Induced pluripotent stem cell-derived cardiomyocytes: boutique science or valuable arrhythmia model? Circ. Res. 112, 969–976; discussion 976. https://doi.org/10.1161/CIRCRESAHA.112.300567

Lian, X., Hsiao, C., Wilson, G., Zhu, K., Hazeltine, L.B., Azarin, S.M., Raval, K.K., Zhang, J., Kamp, T.J., Palecek, S.P., 2012. Robust cardiomyocyte differentiation from human pluripotent stem cells via temporal modulation of canonical Wnt signaling. Proc Natl Acad Sci U S A 109, E1848–E1857. https://doi.org/10.1073/pnas.1200250109

Lian, X., Zhang, J., Azarin, S.M., Zhu, K., Hazeltine, L.B., Bao, X., Hsiao, C., Kamp, T.J., Palecek, S.P., 2013. Directed cardiomyocyte differentiation from human pluripotent stem cells by modulating Wnt/β-catenin signaling under fully defined conditions. Nat Protoc 8, 162–175. https://doi.org/10.1038/nprot.2012.150

Ma, D., Liu, Z., Loh, L.J., Zhao, Y., Li, G., Liew, R., Islam, O., Wu, J., Chung, Y.Y., Teo, W.S., Ching, C.K., Tan, B.Y., Chong, D., Ho, K.L., Lim, P., Yong, R.Y.Y., Panama, B.K., Kaplan, A.D., Bett, G.C.L., Ware, J., Bezzina, C.R., Verkerk, A.O., Cook, S.A., Rasmusson, R.L., Wei, H., 2018. Identification of an INa-dependent and Ito-mediated proarrhythmic mechanism in cardiomyocytes derived from pluripotent stem cells of a Brugada syndrome patient. Scientific Reports 8. https://doi.org/10.1038/s41598-018-29574-5

Ma, D., Wei, H., Lu, J., Ho, S., Zhang, G., Sun, X., Oh, Y., Tan, S.H., Ng, M.L., Shim, W., Wong, P., Liew, R., 2013. Generation of patient-specific induced pluripotent stem cell-derived cardiomyocytes as a cellular model of arrhythmogenic right ventricular cardiomyopathy. Eur Heart J 34, 1122–1133. https://doi.org/10.1093/eurheartj/ehs226

Machiraju, P., Greenway, S.C., 2019. Current methods for the maturation of induced pluripotent stem cell-derived cardiomyocytes. World J Stem Cells 11, 33–43. https://doi.org/10.4252/wjsc.v11.i1.33

Makara, M.A., Curran, J., Little, S.C., Musa, H., Polina, I., Smith, S.A., Wright, P.J., Unudurthi, S.D., Snyder, J., Bennett, V., Hund, T.J., Mohler, P.J., 2014. Ankyrin-G Coordinates Intercalated Disc Signaling Platform to Regulate Cardiac Excitability In Vivo. Circulation Research 115, 929–938. https://doi.org/10.1161/CIRCRESAHA.115.305154

Malhotra, J.D., Thyagarajan, V., Chen, C., Isom, L.L., 2004. Tyrosine-phosphorylated and Nonphosphorylated Sodium Channel β1 Subunits Are Differentially Localized in Cardiac Myocytes. J. Biol. Chem. 279, 40748–40754. https://doi.org/10.1074/jbc.M407243200

Mercier, A., Bois, P., Chatelier, A., 2017. Sodium Channel Trafficking. Voltage-gated Sodium Channels: Structure, Function and Channelopathies 246, 125–145. https://doi.org/10.1007/164_2017_47

Mercier, A., Clément, R., Harnois, T., Bourmeyster, N., Bois, P., Chatelier, A., 2015. Nav1.5 channels can reach the plasma membrane through distinct N-glycosylation states. Biochimica et Biophysica Acta (BBA) - General Subjects 1850, 1215–1223. https://doi.org/10.1016/j.bbagen.2015.02.009

Moriya, H., 2015. Quantitative nature of overexpression experiments. Mol Biol Cell 26, 3932–3939. https://doi.org/10.1091/mbc.E15-07-0512

Multi Channel Systems MCS GmbH, 2019. Multiwell-MEA-System Manual.

Nerbonne, J.M., Kass, R.S., 2005. Molecular Physiology of Cardiac Repolarization. Physiological Reviews 85, 1205–1253. https://doi.org/10.1152/physrev.00002.2005

Nishimura Rick A., Seggewiss Hubert, Schaff Hartzell V., 2017. Hypertrophic Obstructive Cardiomyopathy. Circulation Research 121, 771–783. https://doi.org/10.1161/CIRCRESAHA.116.309348

Noorman, M., Hakim, S., Kessler, E., Groeneweg, J.A., Cox, M.G.P.J., Asimaki, A., van Rijen, H.V.M., van Stuijvenberg, L., Chkourko, H., van der Heyden, M.A.G., Vos, M.A., de Jonge, N., van der Smagt, J.J., Dooijes, D., Vink, A., de Weger, R.A., Varro, A., de Bakker, J.M.T., Saffitz, J.E., Hund, T.J., Mohler, P.J., Delmar, M., Hauer, R.N.W., van Veen, T.A.B., 2013. Remodeling of the cardiac sodium channel, connexin43, and plakoglobin at the intercalated disk in patients with arrhythmogenic cardiomyopathy. Heart Rhythm 10, 412–419. https://doi.org/10.1016/j.hrthm.2012.11.018

Paul J Tesar, M.S.E., 2018. Drug screening for human genetic diseases using iPSC models. Human Molecular Genetics 27, R89–R98. https://doi.org/10.1093/hmg/ddy186

Platonov, P.G., Haugaa, K.H., Bundgaard, H., Svensson, A., Gilljam, T., Hansen, J., Madsen, T., Holst, A.G., Carlson, J., Lie, Ø.H., Kvistholm Jensen, M., Edvardsen, T., Jensen, H.K., Svendsen, J.H., 2019. Primary Prevention of Sudden Cardiac Death With Implantable Cardioverter-Defibrillator Therapy in Patients With Arrhythmogenic Right Ventricular Cardiomyopathy. The American Journal of Cardiology 123, 1156–1162. https://doi.org/10.1016/j.amjcard.2018.12.049

Ponce-Balbuena, D., Guerrero-Serna, G., Valdivia, C.R., Caballero, R., Diez-Guerra, F.J., Jiménez-Vázquez, E.N., Ramírez, R.J., da Rocha, A.M., Herron, T.J., Campbell, K.F., Willis, B.C., Alvarado, F.J., Zarzoso, M., Kaur, K., Pérez-Hernández, M., Matamoros, M., Valdivia, H.H., Delpón, E., Jalife, J., 2018. Cardiac Kir2.1 and NaV1.5 Channels Traffic Together to the Sarcolemma to Control Excitability. Circ Res 122, 1501–1516. https://doi.org/10.1161/CIRCRESAHA.117.311872

Qu, Y., 1996. Phosphorylation of S1505 in the cardiac Na+ channel inactivation gate is required for modulation by protein kinase C. The Journal of General Physiology 108, 375–379. https://doi.org/10.1085/jgp.108.5.375

Qu, Y., Rogers, J., Tanada, T., Scheuer, T., Catterall, W.A., 1994. Modulation of cardiac Na+ channels expressed in a mammalian cell line and in ventricular myocytes by protein kinase C. Proceedings of the National Academy of Sciences 91, 3289–3293. https://doi.org/10.1073/pnas.91.8.3289

Reichart, D., Magnussen, C., Zeller, T., Blankenberg, S., 2019. Dilated Cardiomyopathy - From Epidemiologic to Genetic Phenotypes A Translational Review of Current Literature. J. Intern. Med. https://doi.org/10.1111/joim.12944

Rhett, J.M., Ongstad, E.L., Jourdan, J., Gourdie, R.G., 2012. Cx43 Associates with Nav1.5 in the Cardiomyocyte Perinexus. J Membrane Biol 245, 411–422. https://doi.org/10.1007/s00232-012-9465-z

Rizzo, S., Lodder, E.M., Verkerk, A.O., Wolswinkel, R., Beekman, L., Pilichou, K., Basso, C., Remme, C.A., Thiene, G., Bezzina, C.R., 2012. Intercalated disc abnormalities, reduced Na+ current density, and conduction slowing in desmoglein-2 mutant mice prior to cardiomyopathic changes. Cardiovasc Res 95, 409–418. https://doi.org/10.1093/cvr/cvs219

Roche, J. de la, Angsutararux, P., Kempf, H., Janan, M., Bolesani, E., Thiemann, S., Wojciechowski, D., Coffee, M., Franke, A., Schwanke, K., Leffler, A., Luanpitpong, S., Issaragrisil, S., Fischer, M., Zweigerdt, R., 2019. Comparing human iPSC-cardiomyocytes versus HEK293T cells unveils disease-causing effects of Brugada mutation A735V of NaV1.5 sodium channels. Scientific Reports 9. https://doi.org/10.1038/s41598-019-47632-4

Sato, P.Y., Musa, H., Coombs, W., Guerrero-Serna, G., Patiño, G.A., Taffet, S.M., Isom, L.L., Delmar, M., 2009. Loss of plakophilin-2 expression leads to decreased sodium current and slower conduction velocity in cultured cardiac myocytes. Circ. Res. 105, 523–526. https://doi.org/10.1161/CIRCRESAHA.109.201418

Séverine, P., Anne-Flore, Z., Jakob, O., Elise, B., Nour, R., Said, E.-H., Maxime, A., Philip, B., Stefan, L., E., L.S., N., H.S., Alain, C., Hugues, A., 2011. SAP97 and Dystrophin Macromolecular Complexes Determine Two Pools of Cardiac Sodium Channels Nav1.5 in Cardiomyocytes. Circulation Research 108, 294–304. https://doi.org/10.1161/CIRCRESAHA.110.228312

Strege, P.R., Holm, A.N., Rich, A., Miller, S.M., Ou, Y., Sarr, M.G., Farrugia, G., 2003. Cytoskeletal modulation of sodium current in human jejunal circular smooth muscle cells. American Journal of Physiology-Cell Physiology 284, C60–C66. https://doi.org/10.1152/ajpcell.00532.2001

Syrris Petros, Ward Deirdre, Asimaki Angeliki, Sen-Chowdhry Srijita, Ebrahim Hatim Y., Evans Alison, Hitomi Nobuhiko, Norman Mark, Pantazis Antonios, Shaw Anthony L., Elliott Perry M., McKenna William J., 2006. Clinical Expression of Plakophilin-2 Mutations in Familial Arrhythmogenic Right Ventricular Cardiomyopathy. Circulation 113, 356–364. https://doi.org/10.1161/CIRCULATIONAHA.105.561654

Tamargo, J., Caballero, R., Gómez, R., Valenzuela, C., Delpón, E., 2004. Pharmacology of cardiac potassium channels. Cardiovasc. Res. 62, 9–33. https://doi.org/10.1016/j.cardiores.2003.12.026

Tan, B.Y., Jain, R., den Haan, A.D., Chen, Y., Dalal, D., Tandri, H., Amat-Alarcon, N., Daly, A., Tichnell, C., James, C., Calkins, H., Judge, D.P., 2010. Shared Desmosome Gene Findings in Early and Late Onset Arrhythmogenic Right Ventricular Dysplasia/Cardiomyopathy. J. of Cardiovasc. Trans. Res. 3, 663–673. https://doi.org/10.1007/s12265-010-9224-4

Tanawuttiwat, T., Te Riele, A.S.J.M., Philips, B., James, C.A., Murray, B., Tichnell, C., Sawant, A.C., Calkins, H., Tandri, H., 2016. Electroanatomic Correlates of Depolarization Abnormalities in Arrhythmogenic Right Ventricular Dysplasia/Cardiomyopathy: EAM Correlates of Depolarization in ARVD. J Cardiovasc Electrophysiol 27, 443–452. https://doi.org/10.1111/jce.12925

te Riele, A.S.J.M., James, C.A., Philips, B., Rastegar, N., Bhonsale, A., Groeneweg, J.A., Murray, B., Tichnell, C., Judge, D.P., van der Heijden, J.F., Cramer, M.J.M., Velthuis, B.K., Bluemke, D.A., Zimmerman, S.L., Kamel, I.R., Hauer, R.N.W., Calkins, H., Tandri, H., 2013. Mutation Positive Arrhyhmogenic Right Ventricular Dysplasia/Cardiomyopathy: The Triangle of Dysplasia Displaced. J Cardiovasc Electrophysiol 24, 1311–1320. https://doi.org/10.1111/jce.12222

Undrovinas, A.I., Shander, G.S., Makielski, J.C., 1995. Cytoskeleton modulates gating of voltage-dependent sodium channel in heart. American Journal of Physiology-Heart and Circulatory Physiology 269, H203–H214. https://doi.org/10.1152/ajpheart.1995.269.1.H203

Valdivia, C.R., Ueda, K., Ackerman, M.J., Makielski, J.C., 2009. GPD1L links redox state to cardiac excitability by PKC-dependent phosphorylation of the sodium channel SCN5A. Am J Physiol Heart Circ Physiol 297, H1446–H1452. https://doi.org/10.1152/ajpheart.00513.2009

Wang, W., James, C.A., Calkins, H., 2019. Diagnostic and therapeutic strategies for arrhythmogenic right ventricular dysplasia/cardiomyopathy patient. Europace 21, 9–21. https://doi.org/10.1093/europace/euy063